Calhoun: The NPS Institutional Archive

DSpace Repository

Theses and Dissertations | 1. Thesis and Dissertation Collection, all items

1975-12

Thermographic imaging of electromagnetic fields.

La Varre, Claude Andrews

Monterey, California. Naval Postgraduate School

https://hdl.handle.net/10945/21092

This publication is a work of the U.S. Government as defined in Title 17, United States Code, Section 101. Copyright protection is not available for this work in the United States.

Downloaded from NPS Archive: Calhoun

http://www.nps.edu/library

Calhoun is the Naval Postgraduate School's public access digital repository for research materials and institutional publications created by the NPS community. Calhoun is named for Professor of Mathematics Guy K. Calhoun, NPS's first appointed -- and published -- scholarly author.

Dudley Knox Library / Naval Postgraduate School
411 Dyer Road / 1 University Circle
Monterey, California USA 93943

THERMOGRAPHIC IMAGING OF ELECTROMAGNETIC FIELDS

Claude Andrews La Varre

DUDLEY KNOX LIBRARY
NAVAL POSTGRADUATE SCHOOL
MONTEREY, CALIFORNIA 93940

Report Number NPS-52Zn75121

NAVAL POSTGRADUATE SCHOOL
Monterey, California

THESIS

THERMOGRAPHIC IMAGING OF
ELECTROMAGNETIC FIELDS

by

Claude A. La Varre

December 1975

Thesis Advisor: R. W. Burton

Approved for public release; distribution unlimited.

Prepared for: Air Force Weapons Laboratory
Kirtland Air Force Base, NM 87117

T170809

DUDLEY KNOX LIBRARY
NAVAL POSTGRADUATE SCHOOL
MONTEREY, CALIFORNIA 93940

REPORT DOCUMENTATION PAGE

READ INSTRUCTIONS BEFORE COMPLETING FORM

1. REPORT NUMBER: NPS-52Zn 75121	2. GOVT ACCESSION NO.
3. RECIPIENT'S CATALOG NUMBER	
4. TITLE (and Subtitle): Thermographic Imaging of Electromagnetic Fields	5. TYPE OF REPORT & PERIOD COVERED: Thesis Final Report Jan-Dec 1975
6. PERFORMING ORG. REPORT NUMBER	
7. AUTHOR(s): Claude A La Varre, LCDR, USN in conjunction with R.W. Burton	8. CONTRACT OR GRANT NUMBER(s)
9. PERFORMING ORGANIZATION NAME AND ADDRESS: Code 52 Zn Department of Electrical Engineering Naval Postgraduate School Monterey, Ca., 93940	10. PROGRAM ELEMENT, PROJECT, TASK AREA & WORK UNIT NUMBERS: 74-201
11. CONTROLLING OFFICE NAME AND ADDRESS	12. REPORT DATE: December 1975
	13. NUMBER OF PAGES: 155
14. MONITORING AGENCY NAME & ADDRESS(if different from Controlling Office)	15. SECURITY CLASS. (of this report): Unclassified
	15a. DECLASSIFICATION/DOWNGRADING SCHEDULE

16. DISTRIBUTION STATEMENT (of this Report)

Approved for public release; distribution unlimited

17. DISTRIBUTION STATEMENT (of the abstract entered in Block 20, if different from Report)

18. SUPPLEMENTARY NOTES

19. KEY WORDS (Continue on reverse side if necessary and identify by block number)

Thermography
Electromagnetic
Charge Measurement
Current Measurement
Infra-red Photography
EMP

20. ABSTRACT (Continue on reverse side if necessary and identify by block number)

It is recognized that a means of converting electromagnetic fields into visible images would greatly simplify the problem of designing structures to optimize their compatibility with such fields.

Two needs must be met to allow such visualization. First, the fields must be transduced into a phenomenon which is capable of being imaged. Second, there must exist a sensor which senses

that phenomenon and generates an image visible to the human eye.

The bulk of this work was to investigate the parameters and limitations of one possible imaging procedure, called Dye Transfer Modulation (DTM).

On the basis of that work and the development of a new sensor, the AGA Thermovision device was recognized as an exciting alternative to DTM. A brief investigation of its potential was conducted and is presented herein.

Thermographic Imaging Of Electromagnetic Fields

by

Claude Andrews La Varre
Lieutenant Commander, United States Navy
M.S., Naval Postgraduate School, 1975

Submitted in partial fulfillment of the
requirements for the degree of

ELECTRICAL ENGINEER

from the

NAVAL POSTGRADUATE SCHOOL
December 1975

DUDLEY KNOX LIBRARY
NAVAL POSTGRADUATE SCHOOL
MONTEREY, CALIFORNIA 93940

NAVAL POSTGRADUATE SCHOOL
Monterey, California

Rear Admiral Isham Linder
Superintendent

Jack R. Borsting
Provost

This thesis prepared in conjunction with research supported in part by the Naval Postgraduate School.

Reproduction of all or part of this report is authorized.

Released as a
Technical Report by:

ABSTRACT

It is recognized that a means of converting electromagnetic fields into visible images would greatly simplify the problem of designing structures to optimize their compatibility with such fields.

Two needs must be met to allow such visualization. First, the fields must be transduced into a phenomenon which is capable of being imaged. Second, there must exist a sensor which senses that phenomenon and generates an image visible to the human eye.

The bulk of this work was to investigate the parameters and limitations of one possible imaging procedure, called Dye Transfer Modulation (DTM).

On the basis of that work and the development of a new sensor, the AGA Thermovision device was recognized as an exciting alternative to DTM. A brief investigation of its potential was conducted and is presented herein.

TABLE OF CONTENTS

I. SIGNIFICANCE AND APPLICATION..... 10

A. THE PROBLEM..... 10

B. THESIS..... 10

C. THESIS OBJECTIVE..... 11

II. FUNDAMENTAL BASES..... 12

A. THE PHOTOGRAPHIC PROCESS..... 12

B. THE COLOR PROCESS..... 14

III. THE PROCESS OF DYE TRANSFER MODULATION (DTM)..... 16

A. BASIC PRINCIPLE OF DTM..... 16

B. FILM SENSITIZATION..... 17

C. TEMPERATURE BIASING..... 20

D. DEVELOPER ACTIVATION..... 20

E. TRANSFER MODULATION..... 20

IV. PARAMETERS OF THE PROCESS..... 23

A. FILM DENSITY..... 23

B. CONTRAST..... 23

C. APPLIED ENERGY..... 24

1. Power Source..... 24

2. Source Frequency..... 24

3. Source and Target Resonance..... 25

4. Source Radiating Devices..... 25

5. Target Element Placement..... 26

D. PHOTOGRAPHIC PARAMETERS..... 26

1. Color Temperature Of Light Source and Film Sensitivity..... 26

2. Choice of Color Exposure Times for Sensitization..... 29

3. Developer Activation..... 30

E. THERMAL PARAMETERS..... 30

1. Temperature Biasing..... 30

2. Cooling Procedure Parameters..... 30

a. Choice of Coolant..... 31

b. Cooling Device Temperature Variations..... 31
c. Activator Chemical Freezing Point... 31
F. DYNAMIC RANGE..... 31
V. EXPERIMENTAL METHODS AND MODELS..... 33
A. DETERMINATION OF FILM DENSITY..... 33
B. DETERMINATION OF DYNAMIC RANGE..... 35
C. DETERMINATION OF APPLIED ENERGY..... 36
1. Determination of Power Delivered by Waveguide..... 37
a. Field Equations..... 37
b. Time Averaged Power Density..... 38
c. Total Power at Waveguide End..... 39
d. Relation between Total Average Power at Waveguide Source and Load.. 40
e. Relation between Total Power at Source and Power Measured by Meters. 43
f. Summary..... 43
2. Determination of Power Delivered by a Reflector System..... 44
a. Fields of Single Dipole..... 46
b. Effects of Reflections..... 48
c. Summation of Component Fields..... 49
d. Total Time-Averaged Power Density... 50
e. Measurement of Power..... 52
3. Determination of Effect Of System Resonance..... 53
a. Determination of Film Impedance..... 53
b. Determination of System Time Response..... 59
D. DETERMINATION OF THERMAL PARAMETERS..... 60
1. Cooling Box Temperature..... 61
a. Cooling Rate of Box..... 61
b. Effect of Film..... 61
2. Activator Chemical Freezing Point..... 61
3. Temperature Variations in Film

Due to Cooling Method..... 61
a. Dry Ice..... 62
b. Liquid Nitrogen..... 62
4. Warming of Film on Removal..... 62
VI. EXPERIMENTAL RESULTS..... 63
A. SUMMARY OF PARAMETERS..... 63
1. Principal Parameters..... 63
a. Applied Energy..... 63
b. Image Density..... 63
2. Experiment Objective..... 63
B. THERMAL VARIATIONS..... 64
1. Cooling Box Temperature..... 64
2. Film Temperature Variations..... 66
3. Activator Chemical Freezing Point..... 69
C. DENSITY VARIATIONS..... 69
1. Density Variation with Sensitizing Pre-exposure..... 69
2. Density Variations with Initial Temperature..... 71
D. DYNAMIC RANGE MEASUREMENTS..... 73
E. FIELD MEASUREMENTS..... 73
VII. EXPERIMENTAL CONFIGURATIONS..... 78
A. FILM SENSITIZING PARAMETERS..... 78
1. Light Source and Intensity..... 78
2. Filters..... 78
3. Sensitizing Pre-exposures..... 78
B. FILM RADIATION PARAMETERS..... 78
1. Initial Temperature..... 78
2. Radiation Frequency..... 79
3. Radiation Exposure..... 79
C. ALTERNATIVE SOLUTIONS..... 79
VIII. FINAL RESULTS..... 80
IX. CONCLUSION..... 83
A. SUMMARY..... 83
APPENDIX A: BASIC CONCEPTS RELEVANT TO FILM SENSITOMETRY..... 85

A. FILM SENSITIVITY VERSUS EXPOSURE..... 85
B. FILM SENSITIVITY VERSUS COLOR OF LIGHT..... 88
C. FILTERS..... 90
1. Band-pass Filters..... 91
2. Color Conversion Filters..... 92
APPENDIX B 93
APPENDIX C: POWER COMPUTATION COMPUTER PROGRAM..... 96
A. DISCUSSION..... 96
B. PARAMETERS TO BE PROVIDED..... 96
C. DETERMINATION OF PARAMETERS..... 97
1. Defined Parameters..... 97
2. Derived Parameters..... 97
D. SAMPLE PROBLEMS..... 98
1. Two Dimensional Plot (Power vs Y) for fixed D..... 98
2. Two Dimensional Plot (Power versus D) for fixed Y)..... 99
3. Three Dimensional Plot(Power versus Y and D)..... 100
APPENDIX D: MATHEMATICAL PROCEDURES..... 112
APPENDIX E: SMOOTH EXPERIMENTAL DATA..... 114
APPENDIX F: DESCRIPTION OF EXPERIMENTS WITH AGA THERMOVISION..... 131
BIBLIOGRAPHY..... 154
INITIAL DISTRIBUTION LIST..... 155

ACKNOWLEDGEMENT

This thesis represents a summary of my work at the Naval Postgraduate School. Any success in that work is necessarily attributable directly to those other persons who fostered, supported, encouraged and corrected me in that work. Of the many persons to whom I am indebted for their participation in and contribution to my learning experience, there are several who particularly deserve recognition and thanks for their help. These are my friends Patrick and Christina, for whom these three years were the longest cruise ever, and my friends and associates Petty Officer First Class T. W. Nowak, Associate Professor R. W. Burton, and Lucy S. La Varre, all three of whose support and technical abilities were crucial to this work.

I. SIGNIFICANCE AND APPLICATION

A. THE PROBLEM

The design and analysis of devices which interact with electromagnetic fields is of principal interest in many technical areas. One such area directly applicable to the Navy is that of shipboard antenna design and placement. A second is the problem of countering the coupling between a structure and a strong, broad-band signal such as an electromagnetic pulse.

In both cases theoretical approaches, including computer analyses, become severely complicated by the existence of structural discontinuities (junctions) and assymmetric configurations of the structures under study. Even simple models of such structures show significant inconsistencies with experimental measurements.[1]

It would be highly convenient if there existed some simple and direct means of measuring the currents and charges on such structures. One candidate for such a process was suggested by Keigo Iizuka.[2] A more recent investigation of process was made by James Dodd[3] to determine its application to the problem of structures with junctions.

B. THESIS

This thesis is to determine the parameters of that process, to characterize those parameters and their

---

[1]R. W. Burton, The Crossed-Dipole Structure of Aircraft in an Electromagnetic Pulse Environment

[2]Keigo Iizuka, A Method for Photographing Microwave with a Polaroid Film, Technical Report no. 558, Division of Engineering and Applied Physics, Harvard University, Cambridge, Massachusetts, March 1968, p. 3.

[3]Dodd, James L., A Direct Method of Visualizing the Surface Distribution on Antennas at Microwave Frequencies with Application to Cross-Wire Structures, Masters Thesis, U. S. Naval Postgraduate School, Monterey, Calif., 1974.

interactions, and to determine a set of parameters which would optimize the application of the process to the problem of imaging the scattered fields of structures with junctions and thereby to the determination of the currents and charges present.

C. THESIS OBJECTIVE

The objective of this work is to optimize a method for imaging electromagnetic fields. This method is called the Dye Transfer Modulation Process. Optimization is considered to have occurred when the images obtained with the process show the best possible definition of the fields. Ideally one should be able to easily distinguish regions of low energy density from those of high energy density and determine the boundaries between them. Further the range of energy levels distinguishable by the process should match the range of energy present in the fields being measured. In short, it is considered necessary to find the settings of process parameters which would maximize the dynamic range of the process and match it to that of the fields being measured.

II. FUNDAMENTAL BASES

There are three fundamental bases to understanding dye-transfer modulation and to explaining why it may be successful in imaging a field when conventional photography is not. These bases are (1) understanding the basic photographic process (2) understanding the spectral distribution of energy and the application thereof to the basic photographic process and (3) understanding the method of color photography used here.

A. THE PHOTOGRAPHIC PROCESS[4]

A conventional photographic film comprises a structural substrate on which is placed a colloidal suspension of crystals of one or more of the silver halides: silver bromide, chloride or iodide. Each crystal comprises silver and halide ions in a predominantly regular crystalline structure. Within the structure, however, there are a few positive (Ag^+) silver ions which occupy interstitial positions. When a a packet of electromagnetic radiation (a photon) of sufficient energy impinges on a crystal, one or more electrons are broken loose from the halide ions. This results in a modification of the state of the crystal. The few free electrons diffuse through the crystal until they come in contact with some of the interstitial silver ions. The positive silver ions capture the electrons and become metallic silver atoms. A crystal with one or more metallic silver atoms is termed a "sensitized" crystal. On a macroscopic scale, the distribution of these sensitized crystals provides an image of the incoming light pattern. Since the crystals have not changed entirely to metallic silver the image is not normally visible, and is termed a "latent" image. When exposed to a developer, however,

---

[4]Engel, Charles E., Photography for the Scientist, Academic Press, 1968 , p.2.ff.

the atoms of silver catalyze the reaction of the developer with the remainder of the crystal, causing it to convert entirely to metallic silver, and thus forming what is commonly known as the negative. Subsequently, the negative is exposed first to chemicals which neutralize the developer (a "stop" bath) and then to those which remove the unsensitized crystals from the negative (a "fixer" bath).

The chemical reactions described all require energy. In particular the crucial event, that of the halide ion giving up an electron, as in the bromide ion,

$$Br^- \xrightarrow[\text{energy}]{} Br + e^-$$

only occurs when the applied energy is sufficient to break the molecular bond. The energy required is proportional to the oxidation potential of the element and is found to be approximately 10^{-19} joule.[5]

B. FREQUENCY AND ENERGY IN PHOTOGRAPHY

The energy required to break electrons free from a bromide ion must be provided by the photon striking the crystal. The energy of a photon is known from quantum mechanics to have energy proportional to its frequency

$$E = hf$$

where h is Planck's constant, 6.626×10^{-34} joule-sec. and f is the frequency of the radiation.[6] The lowest frequency radiation which is theoretically capable of triggering the process is then found to be approximately

$$\frac{E}{h} = f \cong \frac{10^{-19}}{h} \cong 1.60 \times 10^{14} \text{ Hz}$$

---

[5]Masterton, W. L. and Slowinski, E. J., Chemical Principles, W. B. Saunders, 1973, p.255.

[6]Beiser, Arthur, Perspectives of Modern Physics, McGraw-Hill, 1969, p. 56.

or 160 thousand gigahertz, which corresponds to a wavelength of 2 microns (2 x 10^{-6} meters). (The maximum wavelength that can be imaged by available Kodak films is reported to be 1.15 microns.[7]) By contrast, the radiation associated with the radio spectrum is of the order of ten gigahertz or less, four orders of magnitude lower than the necessary frequency level. Thus, it is not likely that direct irradiation by RF energy shall trigger the photographic process.

B. THE COLOR PROCESS[8]

Imaging fields is possible however, by controlling the events which occur subsequent to the sensitization of the film. In particular, the Polaroid Corporation color process ("Polacolor") uses a diffusion technique which is sensitive to temperature. If the RF energy field can be transduced into a temperature field, modulation of the diffusion process is possible, resulting in an image of the field being formed.

The principle of crystal sensitization in color film is the same as described above for black and white film. The difference between color and black and white film is that color film actually has three emulsions, while black and white film has only one. Each of the three layers is sensitized by a different primary color, the undesired colors having been blocked by filters built into the emulsion. In addition to the silver halide crystals and the color filter, each layer has a chemical (a "dye-coupler") which reacts with the sensitized crystals and the developer to create a dye when the film is developed. It is at this point where the photographic process can be used to provide imaging of electromagnetic energy. Unlike other processes, the Polacolor method causes dyes to be formed in all three

---

[7]Eastman Kodak Company, Kodak Publication No. N-17, Kodak Infrared Films, 1972, p. 2.

[8]Engel, p. 45, ff.

layers of the film independently of the amount of sensitization of the emulsion. Subsequently, sensitized crystals in each of the three emulsions cause some of their respective dyes to become anchored in the emulsion.[9] This anchoring, or leaving behind of selected dyes is termed mordanting. How much of each dye is mordanted (rather than the amount created) is therefore proportional to the amount of sensitization to which the film has been exposed. The unanchored dye molecules then diffuse upward through the multilayered emulsion until reaching the substrate for the print, where they become fixed. It is this diffusion process which is used in dye-transfer modulation to obtain an image.

---

[9]Thirtle, John R., "Chemistry of Color Process," SPSE Handbook of Photographic Science and Engineering, Wiley, 1973 p.567-568.

III. THE PROCESS OF DYE TRANSFER MODULATION (DTM)

The Dye Transfer Modulation (DTM) Process is primarily dependent on the Polacolor diffusion process. The technique comprises four sub-processes.

A. BASIC PRINCIPLE OF DTM

It can be shown[10] that the rate of a chemical reaction is temperature dependent by the expression

$$\log_{10} \frac{R_2}{R_1} = K_1 \frac{T_2 - T_1}{T_1 T_2}$$

where K_1 is a constant, $T_{(i)}$ is the temperature of the reaction and $R_{(i)}$ is the rate of reaction at the corresponding temperature. It can further be shown[11] that the rate of diffusion of a substance through a medium is temperature dependent by the expression

$$j = K_2 \frac{T_2 - T_1}{T_1 T_2}$$

where j is the change in diffusion flow for the indicated change in temperature T and K_2 is another constant. It can be seen that for both rates the effect of a given change in temperature at a low temperature is significantly greater than at a higher temperature. For example, at room temperature a five degree change in reaction temperature gives the ratio

$$\frac{T_2 - T_1}{T_1 T_2} = \frac{5}{300 \cdot 305} = 5.46 \times 10^{-5}$$

while at the temperature of dry ice, approximately 195°K, that same five degree change in temperature yields

$$\frac{T_2 - T_1}{T_1 T_2} = \frac{5}{195 \cdot 200} = 1.28 \times 10^{-4}$$

---

[10] Masterton and Slowinski, p.380-382.

[11] Encyclopaedia Britannica, 1968. v.7, p.424.

2.35 larger than the effect at room temperature. It is clear that temperature variations can be used to modulate the reaction rate in the formation of dyes and, further, to modulate the rate at which the dyes in the unsensitized layers diffuse to the print substrate. It is also clear that a given change in temperature shall have a greater effect on these rates if the ambient temperature is low.

The basic principle of the Dye Transfer Modulation Process is to transduce an energy field, particularly an electro-magnetic field, into a thermal field, then use the thermal field to modulate the rates of reaction and diffusion in the Polacolor process. The term "Dye Transfer Modulation" reflects the fact that the end result is to vary the amount of dye which transfers from the film negative to the print.

B. FILM SENSITIZATION

The schematic drawing of Figure 1 shows the cross-section of a Polaroid Film Pack. Figures 2 and 3 show the actual film packet and its components. Three emulsion layers are placed on the negative substrate, sensitive to red, green, and blue light, in order upward from the substrate. Their developers, when activated, produce cyan, magenta, and yellow dyes.[12] Thus the layer farthest from the surface of the negative is the layer sensitive to red light, which produces cyan dye. Controllability of the diffusion process is maximized by allowing only this deepest dye to escape the negative. This is accomplished, in principle, by exposing the film thoroughly to blue and green light. Such exposure will cause the yellow and magenta layers to be mordanted in the negative, leaving only the cyan, red-sensitive layer free to diffuse to the surface of the negative and thence onto the print surface.

This selective pre-sensitization of the film is effected by exposing the film in a box camera and using

---

[12] SPSE Handbook..., p. 567.

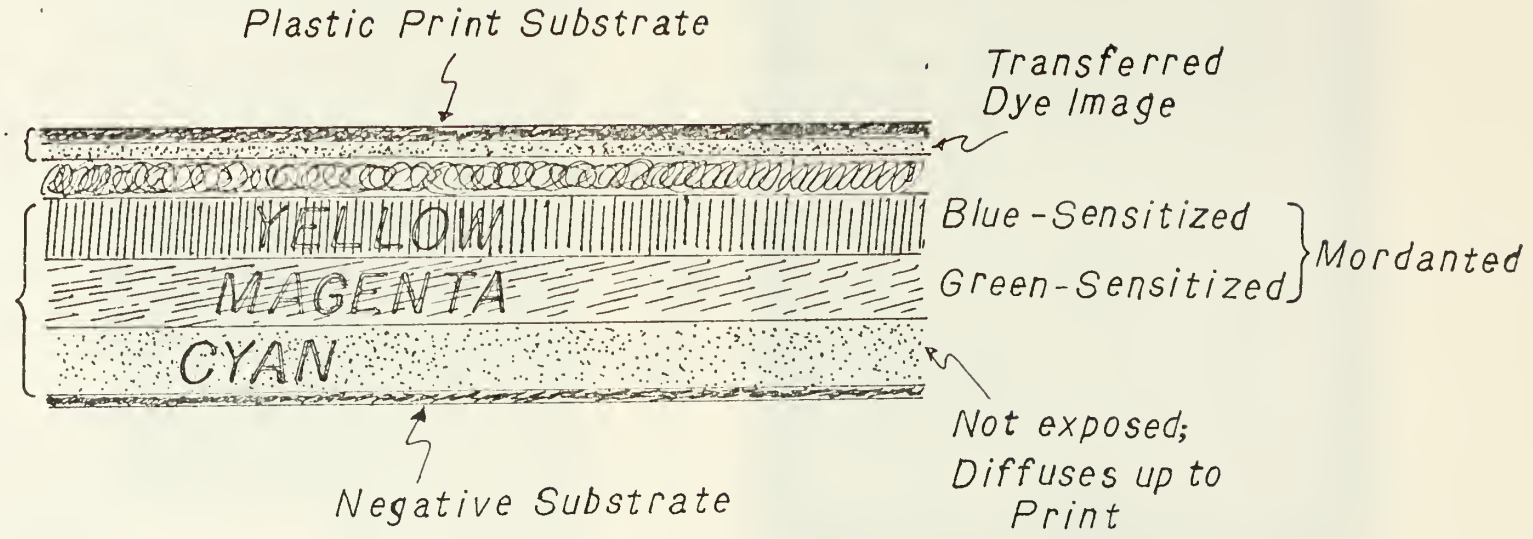

Figure 1
Cross - Section of Polaroid Color
Film Pack (stylized)

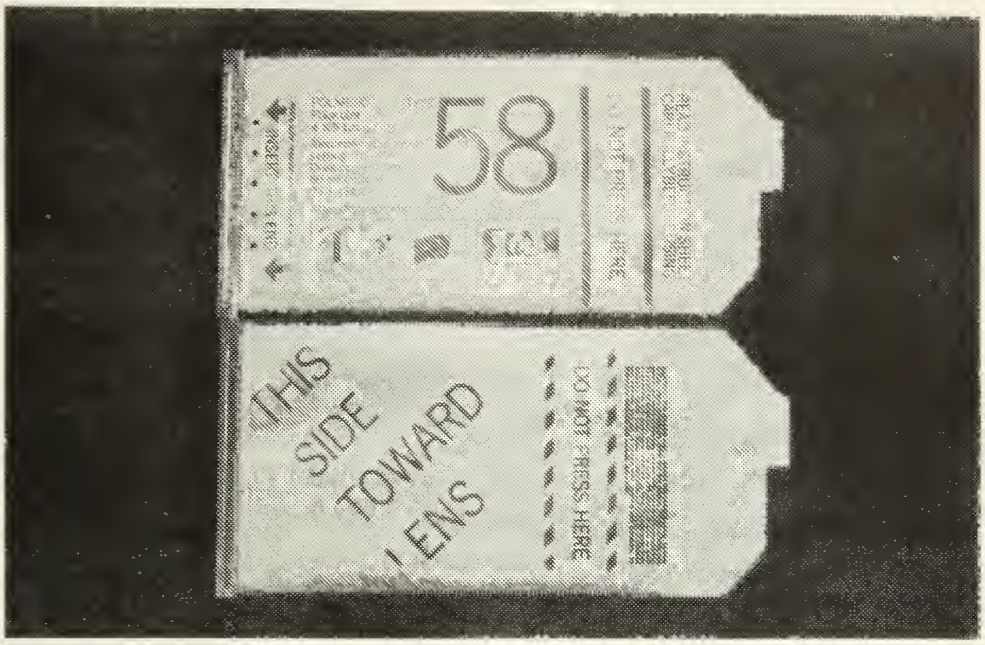

Figure 2
Polaroid Film Pack

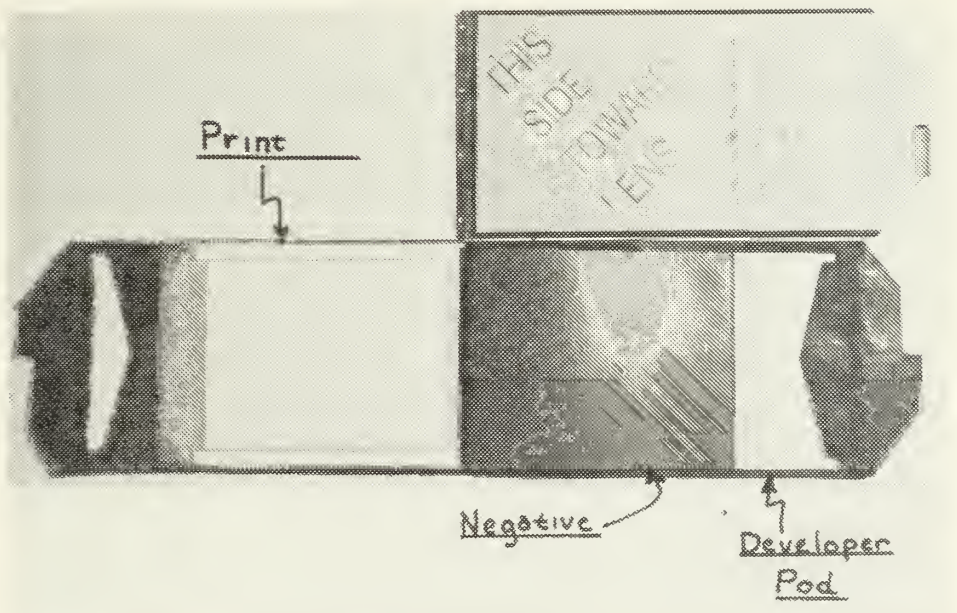

Figure 3
Exploded View

filters to allow only the desired wavelength ranges of blue and green light to reach the film. The sensitization setup is shown in Figure 4. Practical aspects and parameters of this step in the process are discussed below.

C. TEMPERATURE BIASING

The film is then placed in a closed styrofoam container (shown in Figure 5) at a position approximately one centimeter away from a layer of dry ice and allowed to cool to a selected temperature.

D. DEVELOPER ACTIVATION

When properly cooled the developers in the film are activated by passing the film pack through a Polaroid 4 x 5 Land film holder model 500 (figures 6 and 7). The holder has rollers which break a pod containing an alkaline activation chemical (shown in figure 3) and spread the activator between print and emulsion. The activator diffuses into the emulsion and activates the developer.

E. TRANSFER MODULATION

The film pack is then placed in an electromagnetic field. Here, current is induced in the emulsion causing localized heating proportional to the intensity of the electric field.[13] This heating then speeds the diffusion of the cyan dye molecules to the print substrate producing an image of cyan dye in the areas of greater field intensity.

---

[13]Keigo Iizuka, p. 3.

Figure 4
Film Sensitization Setup

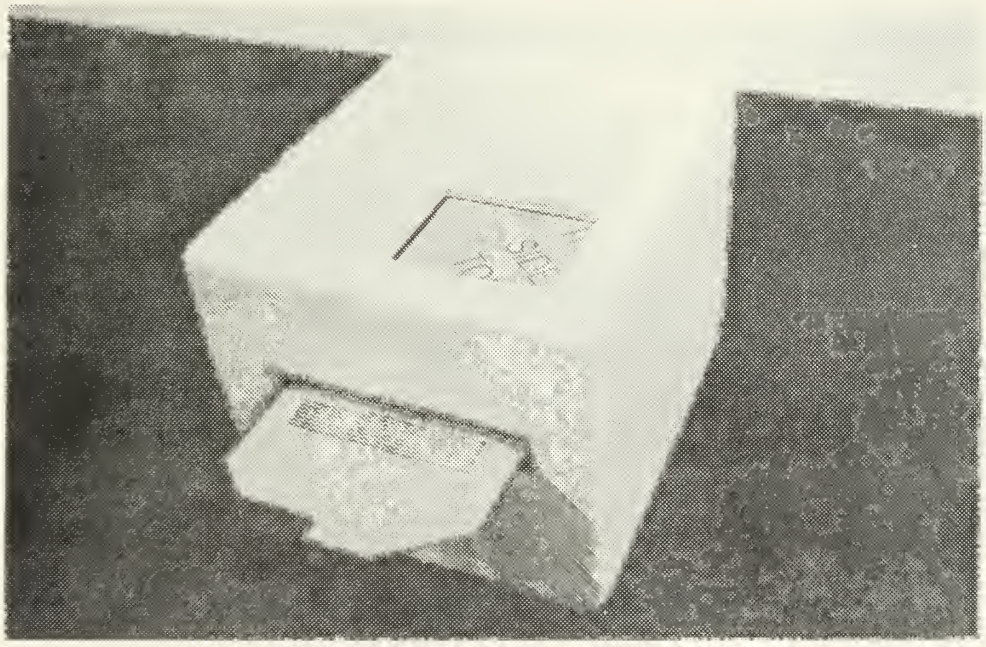

Figure 5
Film Cooling

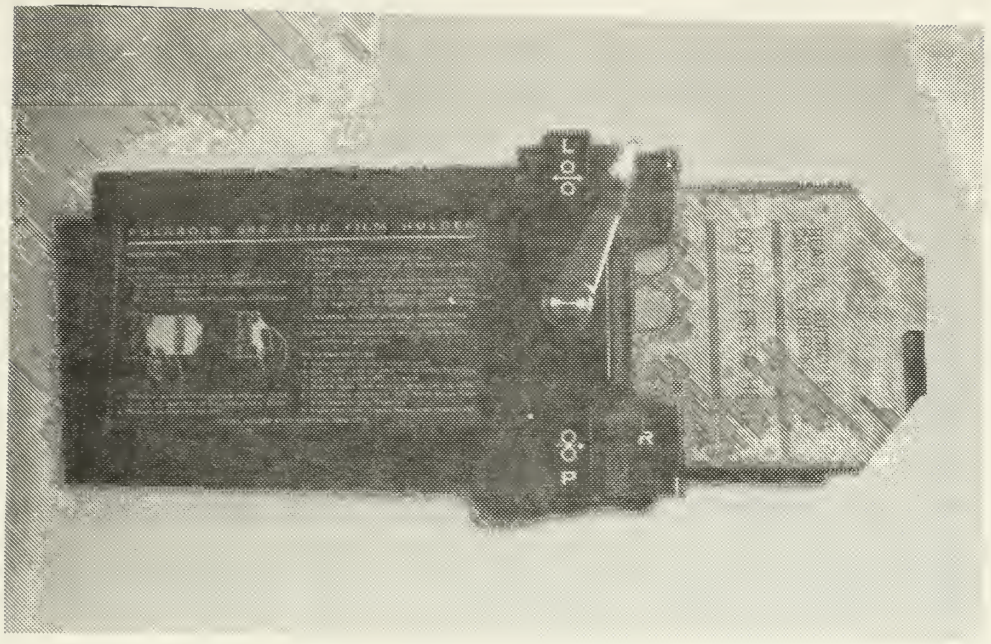

Figure 6
Polaroid Film Holder

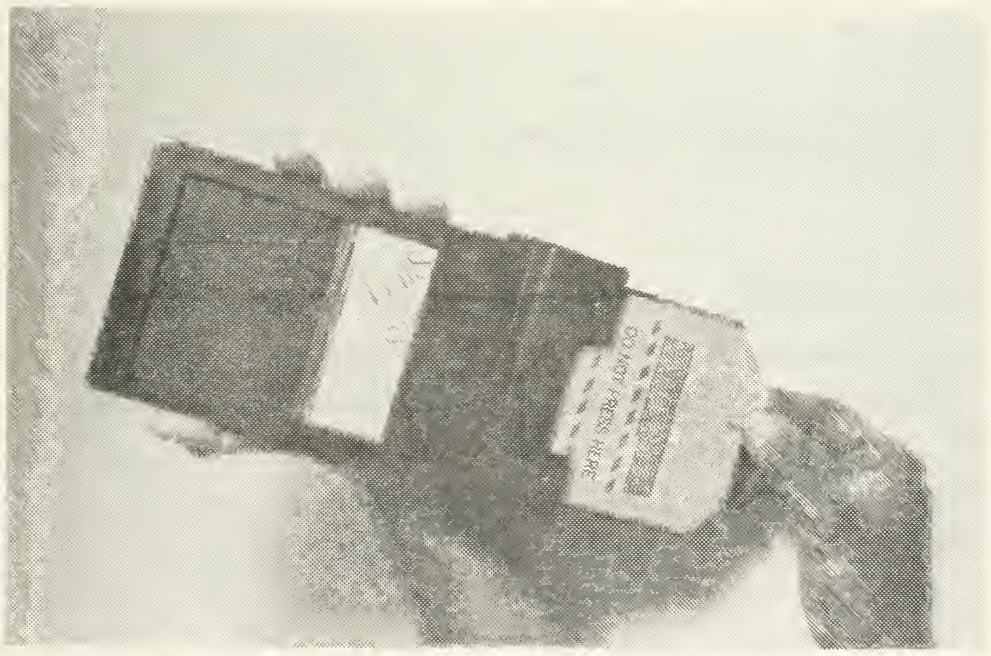

Figure 7
Film Activation

IV. PARAMETERS OF THE PROCESS

The thesis objective was to optimize the dynamic range of the process. The dynamic range is primarily determined by the film characteristics and by the various process parameters which affect those characteristics. This chapter identifies and qualitatively describes some of these parameters.

A. FILM DENSITY

A film characteristic of fundamental value here is the concept of photographic density (D). Density is a measure of the darkness of a film image. It is quantitatively defined in sensitometric terms.[14] In the Polacolor process, how dark the image gets depends on the amount of coloring matter transferred to the print. As described above, the film is subjected to a radiation field after the dye transfer process has been activated. Initially, the print surface is devoid of any color. As the film packet is warmed by the field and by the ambient temperature the dyes in the cyan layer (which has not been exposed to light) begin to transfer to the print by diffusion through the activator chemical which is between them. Obviously, if the transfer process is allowed to continue for a longer time more dye molecules can reach the print.

B. CONTRAST

When measured experimentally, density becomes a space-averaged value and does not provide any information on the relative distribution of light and dark material or of color in the print. Yet the resolution and clarity of the image are apparently highly dependent on both these factors. The quantity contrast provides a measure of the perceived distribution of light and dark regions in a print. It is essentially a subjectively determined quantity, although

---

[14]Appendix A p. 87.

methods exist to represent the contrast characteristic. The industry uses gamma (γ) where γ is the slope of the straight line portion of the characteristic density versus exposure ("D - Log H") curve.[15] Gamma represents the maximum amount of contrast for a given curve. The industry also uses Contrast Index (CI) as a measure of contrast.[16]

C. APPLIED ENERGY

An input parameter of prime significance is that of applied energy. As seen from photographic science, density is highly dependent on the applied energy.[17] Since energy is simply power times time in constant power situations,

$$E = P \cdot T$$

it is concluded that one may relate density to power being expended. The quantity generally used is the rate of energy flow per unit area, or power density, measured in watts per square centimeter. This quantity was found to be significantly dependent on the interaction of several contributory factors:

1. Power Source

The power applied to the DTM process depends most importantly on the sources available. Selection must be made among these on the basis of still more factors. In general the sources available were limited to approximately 300 mw/cm^2. This limitation is due primarily to the factor discussed next.

2. Source Frequency

The operating frequency is bounded below at approximately 1.5 gigahertz. This bound is set by the dimensions of the film and of the target structures whose

---

[15] See Appendix A, p. 87.

[16] Kodak publication #P-315 "KODAK Plates and Films for Scientific Photography", Eastman Kodak Company, 1973, p. 3.

[17] See Appendix A, p.87.

field characteristics are to be investigated. An upper limit is set by the ability to visually differentiate features in a pattern. A selection was possible among sources which have output frequencies between .2 - 10 gigahertz. Lower frequency devices can deliver larger power levels, but their radiating devices and target elements are generally larger than those of the higher frequency equipment, so that, with the available sources, the area to be irradiated varied directly with the power available, resulting in an essentially constant availability of power density. Consequently frequency selection was made only on the basis of the operating frequency bounds. The frequencies ultimately selected were approximately 1.5 and 8 gigahertz.

3. Source and Target Resonances

A second technologically related factor is that of resonance. The limitations on available power density required that experiments be conducted in the near fields of the radiating devices. This situation results in strong interaction of mutual impedances, severely complicating the task of matching the source impedance to its load. The time response of this near-field system has time constants as shown by equation V. C. 23 on page 60. The time constants in these experiments were sufficiently high in some cases to cause the impedances involved apparently to take on a time-varying aspect. That further complicated the task of maximizing the power delivered to the film.

4. Source Radiating Devices

The different radiating devices required for the various scurces result in different field distributions (and, consequently, differing power densities) being applied to the target elements. Ultimately two devices were selected which maximized power density available at the selected frequencies. A quarter-wavelength monopole over a ground plane with a corner reflector was used for the lower frequency work, while an open ended waveguide was used at the upper frequency.

5. Target Element Placement

A final power-related aspect is that of target element placement, which affects interaction among the various elements of the near field scenario and the consequent resultant load impedance presented to the source.

D. PHOTOGRAPHIC PARAMETERS

The photographic parameters are those which affect the print through mechanisms primarily related to photographic science.

1. Color Temperature of Light Source and Film Sensitivity

Appendix A provides an overview of quantitative photographic terms and concepts which shall be used in the discussion which is to follow. Figure 8 provides a representative[18] sensitivity plot for Polaroid type 58 film and indicates peak sensitivities to blue, green, and red light (of the yellow, magenta, and cyan layers respectively) of

Blue	350nm.
Green	350nm., 572nm.
Red	645nm.

It is particularly interesting to note that the green-sensitive layer has two sensitivity spectra, one which is a proportional mapping of the same spectrum to which the blue layer is reported to be sensitive. It is stressed that the dyes do not function completely independently:

> Although each dye absorbs in one principal spectral region..., it also has unwanted density in the other spectral regions. These unwanted densities desaturate and darken colors in a photograph, thus distorting color reproduction.[19]

This duality in spectral sensitivity, and the relatively large separation between the blue-green spectrum

---

[18]Polaroid Corporation letter received March 1974 and appended as Appendix B. Note the caveat that these curves are not to be considered as average or a product specification. Data confirmed as being equally applicable to type 58 as to type 108 by telephone conversation 21 June 1974 with Polaroid Corporation Technical Assistance Division representative Mr. Brooks Corl, who reported that the type 58 and 108 films use the same identical emulsion.

[19]SPSE Handbook..., p. 452-453.

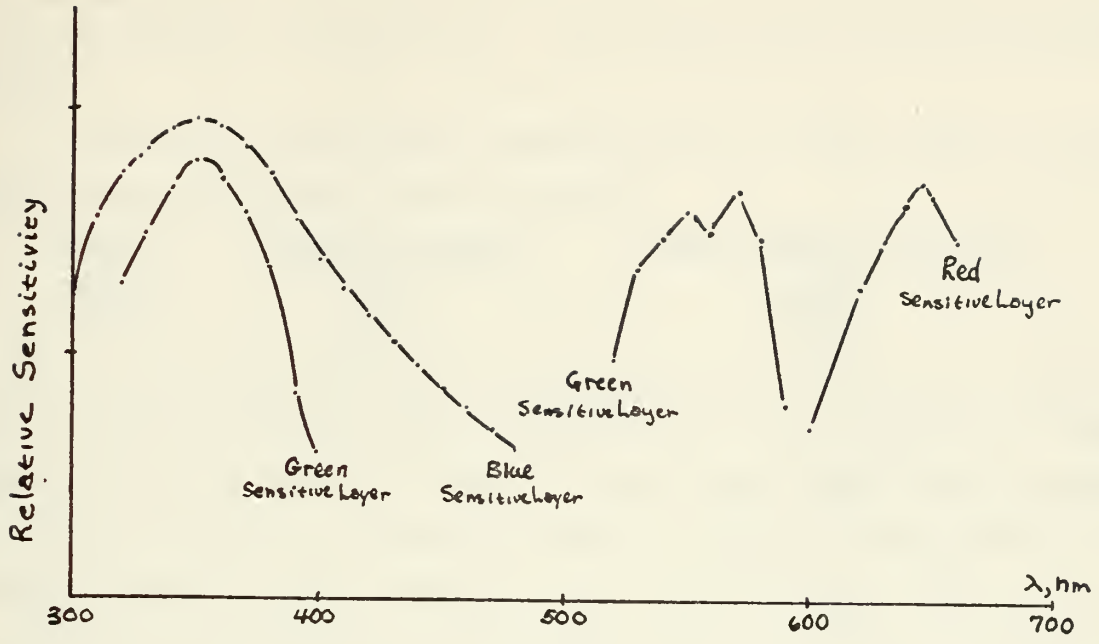

Figure 8
Sensitivity of Polaroid Type Film

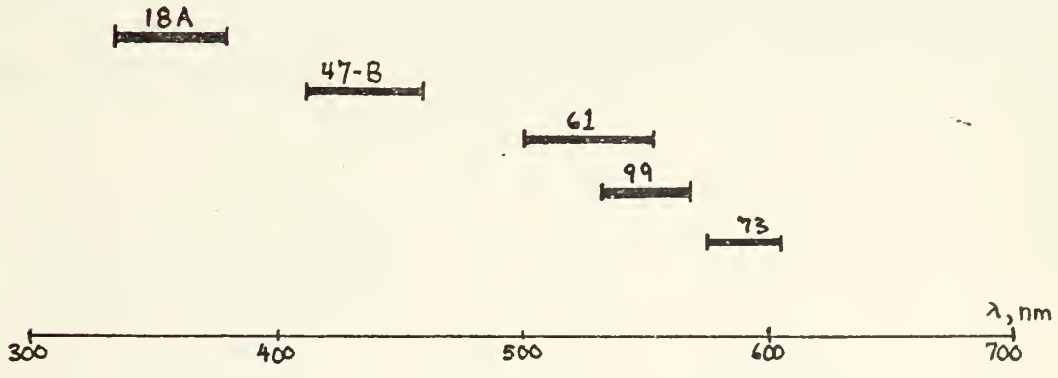

Figure 9
Passbands of Selected Wratten Filters

and the red-sensitive region tend to indicate use of the red-sensitive layer for the dye image, since the blue and green-sensitive layers should be able to be mordanted in the negative without excessively activating the red-sensitive layer.

The color temperature corresponding to the color to be used for sensitizing the film are[20]

Color	Wavelength(nm)	Color Temperature(°K)
Blue	350	8279
Green	350	8279
	572	5066

These colors are provided approximately by Wratten filters 18A (at 360 nm) and 99 (at 550 nm). See Figure 9. The use of filters such as these, whose pass-band half-widths are 45 and 35 nm., respectively,[21] minimizes the problem of trying to match color balance of the film as long as a constant intensity of sensitizing light is used. (Increased exposure at any particular wavelength gives less negative density.[22] Thus, sufficient increase in exposure may override the attenuation characteristic of the filter.)

If large variations in exposure are to be used, then the light source must be matched to the color temperature balance of the film using a color conversion filter with an appropriate Mired-Shift-Value (MSV).[23] Polaroid film is color balanced for 5500°K.[24] For use with 4800°K blue photoflood lamps a color conversion filter with an MSV of -26.5 is indicated, which corresponds approximately to a Wratten 78C (whose MSV is -24).[25]

---

[20]Appendix A, p. 88.

[21]SPSE Handbook..., p. 308-309.

[22]c.f. Appendix A, p. 87.

[23]Ibid., p. 92.

[24]Polaroid Corporation publication PX 850, December 1972, p. 1.

[25]SPSE Handbook..., p.315.

In summary, the cyan dye layer is indicated to be the most useful layer for the modulation process. The yellow and magenta layers should be mordanted in the negative by exposure of the film to blue light of 350nm. and green light of 572nm. approximately derived by exposing the film to a 4800°K light source first through a Wratten 18A blue filter, then a Wratten 99 green filter. If various exposure settings are anticipated the light source should be compensated to 5500°K by concurrent additional use of a Wratten 78C color conversion filter.

2. Choice of Color Exposure Times for Sensitization

The film negative has been described as comprising three basic dye layers. The pre-exposure of the film is seen to be a method of selectively mordanting dye layers in the negative to allow only the deepest (cyan-colored) layer to diffuse up to the print. It is not considered likely that in practice the two higher layers are completely mordanted. Rather, it is apparent that to some extent the yellow mixes with cyan to provide a green tone, while magenta mixes to provide blue. The relative proportions of these can be controlled by varying the amount of light each receives during pre-exposure. Increasing blue light results in less yellow being transferred. Increasing green light results in less magenta being transferred.

As a consequence, rather than a single D-log H curve, there are two density curves in this process; density versus blue exposure for selected values of green exposure, and density versus green exposure for selected blue exposure. It is possible to select values of blue and green pre-exposure which set an operating point on the three dimensional contour which provides the largest value of gamma.

These curves are found also to vary with respect to the initial temperature selected, as discussed below.

3. Developer Activation

The film packet must be pulled through the film holder at a rapid and uniform rate. Any hesitation while pulling the packet through the rollers results in uneven distribution of the dye-developer activator with a resultant ridging in the final image.

E. THERMAL PARAMETERS

1. Temperature Biasing

The film packet must be sufficiently cooled to ensure that the only modulation of diffusion and development which occurs is due to the localized heating by the incident energy field. If chilled excessively reactions cannot occur. Further cooling of the reagent pod will cause it to solidify and thus prevent activation of the developers. Conversely, if the packet is not sufficiently cooled the development and dye transfer processes will proceed at a rate too high to allow significant modulation by the incident field. The effect of these varying factors is seen primarily as a change in print density. It can be understood that if the film is cooled for different amounts of time or with different materials, its temperature, when initially inserted in the radiation field, shall be different. For a lower initial temperature a film should be expected to require more heating (longer radiation time or higher incident energy density) to acquire a particular density reading. It may be then concluded that the print density is dependent on initial temperature as well as on applied energy.

2. Cooling Procedure Parameters

Several aspects of the cooling technique were investigated, primarily as a means of calibrating the temperature of the film.

a. Choice of Coolant

Two methods were used to cool the film. Liquid nitrogen was used for very low temperature work (at

temperatures below -30°C), and dry ice was used for temperatures between -30° and 20° C.

b. Cooling Device Temperature Variations

These were found to be essentially exponential responses in time, and highly predictable.

c. Activator Chemical Freezing Point

This value was investigated in order to determine a lower bound on the temperature for pre-chilling the film.

F. DYNAMIC RANGE

For a given setting of other process parameters, the amount of density (D) appears to be proportional to the amount of energy (E) present in the fields being measured. Therefore one measure of dynamic range might be the range of energies over which noticeable changes in density occur. Referring to the D - log H curve[26] one can see that dynamic range can be measured by the range of energies over which there is a slope to the curve.

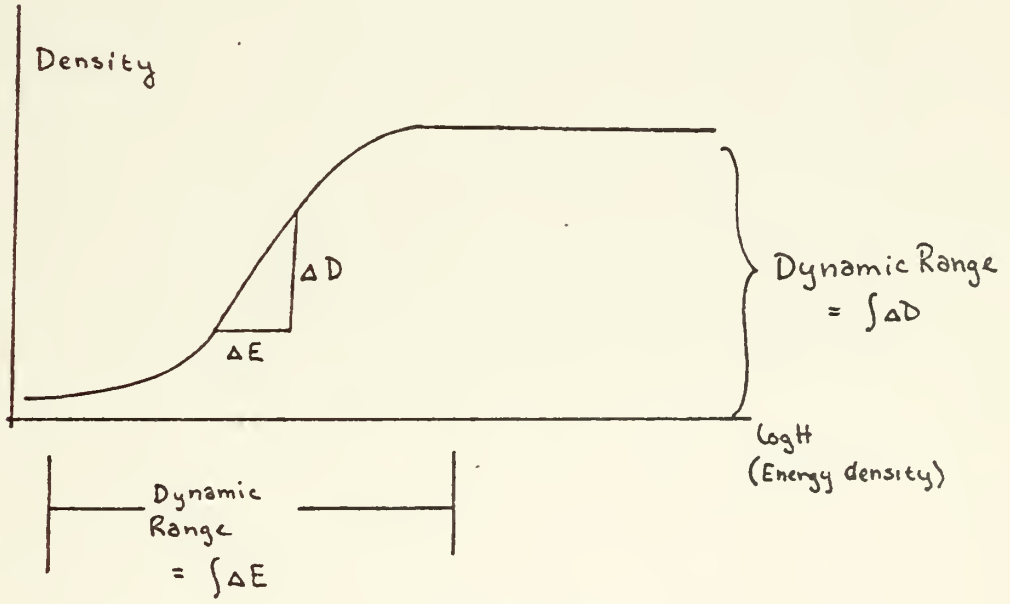

Figure 10
Typical D - Log H Curve

---

[26]Appendix A p. 87.

Alternatively, it can be seen that the dynamic range is also affected by the total amount of change in density. A large range of energies is of little use if there is only a slight change in the density over that range. Therefore it is concluded that the range of values over which the film density varies for different energy settings is also an important measure of the dynamic range of the process.

A performance measure of the dynamic range of the process, which takes into consideration ranges of density and energy, is a quantity defined as sigma (σ):

$$\sigma = \iint \delta D \, \delta E = \Delta D \cdot \Delta E$$

It is considered desirable to find the settings of other process parameters which result in an optimization of sigma over its range of values.

V. EXPERIMENTAL METHODS AND MODELS

Several characteristics and parameters affecting optimization of the process have been identified. The quantification of these factors was achieved through various experiments. The following is a description of those experiments and of the models used to develop them.

A. DETERMINATION OF FILM DENSITY

1. Film Density Standard

Film density was deemed a fundamental characteristic. An ability to measure it was considered essential for other experiments. Facilities were not available for direct density measurements in small areas of the film. Therefore a set of prints was developed as a comparison standard for selected combinations of blue and green sensitization. Other photographs could then be compared visually with the standards in order to determine density values in different regions.

The standards were developed as follows:

a. A particular ratio of blue and green sensitizing exposure was selected; e.g. 2:1.

b. Successive exposures were made of a uniform surface (white cardboard) with a constant light source (4800°K at 225 foot-candles.) Each exposure was made with the selected ratio but with increasing fractions of seconds of exposure for each color; e.g.: $\frac{1}{5}$sec. blue $\frac{1}{10}$sec. green; $\frac{2}{5}$sec. blue $\frac{1}{5}$sec. green; 1sec. blue $\frac{1}{2}$sec. green; etc.

c. Each exposure was developed at a uniform temperature (23° C) for 60 seconds.

d. A method was devised to provide the opacity (O) reading:

$$O = \frac{\text{Incident Intensity } (I_i)}{\text{Reflected Intensity } (I_{ref})}$$

from which the density (D) was computed

$$D = \log_{10}(O)$$

The method used fluorescent light on a white cardboard surface to reflect uniform light on the print. The light (I_i) incident on the print from the cardboard and the light (I_{ref}) reflected from the print were measured with a light meter[27] in foot-candles. Figure 11 shows the measurement method. Densities (D) were obtained for each exposure for three different values of I_i (38, 50, and 60 foot-candles). These values were then averaged to give a value of average density ($\bar{D}$).

e. A different ratio of blue and green was selected and the process repeated.

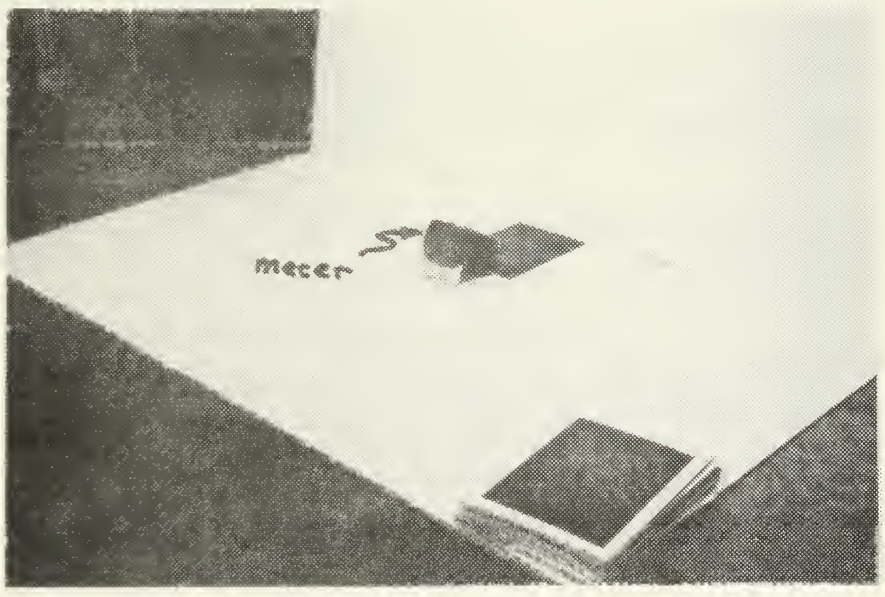

Figure 11
Density Measurement Method

2. Variation of Density with Preexposure Light Intensity and Color Balance

The combined effect of intensity and color balance on film density was obtained by plotting the various values of Density obtained above in a three dimensional display of D versus Log H for blue and green preexposure.

---

[27]General Electric Model 8DW58YI

B. DETERMINATION OF DYNAMIC RANGE

Another fundamental characteristic of the process to be measured was the Dynamic Range, the breadth of which is to be characterized by the quantity σ (sigma):

$$\sigma \stackrel{D}{=} \Delta D \Delta E$$

where ΔD is the range of print densities resulting from a range of applied energy ΔE. The value of this performance measure was to be found for various ratios of blue and green light sensitization, for different levels of total applied energy and for different settings of other process parameters. These quantities were measured as follows:

1. A particular ratio of blue to green sensitization exposure was selected.

2. The film was pre-chilled to a specified temperature, activated and placed at the open end of a waveguide. The power supply was turned on, irradiating the film for a specified interval of time during which power levels were recorded.

3. At the end of the radiation period the power supply was turned off and the print was separated from the negative to halt the transfer process.

4. If an image was visible in the region of the waveguide aperture then the power was reduced using a calibrated attenuator. The process was repeated until there was a just barely noticeable change in density. At that point the highest energy level Emax of the energy range was considered to have been reached.

5. The width of the image was measured between points at which an image was just barely visible. This width could be converted to a power difference with respect to the maximum power.[28] At that point it was considered that the lowest energy level Emin had been reached for the selected

---

[28] (see paragraph V C below).

ratio. Therefore a new ratio was selected and the experiment repeated.

6. When all desired ratios had been tested the recorded power levels were adjusted for factors such as reflections[29] to find the actual power delivered to the film. The quantity ΔE was then found to be the difference between the adjusted highest power level Emax' and the adjusted lowest power level Emin':

$$\Delta E = Emax' - Emin'$$

7. The prints at Emax' and Emin' were measured for density by comparison with the density standards. The difference in density at the two respective energy levels was taken to be ΔD.

C. DETERMINATION OF APPLIED ENERGY

Since the object of this work was to image applied fields, it was necessary to establish a means of measuring the power applied to the film by the selected sources. There are two aspects to this problem. One is measuring the power applied to the film placed at the end of the waveguide for dynamic range measurements. The other is measuring the power applied to the film placed in the field of an array of dipoles. In either case energy E is taken to be the product of time averaged power (P) and the radiation period (T).

$$E = P \cdot T$$

In both cases there were system time constants which resulted in a slow change in power delivered. These constants are considered to be due primarily to impedance characteristics of the film[30] since pains were taken to maintain the power supply frequency and power output constant. Because of these time constants the steady state power levels were taken as the values to be recorded. The

---

[29] Ibid.

[30] (see paragraph V. C. 3 below).

following derivations therefore assume steady state conditions.

The schematic of the power measurement setup is shown in Figure 12.

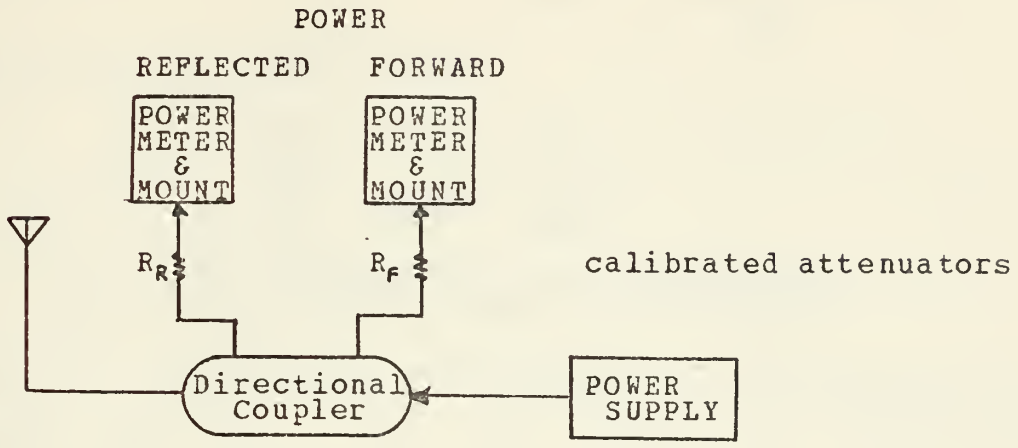

Figure 12
Power Measurement Setup

In both cases power was measured through directional couplers, thermistor mounts and power meters. The equipment used were:

Hewlett Packard:
Model 430C Power Meter
with
Model 477B Thermistor Mount

766D Directional coupler
Assorted calibrated attenuators

1. Determination Of Power Delivered by Waveguide

a. Field Equations

For a rectangular waveguide (Figure 13) driven by a sinusoidal source of such a frequency (ω) as to induce TE_{10} mode operation above cutoff, the solution to the waveguide equations gives the following expressions for the X, Y, and Z components of the electric ($\vec{E}$) and magnetic ($\vec{H}$) fields:[31]

---

[31]Jordan, E.C. and Balmain, K.G., Electromagnetic Waves and Radiating Systems, 2nd Ed, Prentice-Hall, 1968, p. 250.

$$\vec{E}x = 0 \qquad \vec{H}x = \frac{\gamma\pi}{aK_c^2}\tilde{H}_0 \sin\frac{\pi x}{a}\, e^{j\omega t}\,\hat{x}$$

$$\vec{E}y = -j\,\frac{\omega\mu\pi}{aK_c^2}\tilde{H}_0 \sin\frac{\pi x}{a}\, e^{j\omega t}\,\hat{y} \qquad \vec{H}y = 0$$

$$\vec{E}z = 0 \qquad \vec{H}z = \tilde{H}_0 \cos\frac{\pi x}{a}\, e^{j\omega t}\,\hat{z}$$

where for TE_{10} mode above cutoff

$$K_c^2 = \left(\frac{\pi}{a}\right)^2 = \gamma^2 + \omega^2\mu\varepsilon$$

$$\gamma = j\bar{\beta} = j\sqrt{\omega^2\mu\varepsilon - \left(\frac{\pi}{a}\right)^2}$$

a = the X dimension of the waveguide
$\tilde{H}_0$ = an arbitrary complex constant $|H_0|e^{j\phi}$

μ and ε are respectively the permeability and permittivity constants, and $\hat{x}$, $\hat{y}$, $\hat{z}$ are unit vectors in rectangular coordinates. When expressed in phasor form these simplify to

$$\vec{E}x = 0 \qquad \vec{H}x = j\,\frac{\bar{\beta}a}{\pi}|H_0| \sin\left(\frac{\pi x}{a}\right)\hat{x}$$

$$\vec{E}y = -j\,\frac{\omega\mu a}{\pi}|H_0| \sin\left(\frac{\pi x}{a}\right)\hat{y} \qquad \vec{H}y = 0 \qquad \text{(V. C. 1)}$$

$$\vec{E}z = 0 \qquad \vec{H}z = |H_0| \cos\left(\frac{\pi x}{a}\right)\hat{z}$$

b. Time Averaged Power Density

The time averaged power density is known to be[32] a vector quantity

$$P = \frac{1}{2}\,\mathrm{Re}\,\{\vec{E} \times \vec{H}^*\} \qquad \text{(V. C. 2)}$$

When the cross product $\vec{E} \times \vec{H}^*$ is taken, the real component is simply $E_y H_x^* \hat{z}$ so that time averaged power flow $(\vec{P}(x))$ in watts per square meter is

$$\vec{P}(x) = \frac{1}{2}(E_y H_x^*)\,\hat{z}$$

$$= \frac{\bar{\beta}\omega\mu a^2}{2\pi^2}|H_0|^2 \sin^2\left(\frac{\pi x}{a}\right)\hat{z} \qquad \text{(V. C. 3)}$$

Figure 13 shows this distribution as seen across the face of the waveguide. It shows a flow of power down the waveguide in the z direction, uniformly distributed in the y-direction but tapering off sinusoidally as it moves away from the

---

[32] Ibid., p. 171.

center in the x-direction. Figure 14 is a photograph of the waveguide cross section showing that distribution in fact.

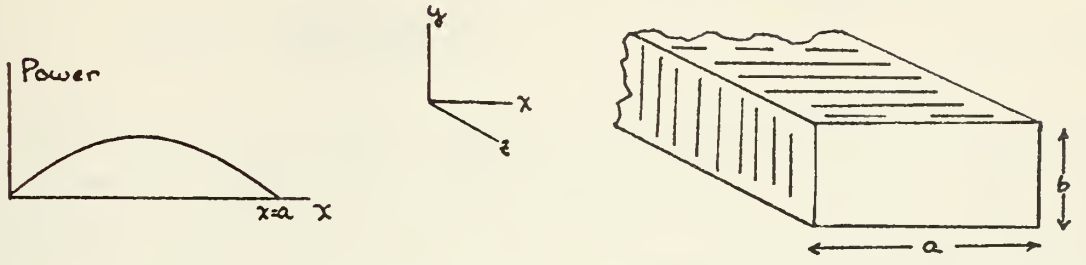

Figure 13 Waveguide Dimensions and Power Distribution

Figure 14
Photograph of Power Distribution across Face of Waveguide

Clearly, there is in fact a power distribution across the waveguide. The problem is how to relate those levels to the levels measured at the entry port of the waveguide. It is considered that the following discussion supplies that relation.

c. Total Power at Waveguide End

The expression for $\vec{P}(x)$ in (V. C. 3) above gives the spatial distribution of power as a time average. The integral of that expression over the face of the waveguide gives the total time average power in watts delivered to the open end of the waveguide ($\bar{P}(o)$):

$$\bar{P}(o) = P_{\substack{\text{total} \\ \text{avg}}} = \int_o^b \int_o^a |\vec{P}(x)| dx dy$$

$$= \int_o^a K \sin^2\left(\frac{\pi}{a}x\right) dx \qquad K = \frac{\bar{\beta}\omega\mu a^2 |H_o|^2 b}{2\pi^2}$$

$$\bar{P}(o) = \frac{\bar{\beta}\omega\mu a^3 |H_o|^2 b}{4\pi^2} \qquad \text{(V. C. 4)}$$

If the power measurement system were lossless and there were no reflected power, the power measured as going down the waveguide (P(s)) would be the value $\bar{P}(o)$. By comparison with P in (V. C. 3), it is seen that the power being delivered at the center of the waveguide (P peak) is:

$$\vec{P}(x) \text{ peak} = \frac{2}{ab} \bar{P}(o) \hat{z} \qquad \text{(V. C. 5)}$$

The relationship now to be investigated is that between the total power going down the waveguide, measured at the power measurement system, $\bar{P}(s)$, to the total power being delivered at the open end of the waveguide, $\bar{P}(o)$.

d. Relation between Total Average Power at Waveguide Source and Load

Because of reflections from the load there are standing wave patterns in the waveguide. It is known that the current and voltage standing wave patterns are periodic with a period of half the waveguide wavelengths and are shifted with respect to each other by a quarter wavelength. Figure 15 shows the patterns for an open ended transmission line.[33] Since the power delivered is a product of voltage and current, it would be expected that there be regions of maximum and minimum power availability. In a real system, if there is no load present to accept that power, then currents shall flow on the outer surface of the waveguide, and the power shall be expended in the losses of the waveguide.

---

[33] Ibid., pp. 219 - 220.

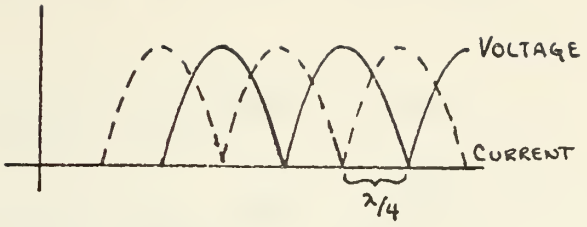

Figure 15

The presence of these power standing waves can be shown analytically:

Defining the voltage reflection coefficient to be the ratio of reflected to forward electric fields

$$\Gamma \stackrel{D}{=} \frac{E_R}{E_F} = \frac{V_R}{V_F}$$

and the origin of the z-axis to be at the film end of the waveguide as shown in Figure 16:

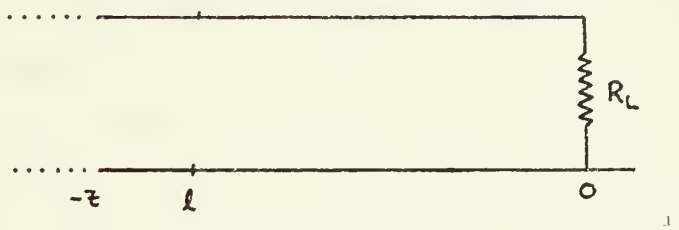

Figure 16
Wave guide Transmission Line Coordinates

At a point $z = -\ell$ the incident electric field $\vec{V}_F$ is:

$$\vec{V}_F = V_0 e^{-j\beta(-\ell)} = V_0 e^{j\beta\ell}$$

where V_0 is the peak value (in time and space) of the incident electric field. The reflected field $\vec{V}_R$ is

$$\vec{V}_R = [V_R] e^{-j\beta\ell} = \Gamma V_0 e^{-j\beta\ell}$$

and the total electric field at point $z = -\ell$ is

$$\vec{V}_F + \vec{V}_R = V_0 (e^{j\beta\ell} + \Gamma e^{-j\beta\ell})$$

or generally

$$V(z) = V_0 (e^{-j\beta z} + \Gamma e^{+j\beta z})$$

$$I(z) = \frac{V_0}{Z_0} (e^{-j\beta z} - \Gamma e^{j\beta z}) \qquad \text{(V. C. 6)}$$

the time average power density at any point z then is

$$\bar{P}(z) = \frac{1}{2} \operatorname{Re} \{V(z) \cdot I(z)\}$$

$$= \frac{1}{2} \operatorname{Re}\left\{\frac{V_0^2}{Z_0}\left[1 + \Gamma e^{j2\beta z} - \Gamma^* e^{-j2\beta z} - \Gamma\Gamma^*\right] e^{-j\phi}\right\} \qquad \text{(V. C. 7)}$$

where we indicate the complex conjugate of a function A by A^* and take

$$V(z,t) = V(z) \cos\omega t$$
$$I(z,t) = I(z) \cos(\omega t + \phi)$$

V_0 is a real number, the peak value of incident electric field, ϕ is a time-phase difference between electric and magnetic field peaks.

At the source, where the power measurement setup is located, the power measured must be $\bar{P}(z)$ evaluated at $z = -\ell$, which must also be the power being measured at the source after corrections are made for losses in the measurement system. That is, $\bar{P}(s)$ is the resultant of incident and reflected power

$$\bar{P}(s) = \bar{P}_F - \bar{P}_R$$

$$= \frac{1}{2} \operatorname{Re}\left\{\frac{V_0^2}{Z_0}\left[1 + (\Gamma e^{-j2\beta\ell} - \Gamma^* e^{j2\beta\ell}) - \Gamma\Gamma^*\right] e^{-j\phi}\right\}$$

We can relate $\bar{P}(s)$ to $\bar{P}(o)$ by noting that by (V. C. 7), for $z=0$

$$\bar{P}(o) = \frac{1}{2} \operatorname{Re}\left\{\frac{V_0^2}{Z_0} (1 + \Gamma - \Gamma^* - \Gamma\Gamma^*) e^{-j\phi}\right\}$$

so that

$$\frac{\bar{P}(o)}{\bar{P}(s)} = f(\Gamma)$$

$$\bar{P}(o) = f(\Gamma)\bar{P}(s)$$

$$\bar{P}(o) = Re\left\{\frac{1 + (\Gamma - \Gamma^*) - \Gamma\Gamma^*}{1 + e^{-j2\beta\ell} - \Gamma^* e^{j2\beta\ell} - \Gamma\Gamma^*}\right\} \cdot \bar{P}(s) \qquad \text{(V. C. 8)}$$

e. Relation between Total Power at Source and Power Measured by Meters

The final step in finding the value of power being delivered is to relate $\bar{P}(s)$ to the power levels read at the meters. The losses in the power meters and thermistor mounts are provided by the manufacturer as a parameter called the calibration factor (CF), which compares meter reading (P_M) to the power incident on the thermistor mount (P_I)

$$CF = \frac{P_M}{P_I}$$

For the general case in which there is both forward (P_F) and reflected (P_R) power being read,

$$\bar{P} = P_F - P_R$$

$$= \frac{P_{MF}}{CF_F} - \frac{P_{MR}}{CF_R}$$

where P_{MF}, P_{MR} are the forward and reflected power meter reading and CF_F, CF_R are their respective calibration factors.

In these experiments the power levels were such that in-line attenuators R_F and R_R were required. Thus,

$$\bar{P}(s) = \left[\frac{P_{MF}}{CF_F} + R_F\right] - \left[\frac{P_{MR}}{CF_R} + R_R\right] \qquad \text{(V. C. 9)}$$

f. Summary

In summary, beginning with assumptions of TE_{10} mode operation above cutoff the spatial distribution of average power across the waveguide ($\vec{P}(x)$) was found. Next the spatial total average power at the load ($\bar{P}(o)$) was developed. That value was then related to the average power

applied at the source ($\bar{P}(s)$). Finally, the relationship between the source power $\bar{P}(s)$ and the incident and reflected power meter readings (P_{MF}, P_{MR}) was established. Thus the equations used to relate meter readings to peak spatial average power $\vec{P}(x)$ evaluated at $x = \frac{a}{2}$ were:

$$\vec{P}(x)\,\text{peak} = \frac{2}{ab}\,\bar{P}(o)\,\hat{z} \qquad \text{(V. C. 5)}$$

$$\bar{P}(o) = \text{Re}\left[\frac{1 + \Gamma - \Gamma^* - \Gamma\Gamma^*}{1 + \Gamma e^{-j2\beta\ell} - \Gamma^* e^{j2\beta\ell} - \Gamma\Gamma^*}\right] \cdot \bar{P}(s) \qquad \text{(V. C. 8)}$$

$$\begin{aligned}\bar{P}(s) &= P_F - P_R \\ &= \left[\frac{P_{MF}}{C\bar{F}_F} + R_F\right] - \left[\frac{P_{MR}}{C\bar{F}_R} + R_R\right]\end{aligned} \qquad \text{(V. C. 9)}$$

where

a = x-dimension of waveguide

Γ = voltage reflection coefficient

ℓ = length of waveguide from lead to power measurement setup

P_M = power meter reading

CF = thermistor mount calibration factor

R = in-line calibrated attenuators

These formulas were used to measure the power delivered to the center of the end of the waveguide.

2. Determination of Power Delivered by a Reflector System

A driven monopole and 60° corner reflector over a ground plane were used to produce the field for some of the experiments. The use of a conducting reflector permitted application of image and array theory to determine the field in the vicinity of the system. Such a determination was considered necessary in order to select the placement of the reflector and of the target element which would optimize the field at the target element. The geometry of the system is shown in Figure 17.

The field reflected by a perfectly conducting ground plane and corner reflector can be considered to be produced by five image elements arranged in a hexagonal

pattern.[34] Phasor addition of the individual fields from all six elements then gives an approximation of the resultant field. Because of the different element-to-target distances involved, there are phase and magnitude differences which may vary significantly along the axis of symmetry. The following development explores these possibilities.

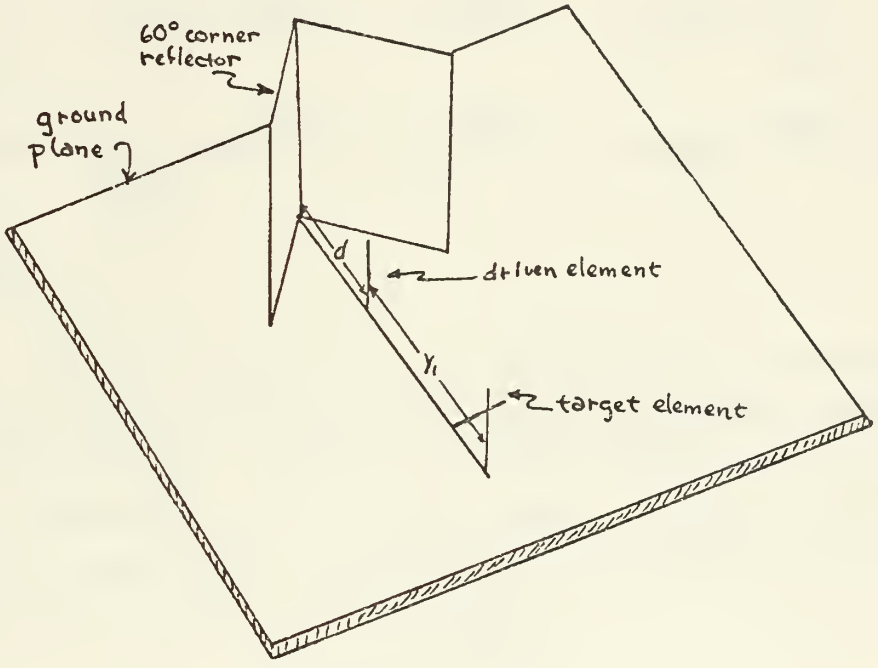

Figure 17a
Perspective View of Reflector System

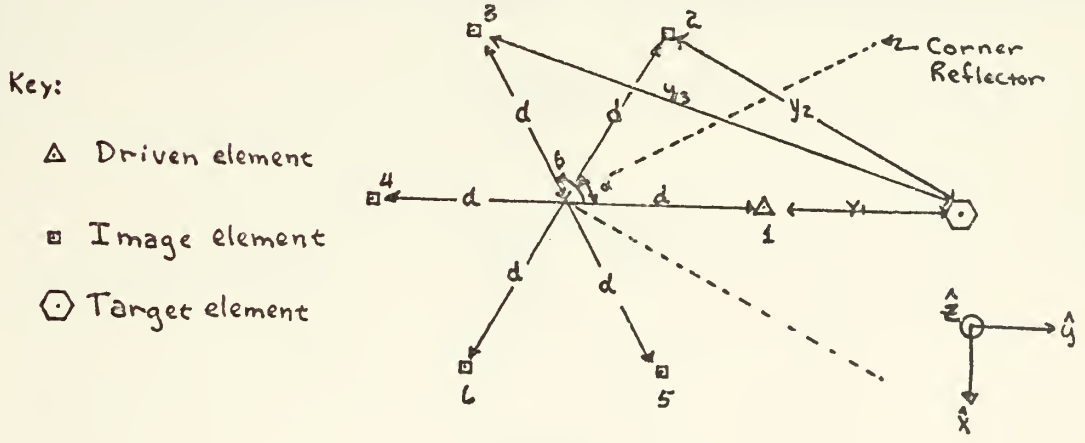

Figure 17b
Dimensions of Reflector-Image System

---

[34]Kraus, p. 330.

a. Fields of a Single Dipole

The near field of a single dipole has been derived[35] giving the following expressions for the electric and magnetic field components of a quarterwave monopole over a conductive ground plane. The subscript m shall be used to indicate that the mth element is being considered.

$$\vec{E_{z_m}} = E_{z_m}' \hat{z} = -jE_{z_0}' \left(\frac{e^{-j\beta R_{1m}}}{R_{1m}} + \frac{e^{-j\beta R_{2m}}}{R_{2m}} - 2\cos\beta H \frac{e^{-j\beta r_m}}{r_m} \right) \qquad \text{(V. C. 10)}$$

$$\vec{H_{\phi_m}} = H_{\phi_m}' \hat{\phi} = \frac{jE_{z_0}'}{\eta y_m} \left(e^{-j\beta R_{1m}} + e^{-j\beta R_{2m}} - 2\cos\beta H e^{-j\beta r_m} \right)$$

$$E_{z_0}' = 30 I_m'$$

where I_m' is the element source current, H is the monopole length (dipole half-length), β is the propagation constant, η is 377 ohms, $\hat{z}$ and $\hat{\phi}$ are unit vectors in their respective directions, and the R_{im}, r_m, and y_m are defined for the mth element of Figure 17b by the geometry of Figure 18. From that figure it is seen that

$$r_m = \sqrt{y_m^2 + z^2}$$

These variables can be reduced to multiples of a wavelength (λ) by defining

$$\begin{aligned} r_m &\triangleq \rho_m \lambda \\ H &\triangleq h\lambda \\ R_{im} &\triangleq r_{im}\lambda \\ z &\triangleq s\lambda \\ y_m &\triangleq K_m \lambda \\ d &\triangleq c\lambda \end{aligned} \qquad \text{(V. C. 11)}$$

---

[35] Jordan and Balmain, p. 336.

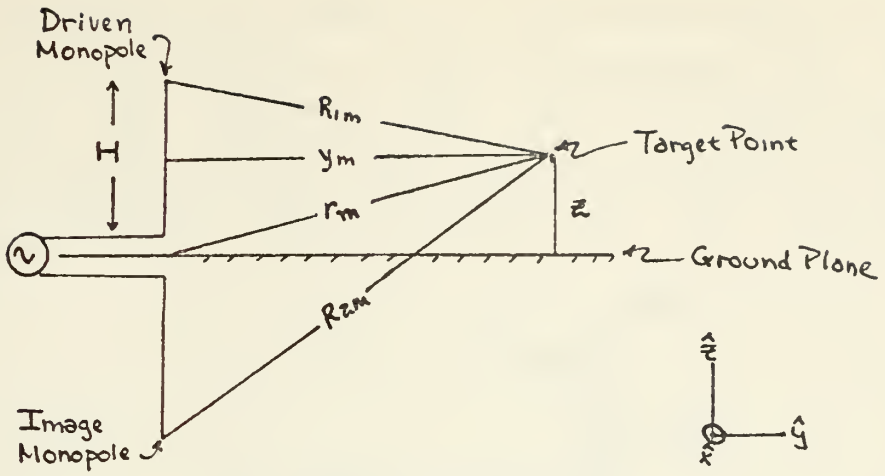

Figure 18
Geometry of a Monopole over a Perfectly Conducting Ground Plane

Substituting (V. C. 11) in (V. C. 10) results in

$$E'_{zm} = -jE_{z0}\left[\left\{\frac{\cos\theta_{1m}}{r_{1m}} + \frac{\cos\theta_{2m}}{r_{2m}} - \frac{2\cos\theta_3\cos\theta_{4m}}{\rho_m}\right\}\right.$$
$$\left. -j\left\{\frac{\sin\theta_{1m}}{r_{1m}} + \frac{\sin\theta_{2m}}{r_{2m}} - \frac{2\cos\theta_3\sin\theta_{4m}}{\rho_m}\right\}\right]$$

where

$$\theta_{1m} = 2\pi r_{1m}$$
$$\theta_{2m} = 2\pi r_{2m}$$
$$\theta_3 = 2\pi h$$
$$\theta_{4m} = 2\pi\rho_m$$
$$E_{z_0} = \frac{E'_{z_0}}{\lambda}$$

Separating E'_{z_m} into its real and imaginary parts yields

$$E'_{zm} = \mathrm{Re}\{E'_{zm}\} + j\mathrm{Im}\{E'_{zm}\}$$

$$\mathrm{Re}\{E'_{zm}\} = -E_{z_0}\left[\frac{\sin\theta_{1m}}{r_{1m}} + \frac{\sin\theta_{2m}}{r_{2m}} - \frac{2\cos\theta_3\sin\theta_{4m}}{\rho_m}\right] \qquad \text{(V. C. 12a)}$$

$$\mathrm{Im}\{E'_{zm}\} = -E_{z_0}\left[\frac{\cos\theta_{1m}}{r_{1m}} + \frac{\cos\theta_{2m}}{r_{2m}} - \frac{2\cos\theta_3\cos\theta_{4m}}{\rho_m}\right]$$

A similar operation on H_m results in

$$\mathrm{Re}\{H'_{\phi m}\} = \frac{E_{z0}}{\eta K_m}(\sin\theta_{1m} + \sin\theta_{2m} - 2\cos\theta_3\sin\theta_{4m}) \qquad \text{(V. C. 12b)}$$

$$\mathrm{Im}\{H'_{\phi m}\} = \frac{E_{z0}}{\eta K_m}(\cos\theta_{1m} + \cos\theta_{2m} - 2\cos\theta_3\cos\theta_{4m})$$

From the geometry of Figure 17b it is clear that all the $\vec{H}_{\phi m}$ shall not be aligned, so that the magnetic field resulting from all six elements shall have two components, one parallel ($\vec{H}y$) and one normal ($\vec{H}x$) to the axis of symmetry. These components are determined by the geometry of Figure 19.

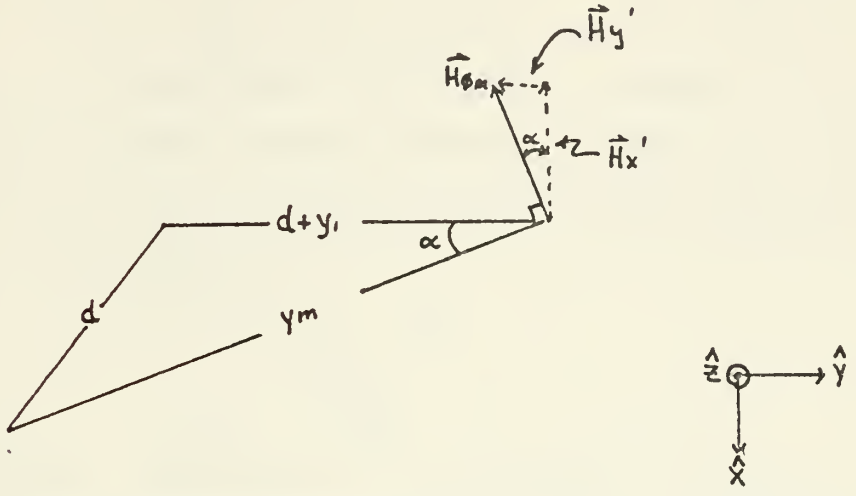

Figure 19
Normal and Parallel Components of the mth Magnetic Field

From that figure and the law of cosines, the included angle (α) is

$$\alpha = \cos^{-1} \frac{y_1^2 + y_m^2 + 2dy_1}{2(d + y_1)y_m}$$

$$= \cos^{-1} \frac{K_2^2 + K_m^2 + 2CK_1}{2(C + K_1)K_m}$$

so that $\vec{H}_{\phi m}'$ can be broken into its components,

$$\vec{H}_{\phi m}' = -[H_{xm}' \, x + H_{ym}' \, \hat{y}]$$
$$H_{xm}' = H_{\phi m}' \cos\alpha$$
$$H_{ym}' = H_{\phi m}' \sin\alpha$$

Examination of the geometry of Figures 17b and 19 shall reveal that the $\vec{H}y$ components of elements 2 and 3 cancel the $\vec{H}y$ components of elements 6 and 5 respectively.

b. Effects of Reflection

The development to this point assumes a perfectly conducting ground plane and corner reflector with perfect connection to the ground plane. In such a case the

reflection coefficient is -1. The (tangential) electric field is reversed upon reflection. The tangential magnetic field component is unchanged, while the normal magnetic field component changes sign. The net effect is that of the source current in the image element being 180 degrees out of phase with that of the driven element.[36] If, however, the reflector is not in perfect contact with the ground plane the reflection coefficient (Γ) becomes complex. In such a case the image source current suffers a phase lag as well as attenuation, and the reflected electric field (E_{zm}) is the product of the reflection coefficient and the incident field (E_{zm}') for each reflection:

$$\tilde{\Gamma} = |\tilde{\Gamma}| e^{j\phi_r}$$

$$E_{z_m} = \tilde{\Gamma} E_{z_m}'$$

For multiple reflections the resultant electric field arriving at the target element is the original source field multiplied by the appropriate power of the reflection coefficient

$$E_{zm} = \tilde{\Gamma}_m E_{zm}'$$

$$\tilde{\Gamma}_m = 1 \text{ for } m = 1 \qquad \text{(V. C. 13a)}$$

$$\tilde{\Gamma}_m = \Gamma \text{ for } m = 2,4,6$$

$$\tilde{\Gamma}_m = (\tilde{\Gamma}_m)^2 \text{ for } m = 3,5$$

and

$$\vec{H_{\phi m}} = \tilde{\Gamma}_m \vec{H_{\phi m}} = \Gamma_m (H_{xm}' \hat{x} + H_{ym}' \hat{y})$$

and (V. C. 13b)

$$H_{xm} = \tilde{\Gamma}_m H_{xm}'$$

c. Summation of Component Fields

For the array of real and imaged dipoles shown in Figure 17b at a point $y_i = K_i \lambda$ along the axis of symmetry from the driven element the total fields are found by phasor addition of the contributions from each element, taking into

---

[36]Jordan and Balmain, p. 470 - 471.

consideration the phase and angular variations of the electric and magnetic fields described above:

$$\vec{E}_{zt} = E_{zt}\,\hat{z} \qquad \text{(V. C. 14a)}$$

where

$$E_{zt} = \mathrm{Re}\{E_{zt}\} + j\mathrm{Im}\{E_{zt}\}$$

$$\mathrm{Re}\{E_{zt}\} = \sum_{m=1}^{6} (\mathrm{Re}\{E_{zm}\})$$

$$\mathrm{Im}\{E_{zt}\} = \sum_{m=1}^{6} (\mathrm{Im}\{E_{zm}\})$$

Also,

$$\vec{H}_{\phi t} = - H_{xt}\,\hat{x} \qquad \text{(V. C. 14b)}$$

where

$$H_{xt} = \sum_{m=1}^{6} H_{xm} = \sum_{m=1}^{6} \mathrm{Re}\{H_{xm}\} + j \sum_{m=1}^{6} \mathrm{Im}\{H_{xm}\}$$

and the mth contributions to these sums are described by equations (V. C. 12) and (V. C. 13).

d. Total Time Averaged Power Density

The total time averaged power density $\vec{P}_t$ impinging on that point y_1 is then found by applying equation (V. C. 2) to these total fields:

$$P_{av} = \frac{1}{2} \mathrm{Re}\{\vec{P}_t\}$$

where

$$\vec{P}_t \triangleq \vec{E}_{zt} \times H^*_{\phi t}$$

That cross product is found from

$$(\vec{E}_{zt} \times H^*_{\phi t}) = \det \begin{bmatrix} x & y & z \\ Ex & Ey & Ez \\ -Hx^* & 0 & 0 \end{bmatrix}$$

$$= \vec{P}_t = P_{yt}\,\hat{y} + P_{zt}\,\hat{z} \qquad \text{(VI. C. 15)}$$

so that

$$P_{yt} = -EzHx^*$$

$$P_{zt} = EyHx^*$$

From the geometry of Figure 18 R_{im} can be found in terms of z and the various y_m, hence r_{im} in terms of s and Km:

$$r_{1m}^2 = \left(\frac{R_{1m}}{\lambda}\right)^2 = (Km^2 + s^2 + h^2) - 2hs$$

$$r_{2m}^2 = \left(\frac{R_{2m}}{\lambda}\right)^2 = (Km^2 + s^2 + h^2) + 2hs \qquad \text{(V. C. 16)}$$

To find the K_m we use the geometry of Figure 17b and the law of cosines, where the angles α and β are seen to be sixty and 120 degrees respectively:

$$y_2^2 = (d + y_1)^2 + d^2 - 2(d + y_1) \cdot d \cdot \cos 60^\circ$$

$$y_3^2 = (d + y_1)^2 + d^2 - 2(d + y_1) \cdot d \cdot \cos 120^\circ$$

When simplified these give

$$y_2^2 = d^2 + y_1 d + y_1^2$$

$$y_3^2 = 3d^2 + 3y_1 d + y_1^2 \qquad \text{(V. C. 17)}$$

Taking

$$\begin{aligned} y_1 &= K_1 \lambda \\ y_2 &= K_2 \lambda \\ y_3 &= K_3 \lambda \\ y_4 &= K_4 \lambda \\ y_5 &= K_5 \lambda \\ y_6 &= K_6 \lambda \\ d &= C \lambda \end{aligned} \qquad \text{(V. C. 18)}$$

results in

$$K_2^2 = C^2 + CK_1 + K_1^2$$

$$K_3^2 = 3C^2 + 3CK_1 + K_1^2 \qquad \text{(V. C. 19)}$$

By symmetry, then

$$\begin{aligned} K_4 &= 2C + K_1 \\ K_5 &= K_3 \\ K_6 &= K_2 \end{aligned} \qquad \text{(V. C. 20)}$$

Then, using equations (V. C. 19) and (V. C. 20) with

equations (V. C. 14) the total power present at a point $y_i = K_i\lambda$ along the axis of symmetry can be found by summing the contributions from all six elements.

e. Measurement of Power

The instrumentation of Figure 12 was used to monitor the power being fed to the driven element of the system. Additionally a probe was used to measure the field along the axis of symmetry. The probe, shown in Figure 28, sampled the radial component of power flow. The sample was then measured with a thermistor and power meter arrangement such as that described on page 37 above. Since the probe is aligned vertically, it is considered that it only sampled the radial component of power flow. In order to compare experimental results with the expectations of equation (V. C. 15), the resultant value of P_{yt} was first integrated numerically using Simpson's rule over the range in wavelengths, which corresponded to the length of the probe:

$$P_{tt} = \int_0^{.05\lambda} \overline{Pr}\, ds = \int_0^{.05\lambda} Px\, ds + \int_0^{.05\lambda} Py\, ds$$

A listing of the program written to carry out the indicated summations, products, and numerical integration is contained in Appendix C. It was found that fluctuations occured in the power being delivered to the system (P_{inc}) when either the probe or corner reflector was in the very near field of the driven element. The effect of these variations on the measured power magnitude (P_{ttm}) was corrected for by applying a correction multiplier (ξ) such that

$$P_{tt} = \xi \cdot P_{ttm}$$

The incident power was measured with the offending element moved far away from the driven element. This value (P_o) was taken as a reference. The ratio between distant spacing to near field power values was taken as the multiplier, that is

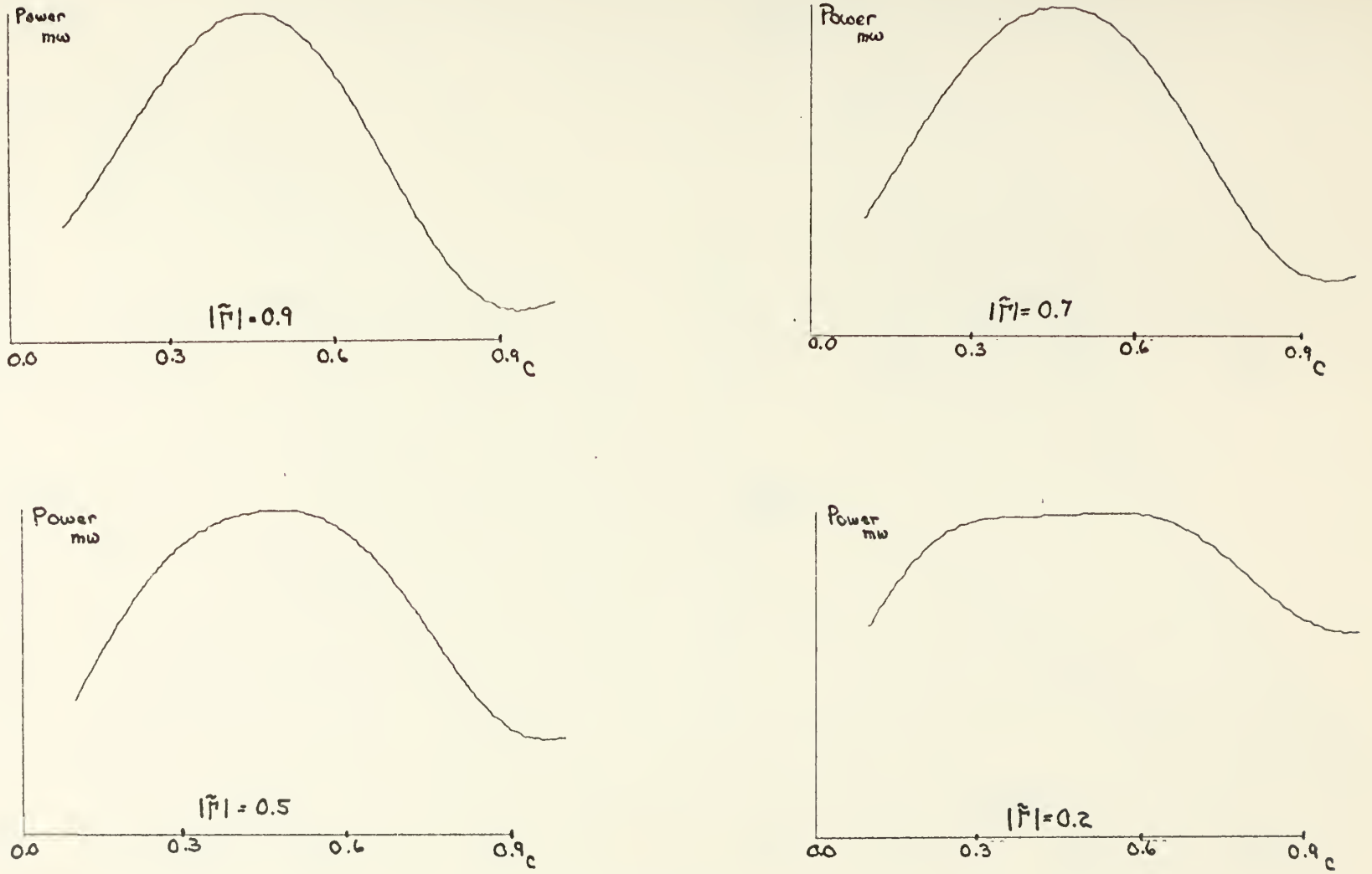

Figure 20
Power vs Corner Spacing ($D=C\lambda$), showing changes which occur for different values of Reflection Coefficient Magnitude ($|\tilde{\Gamma}|$). Power magnitudes are normalized to an arbitrary scale.
$\tilde{\Gamma} = |\tilde{\Gamma}| \angle -225°$

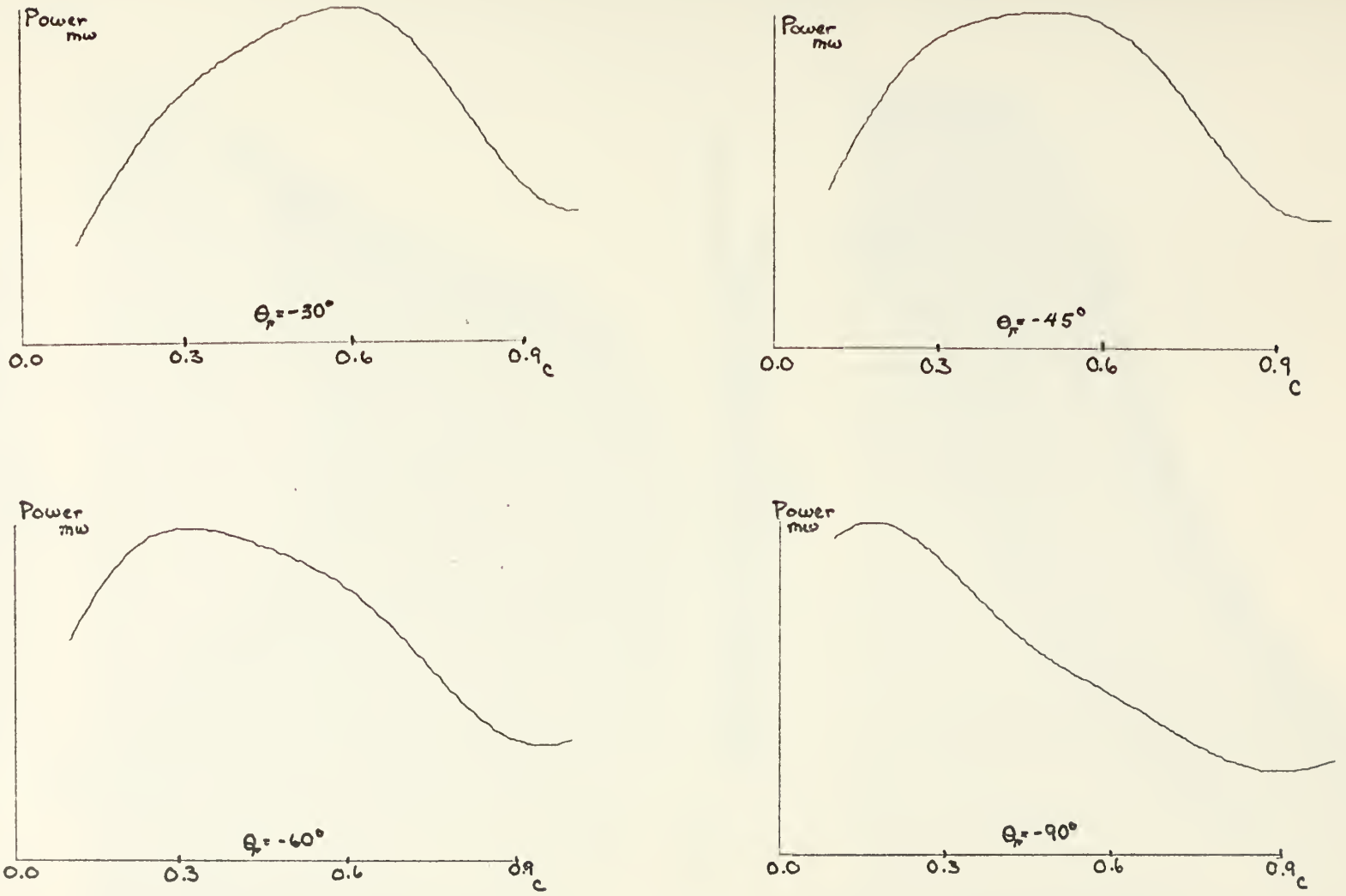

Figure 21
Power vs Corner Spacing (D=Cλ), showing changes which occur for different values of Reflection Coefficient Phase Angle (θ_r). Power magnitudes are normalized to an arbitrary scale.
$\Gamma = -0.4\angle\theta_r$

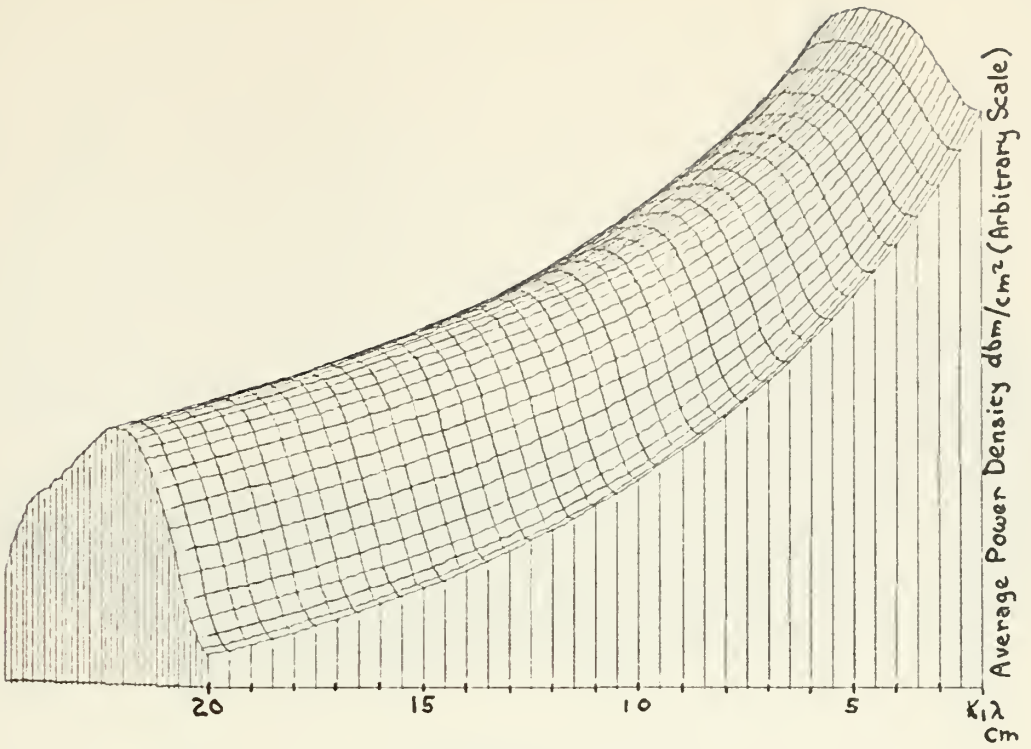

Figure 22
Power vs Spacing in the Field of a
60° Corner Reflector Radiator
(Monopole to Probe Distance is Principal Axis)

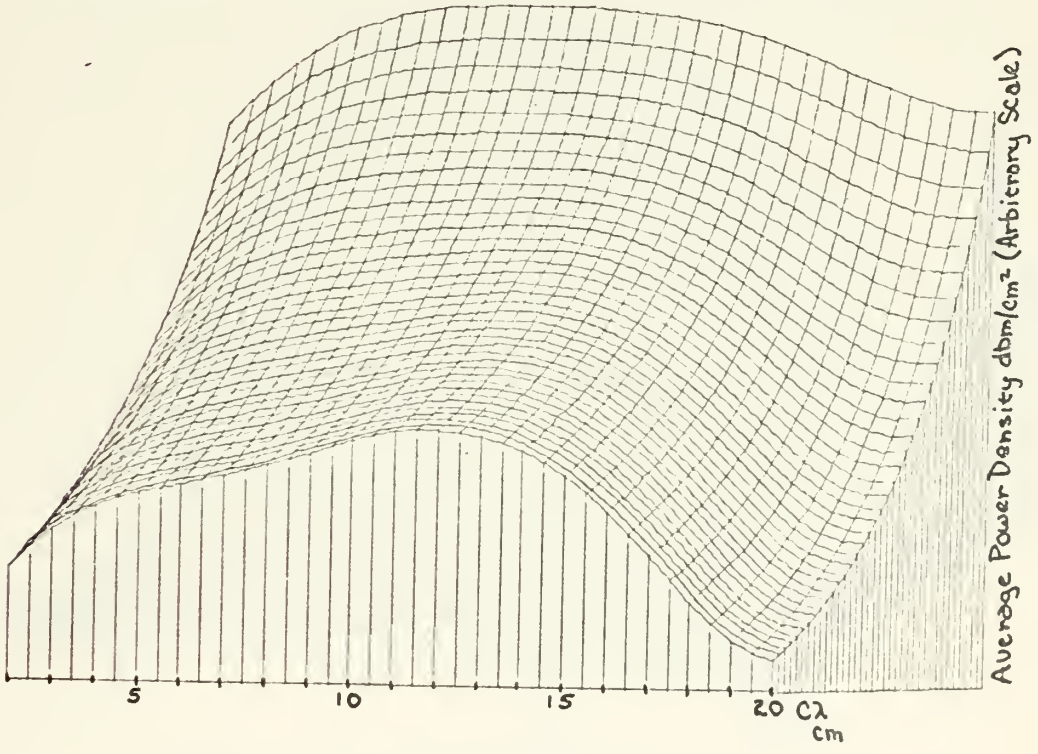

Figure 23
Power vs Spacing in the Field of a
60° Corner Reflector Radiator
(Corner to Monopole Distance is Principal Axis)

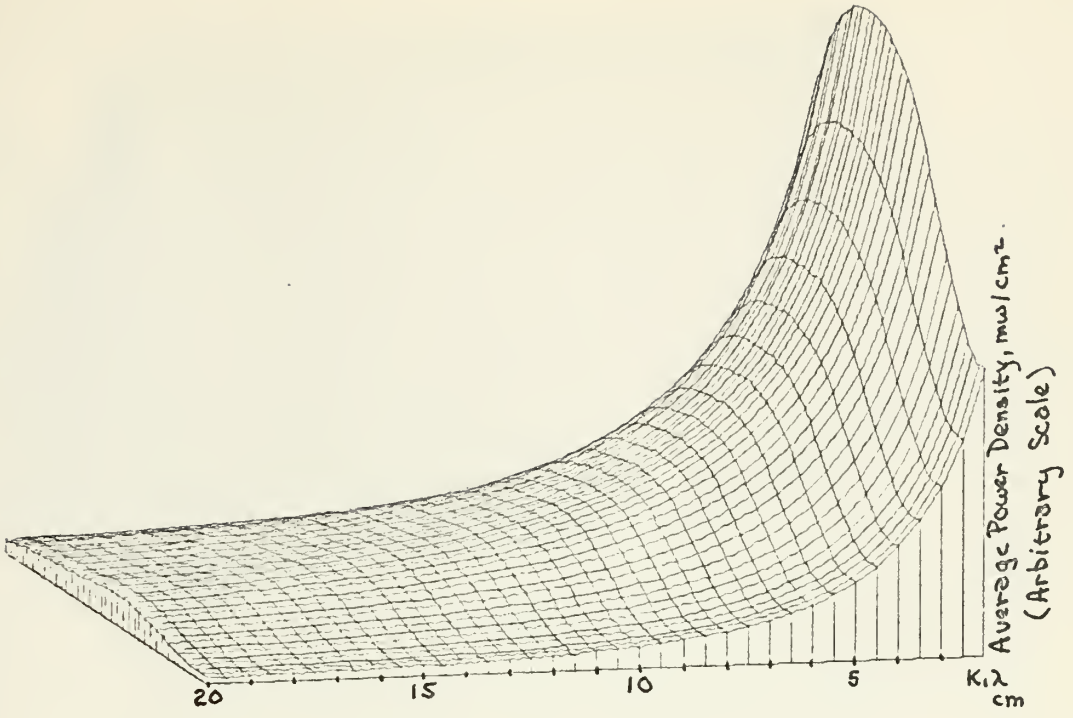

Figure 24
Power vs Spacing in the Field of a
60° Corner Reflector Radiator
(Monopole to Probe Distance is Principal Axis)

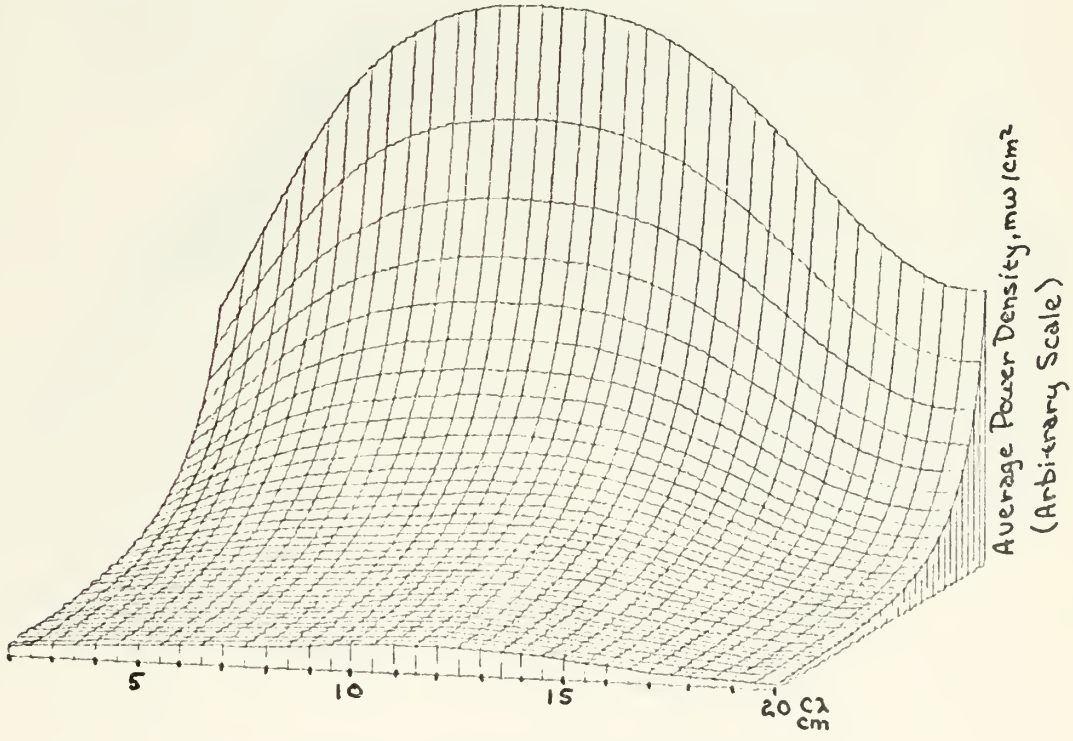

Figure 25
Power vs Spacing in the Field of a
60° Corner Reflector Radiator
(Corner to Monopole Distance is Principal Axis)

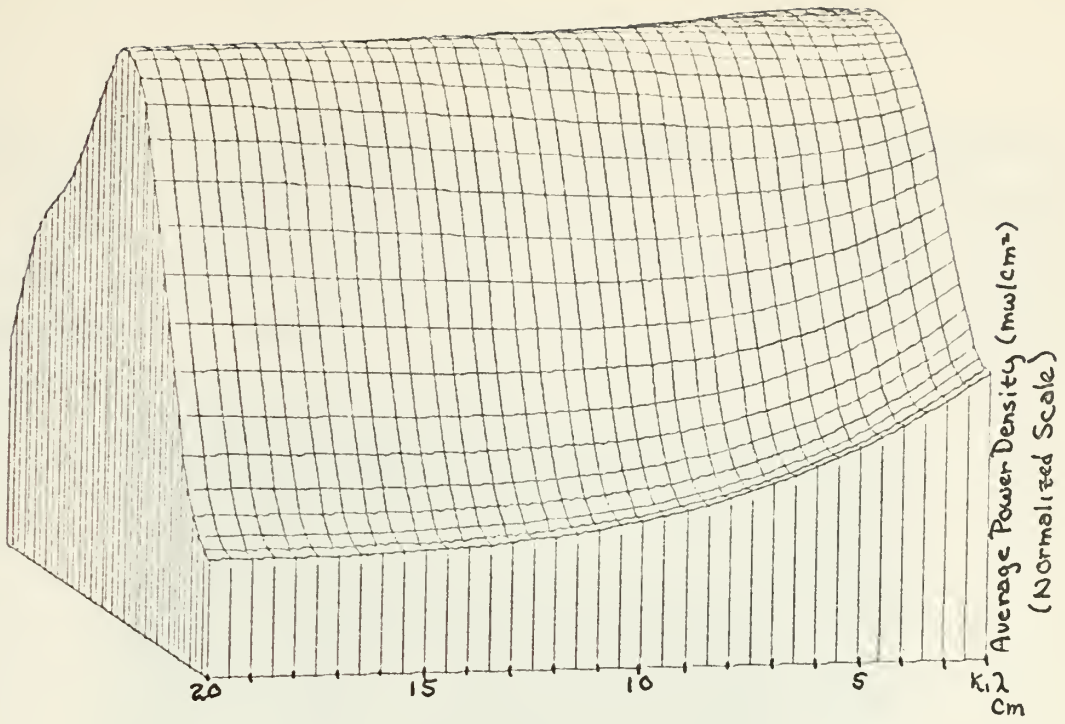

Figure 26
Normalized Power vs Spacing

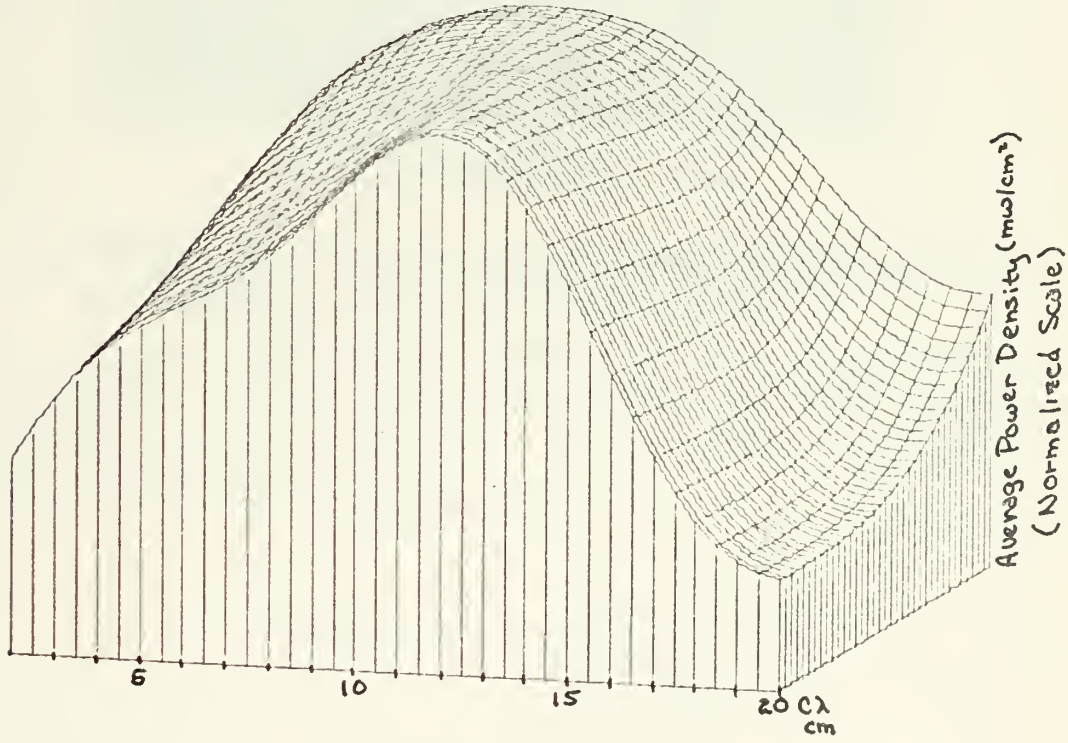

Figure 27
Normalized Power vs Spacing

$$\xi = \frac{P_a}{P_{INC}}$$

Figures 20 and 21 show plots of the results of integration for different values of the parameter $\tilde{\Gamma}$. Figure 22 through 25 show the composite dependence on spacing. Figures 22 and 23 give power on a dbm scale. Figure 24 and 25 show power in milliwatts. Figures 26 and 27 are normalized to show the shift in peak power with different spacings.

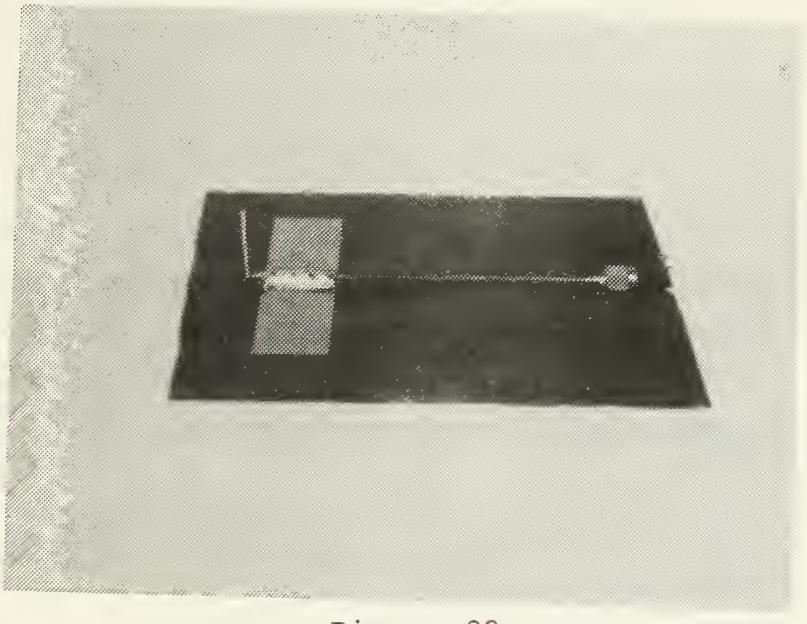

Figure 28
Field Power Sensing Probe

3. Determination of the Effects of System Resonance

a. Determimation of Film Impedance

To determine the effects of system resonance it was considered necessary to model the film, then determine the response of that model to an applied field. A resonant circuit was considered likely:

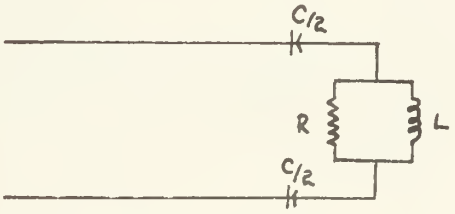

This is seen to be equivalent:

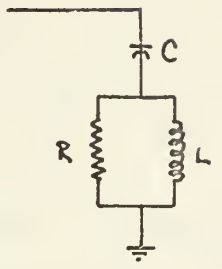

The capacitance is provided by the gap between waveguide and the conductive film negative. The resistance and inductance are present in parallel in the conductive media (the film negative and the activating chemicals).

The Laplace transform of the impedance of such a circuit:

$$z(s) = \frac{1}{sC} + \frac{1}{\frac{1}{R} + \frac{1}{Ls}}$$

$$= \frac{s^2RLC + sL + R}{s^2LC + sRC}$$

$$z(s) = R + \left\{\frac{L - R^2C}{LC}\right\} \cdot \left\{\frac{s + \frac{R}{L - R^2C}}{s^2 + s(R/L)}\right\}$$

letting $a = P$, $b = \frac{L - R^2C}{LC}$, $c = \frac{R}{L - R^2C}$, $d = \frac{R}{L}$ the impedance becomes

$$Z(s) = a + \frac{b(s + c)}{s(s + d)} \qquad \text{(V. C. 21)}$$

b. Determination of System Time Response

The experiment consisted of applying a signal to the film to determine its characteristics, and, later, to obtain images. The response of the model to such a signal, considered to be cosinusoidal and of unit amplitude is found from a transmission line analogy, using Laplace transforms.

$$i(t) = \cos\omega t$$

$$I(s) = \frac{s}{s^2 + \omega^2}$$

$$V(s) = I(s) \cdot Z(s) \qquad \text{(V. C. 22)}$$

By expanding (V. C. 22) using partial fractions and combining certain terms, the total response transform becomes

$$V(s) = \frac{s[a + bC_1(\omega)\cos[\phi(\omega)]]}{s^2 + \omega^2} + \frac{-[bC_1(\omega)\sin[\phi(\omega)]]}{s^2 + \omega^2} - \frac{bC_2(\omega)}{s + d}$$

where

$$C_1(\omega) = \frac{1}{\omega}\sqrt{\frac{c^2 + \omega^2}{d^2 + \omega^2}}$$

$$C_2(\omega) = \sqrt{\frac{c + d}{d^2 + \omega^2}}$$

$$\phi(\omega) = \tan^{-1}\left\{\frac{\omega}{c}\right\} - \tan^{-1}\left\{\frac{\omega}{d}\right\}$$

for which the inverse transform is

$$V(t) = K_1(\omega)\cos[\omega t - \Theta(\omega)] - K_2(\omega)e^{-dt} \qquad \text{(V. C. 23)}$$

where

$$K_1(\omega) = \sqrt{a^2 + b^2C_1^2(\omega) + 2abC_1(\omega)\cos[\phi(\omega)]}$$

$$K_2(\omega) = bC_2(\omega)$$

$$\Theta(\omega) = \tan^{-1}\left\{\frac{bC_1(\omega)\sin[\phi(\omega)]}{a + bC_1(\omega)\cos[\phi(\omega)]}\right\}$$

D. DETERMINATION OF THERMAL PARAMETERS

Various thermal parameters were measured. All thermal measurements were made with a thermocouple and a digital thermocouple indicator[37]. The ambient temperature was 22° Centigrade (71.6°F). Variations of temperature with time were determined under various conditions, and changes in film density were determined for different initial temperatures.

---

[37]OMEGA Thermocouple Indicator, Model DS500, Type J

1. Cooling Box Temperature

a. Cooling Rate of Box

It was considered necessary to determine the time required to reach a steady temperature inside the cooling box (Figure 5) in order to ensure uniform data. The box was filled with the appropriate coolant. The thermocouple was passed through a small hole in the side of the cooling box at the level at which the film would be placed. The top to the box was put in place at time zero and the temperature was then recorded at 5 second intervals until steady state had been reached. This experiment was repeated several times, and the average temperature for each time point obtained and plotted versus time.

b. Effect of Film

The temperature changes inside the box when a film packet was inserted was similarly measured and plotted.

2. Activator Chemical Freezing Point

An experiment was conducted to find the approximate freezing point of the chemical. A thermocouple was frozen into a portion of the chemical and readings were taken as the chemical warmed to ambient temperature. The freezing point was considered to be the temperature at which the warming curve was minimum, since at that point energy was being used to change state from solid to liquid.

3. Temperature Variations in Film Due to Cooling Method

Two methods were used to pre-chill the film. Experiments were conducted to determine the temperature changes in the film, with time for the different cooling methods, and thus provide a basis for determining the initial temperature of the film when first placed in the field.

a. Dry Ice

Dry ice was used to cool the film to temperatures between -30° and +20°C. To ensure consistent results the cooling box was always filled to the film

opening with dry ice. Crushed dry ice was used to fill all niches. The thermocouple was inserted through the box wall and used as a film support for all experiments where the ice was used. The probe's position resulted in a fairly constant cooling position for the film. Also the initial temperature of the box before film insertion could be monitored. Consequently the experiment could be conducted under constant conditions. The temperature at the probe consistently was 50°C before film insertion.

b. Liquid Nitrogen

For cooler temperatures liquid nitrogen was used as the coolant. N_2 was poured into a pre-cooled box 30 seconds before film insertion. Precooling was accomplished by pouring 60 ml. of the coolant into the box 1 minute before film insertion and removing it 45 seconds before film insertion.

To measure the temperature inside the film this procedure was modified slightly. The film was inserted in the cooling box at time zero. The temperatures were obtained with the thermocouple previously inserted through a small (2mm square) hole into the space between print and negative in the film packet. The temperatures at 5 second intervals were recorded and averaged over several runs for each point in time, then plotted versus time.

4. Warming of Film on Removal

Finally, data was taken to determine the rate at which the film returned to ambient temperature after removal from the cooling box.

VI. PRESENTATION AND EVALUATION OF EXPERIMENTAL RESULTS

A. SUMMARY OF PARAMETERS

In order to properly consider the results obtained it is considered useful to summarize the various process parameters and their expected relationships.

1. Principal parameters

The process may be viewed as a system for which the input is applied energy and the output is image density.

a. Applied Energy

The energy is applied to the system in three stages:

(1) In the sensitization preexposure phase, the parameters are the amount of preexposure to blue and green light.

(2) In cooling the film, the principal energy parameter is the film packet temperature, which is itself dependent on the temperature of the pre-chill box.

(3) In the radiation phase, the critical factors are initial temperature of the film, ambient temperature in the room where the experiment is being conducted, thermal response of the chemicals involved, strength of the applied energy field and duration of radiation.

b. Image Density

The density (D) of the resultant image is dependent on the interaction of all the above parameters.

2. Experimental Objective

The overall experimental objective was to

a. Characterize the various parameters.

b. Characterize the image density response to those parameters.

c. Examine that response in order to determine an optimal set of parameters which would provide the best image of an electromagnetic field.

These objectives were to be met by three sets of experiments. The first set may be considered to be a set of static tests, where a single parameter is varied on a given run. The results of these tests are presented in paragraphs B and C below.

On the basis of these results certain preferred sets of parameters were selected with which the waveguide experiments were to be conducted. This set of experiments may be considered to be a set of dynamic tests, since these measure the dynamic qualities of ΔD and ΔE, that is, what variations in film density (i.e. contrast, ΔD) occurs in response to a spatial variation in field strength (ΔE). These experiments are discussed in paragraph C.

The final set of experiments is the confirmation set, which were conducted to confirm the conclusions drawn on the first two sets.

B. THERMAL VARIATIONS

1. Cooling Box Temperature

With the cooling box filled with crushed dry ice to the film entry port, the top was put in place at time $t = 0$. The measurements were taken at the position of the film, as seen in Figure 29.

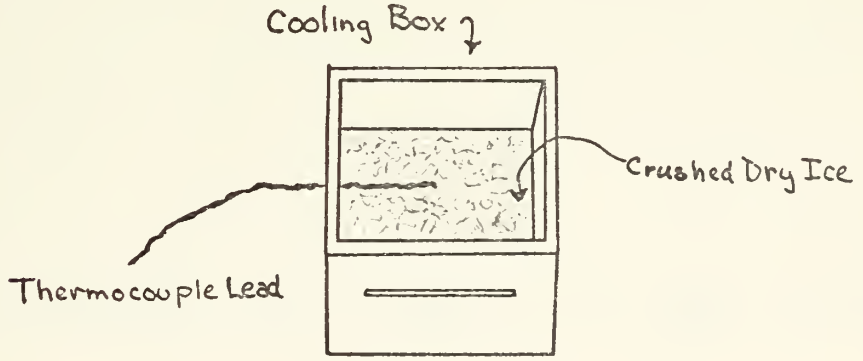

Figure 29
Measurement of Cooling Box Temperatures

The results shown in Figure 30 show that the cooling box is effectively at steady state 4 minutes after being loaded with dry ice. The steady state reached after 15 minutes was consistently within a few degrees of -50°C.

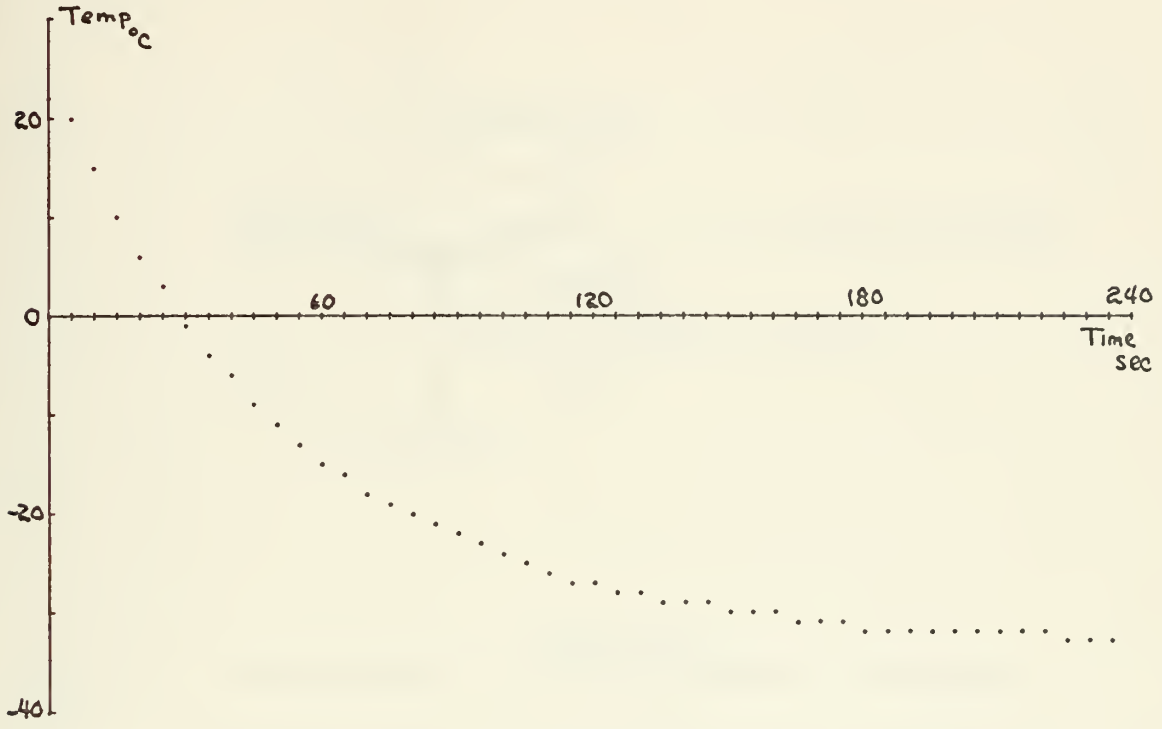

Figure 30
Temperature versus Time for Cooling of Chill Box

Figure 31 shows the change which occurs in the box temperature when a film packet is inserted at time t = 0.

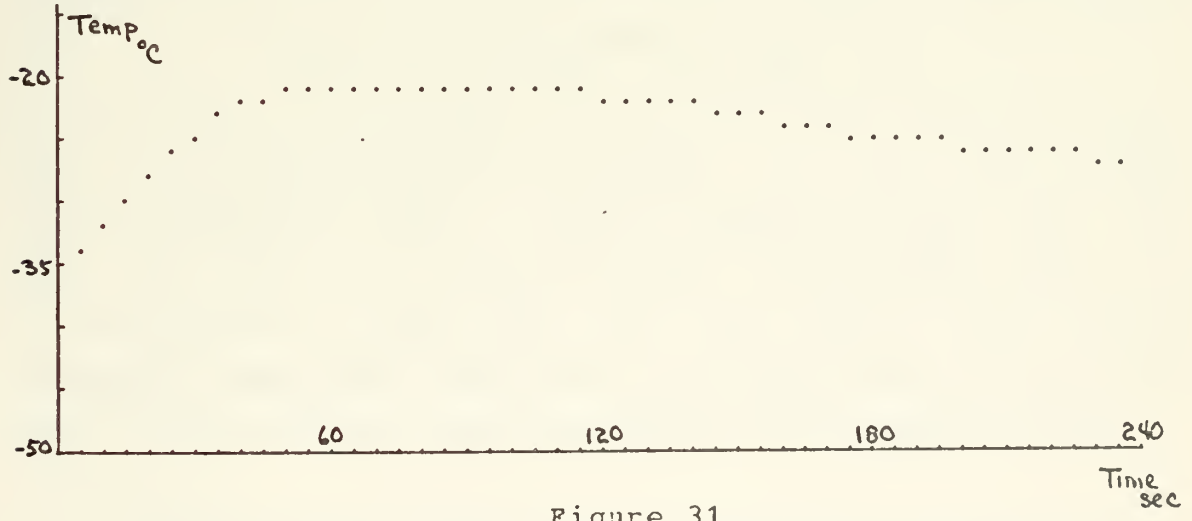

Figure 31
Temperature versus Time for Warming of Chill Box
When Film Is Inserted

2. Film Temperature Variations

Figure 32 shows the method used to record changes in the film temperature during the prechill process.

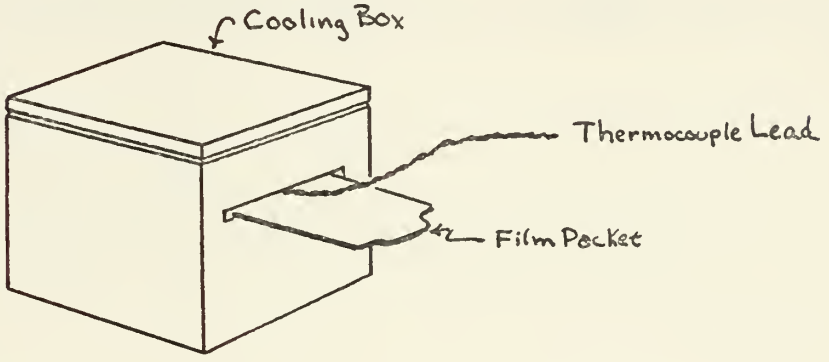

Figure 32
Measurement of Film Temperature Changes

Figures 33 and 34 show the curves for dry ice and liquid nitrogen cooling, respectively. These data are the basis for initial film temperature values assumed throughout for other experiments and data. These curves are of the form

$$T(t) = K_1 + K_2 e^{-t/\tau_1} + K_3 e^{-t/\tau_2}$$

τ_1 has been seen to generally be of the order of 50 seconds, with τ_2 approximately 180 seconds. K_1, K_2, and K_3 have typical values of -35, 7, and 50 respectively for dry ice, 75, 70, and 27 for liquid nitrogen. Each datum represents an average over 3 runs (CO_2) and 5 runs (N_2).[38] The average standard deviation for these data points are 2°.4 and 2°.2 for the dry ice and liquid nitrogen curves, respectively.

---

[38]See Appendix D for definitions of statistical methods used.

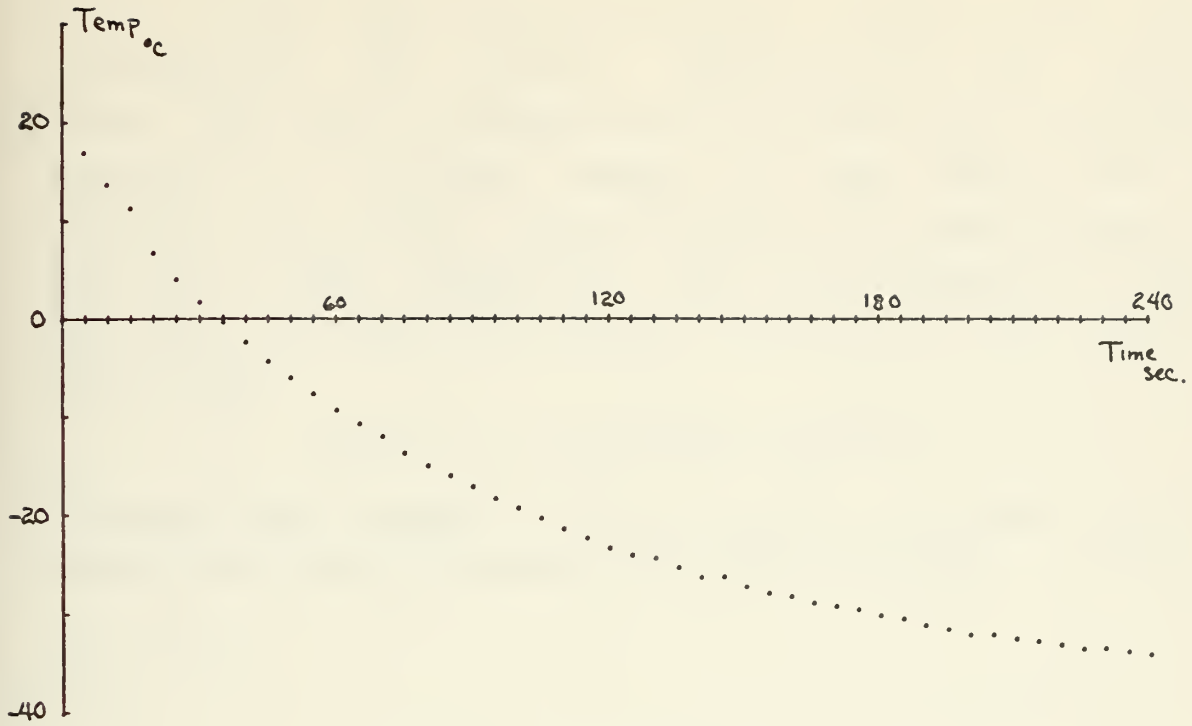

Figure 33
Film Cooling with Dry Ice Coolant

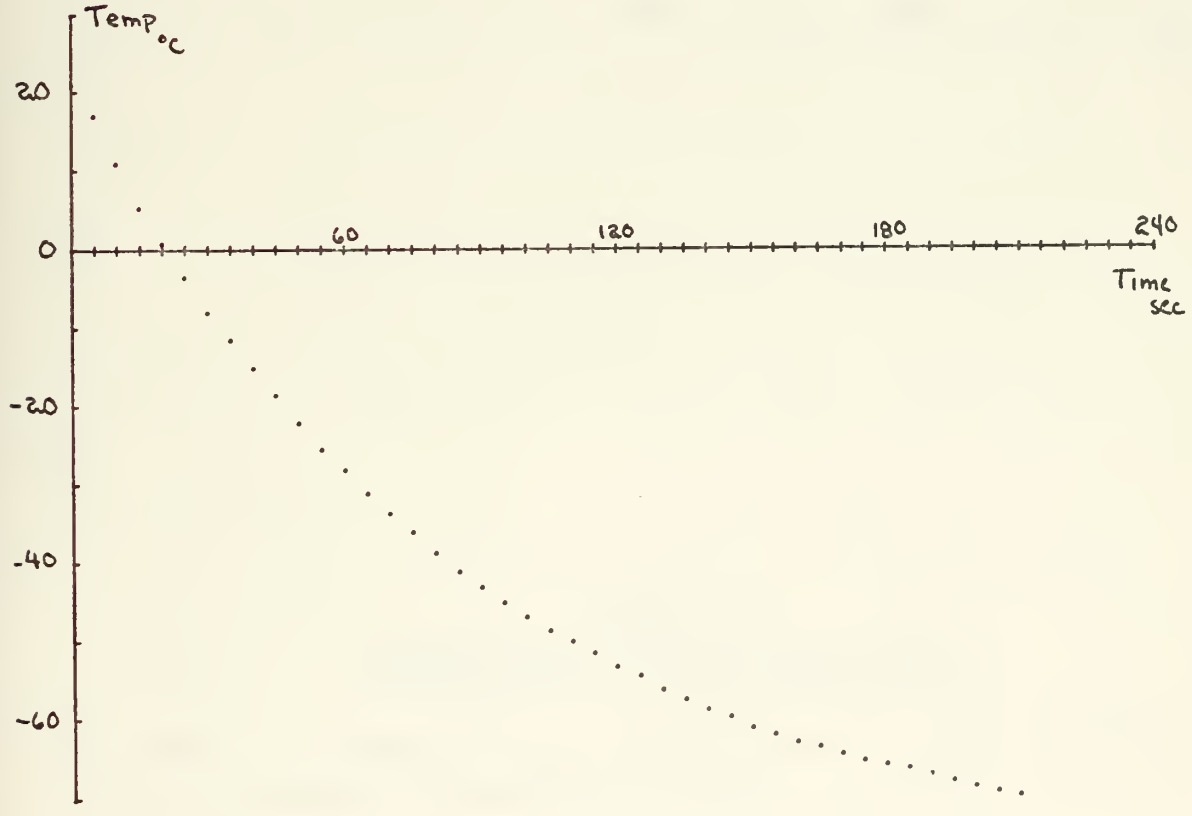

Figure 34
Film Cooling with Liquid Nitrogen Coolant

The film reached apparent steady state after approximately five minutes. Approximately five minutes later the film was removed from the cooling box and placed upright in a position similar to that being used to irradiate the film. Figure 35 shows the time response of the film to these conditions. Time zero represents the time at which the film was removed from the box. This curve is of the form

$$T(t) = K_1 + K_2 e^{-t/\tau_1} + K_3 e^{-t/\tau_2}$$

Representative numbers for K_1, K_2, τ_1, K_3, and τ_2 are, respectively 22,5,15 seconds, 55 and 95 seconds.

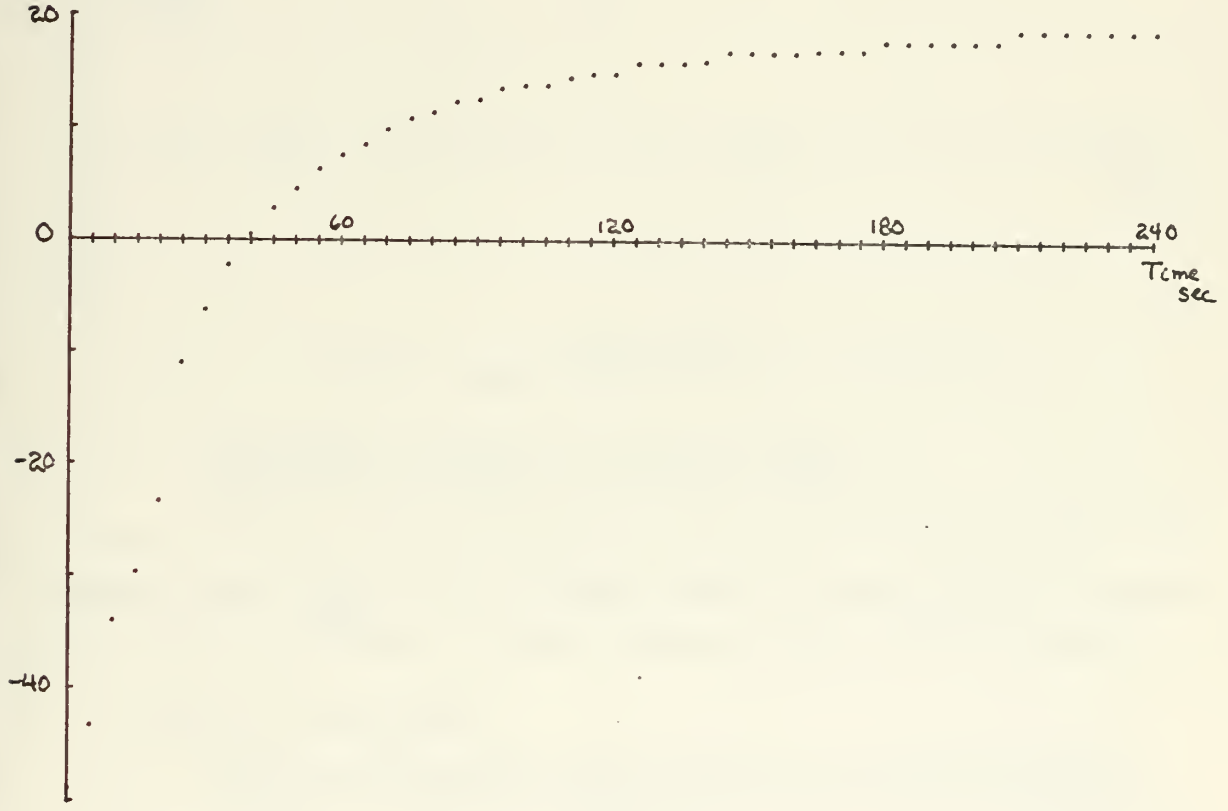

Figure 35
Temperature versus Time for Film
when removed from Cooling Box

The data of Figure 35 was averaged over 4 runs, and had an average standard deviation of $1^{o}.4$.[39]

---

[39] Ibid.

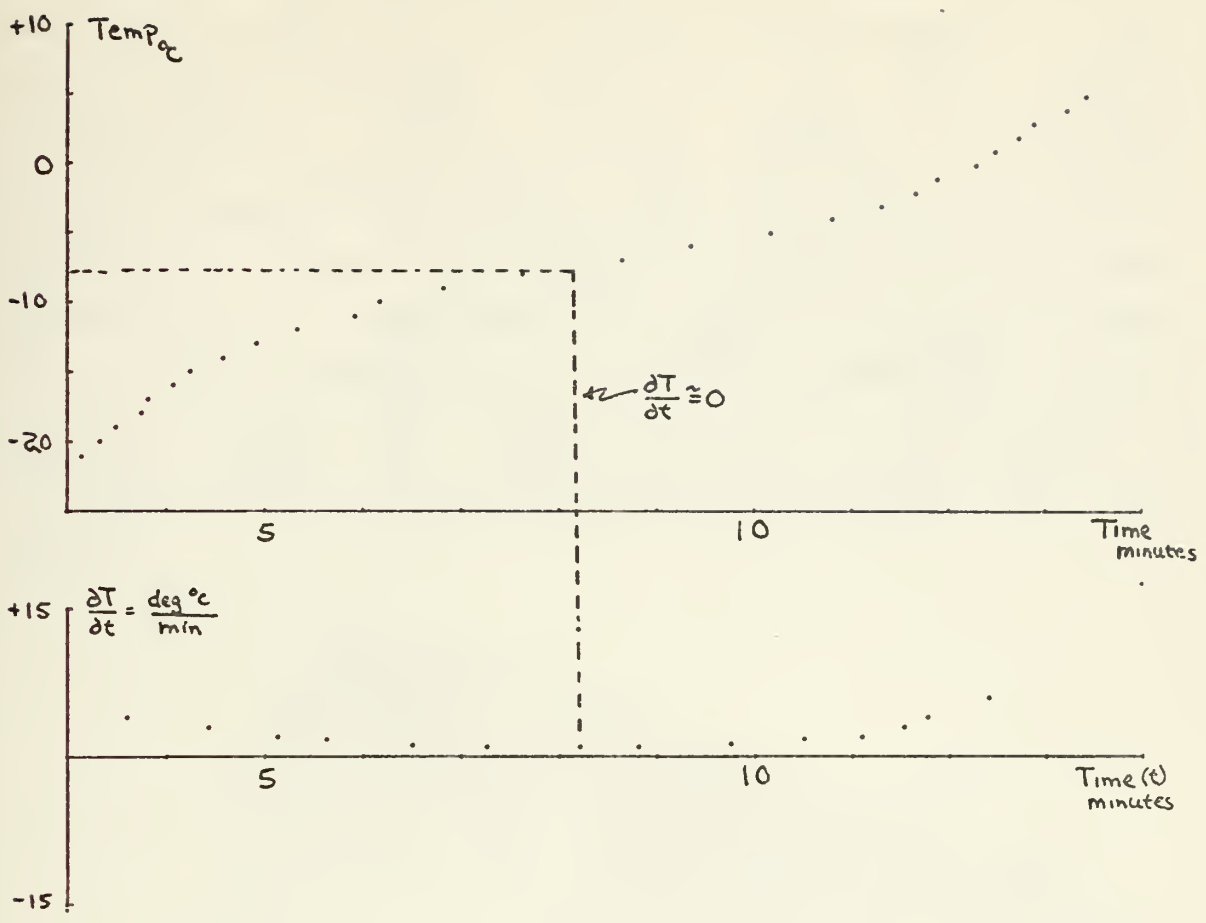

Figure 36
Warming Curve of Activator Chemical

3. Activator Chemical Freezing Point

Figure 36 shows a one run result of an experiment to find the approximate freezing point of the chemical. The minimum slope ($\frac{D^2T}{dt^2} = 0$) occurs when the temperature reaches -7°C, which is taken as the freezing point of the chemical.

C. DENSITY VARIATIONS

1. Density Variation with Sensitizing Pre-exposure

Figure 37 and 38 display the density variations as a function of two parameters on logarithmic axes. These are the results of the experiment described in paragraph V. A. above. The horizontal axes represent the composite amount of pre-exposure to filtered blue and green light (Log H (Blue) and Log H (Green)). The vertical axis is representative of the average film density (D) which

resulted from such pre-exposure. Each figure provides a view of the same data from different viewing angles to allow observation of different aspects of the film's response characteristic. These figures reveal a significant variation in dynamic range over the field of measured exposure levels. The steepest slope appears to exist in the vicinity of (-1.55, -.5) which corresponds to a blue-green pre-exposure of approximately $\frac{3}{100}$sec. blue, $\frac{3}{10}$sec. green. The gradient appears to be aligned diagonally to both horizontal axes. The nearest corner of the density function surface shows the lowest response, corresponding to preexposures of 3 seconds for blue and 2 seconds for green light.

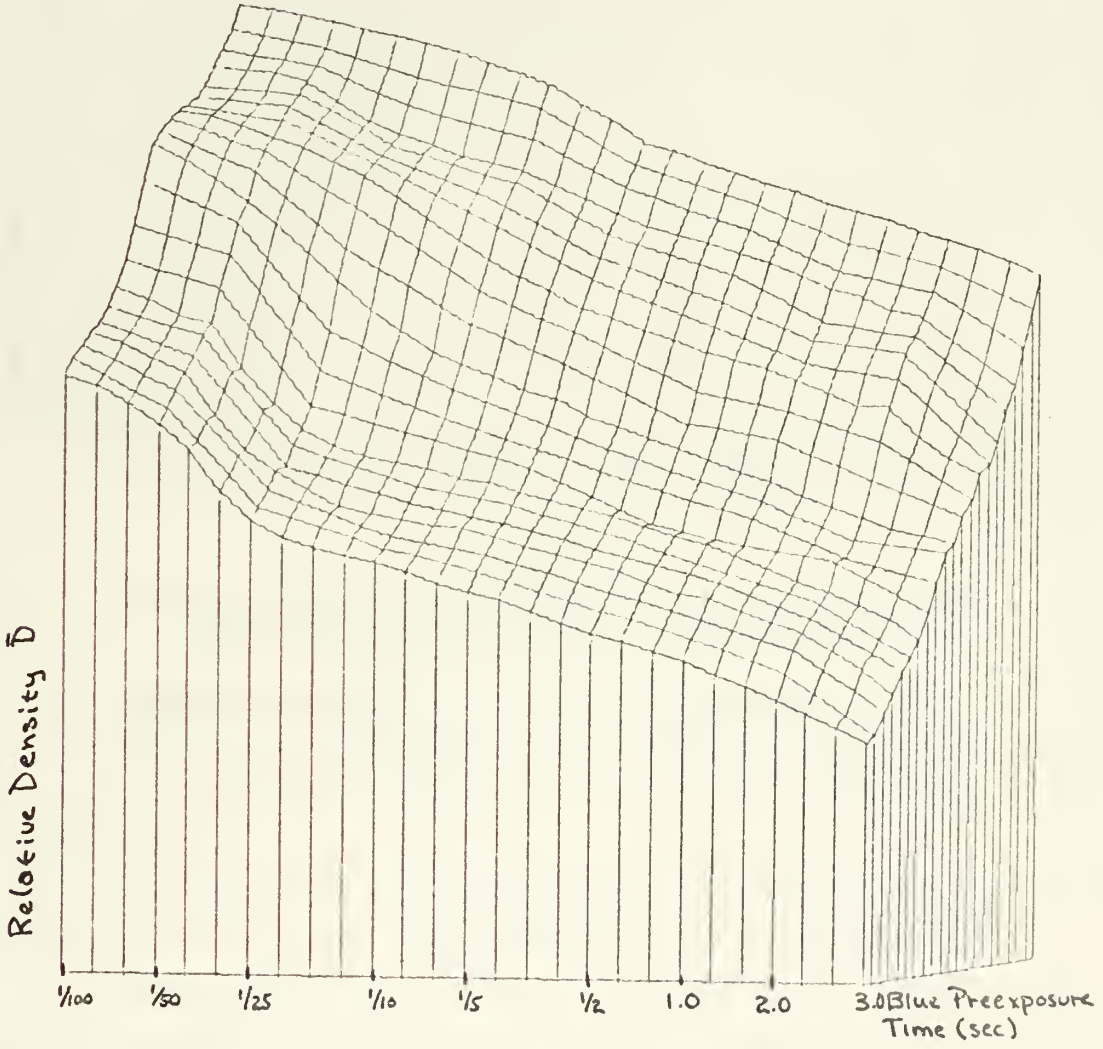

Figure 37
Average Film Density versus Preexposure Time
(Principal Axis is Blue Preexposure)

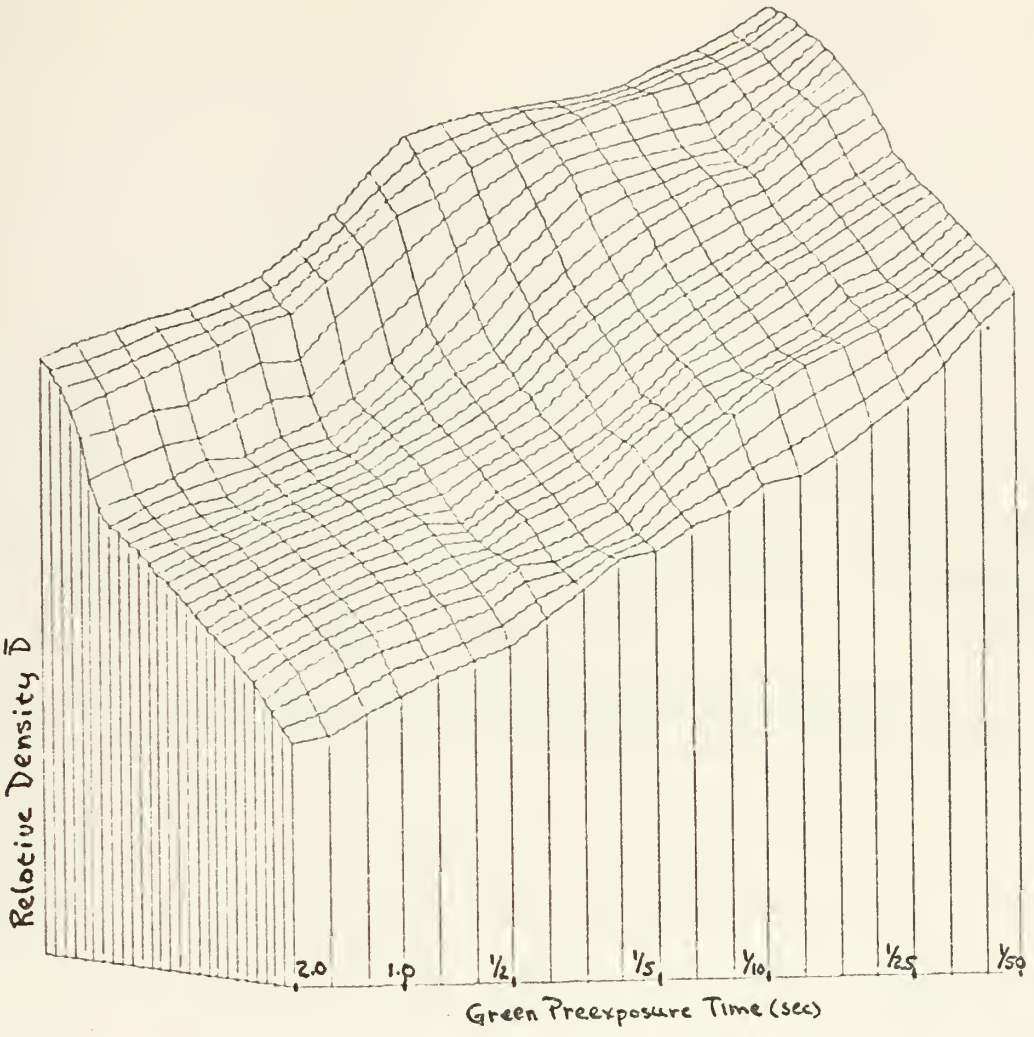

Figure 38
Average Film Density versus Preexposure Time
(Principal Axis is Green Preexposure)

2. Density Variation with Initial Temperature

Figure 39 and 40 show the changes in density which occur for different values of initial temperature and applied energy.

The steepest slope appears to be in the vicinity of the temperature-energy coordinates of (0°, 1000 joules).

The gradient is aligned diagonally to both axes, showing an overall dependence on total energy applied during the radiation phase.

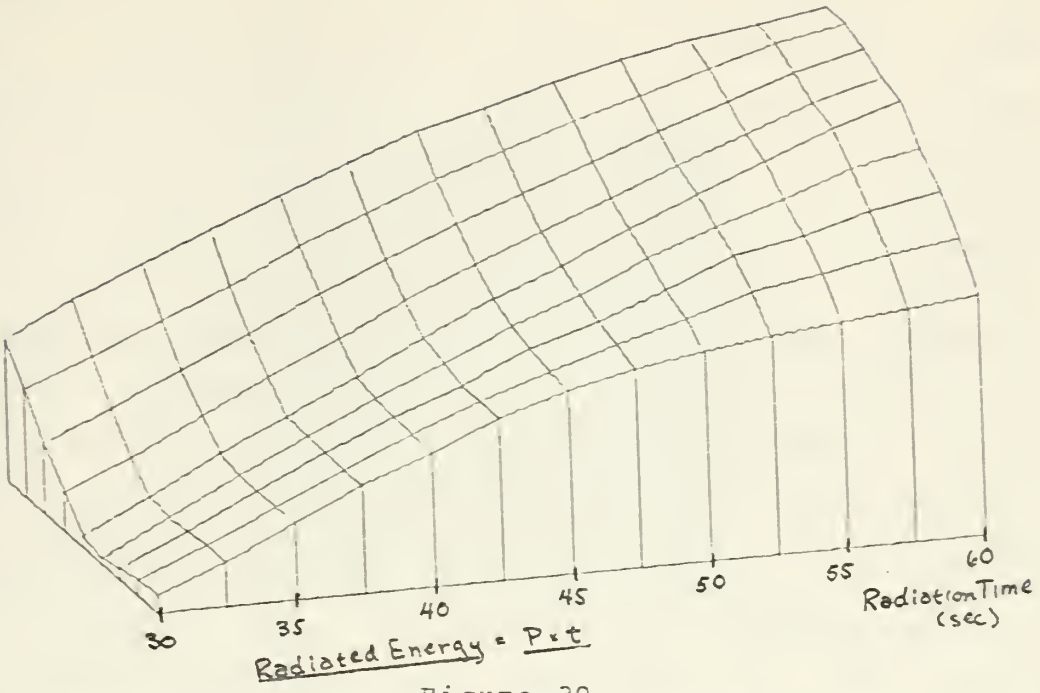

Figure 39
Density versus Radiation Parameters
(Principal Axis is Nominal Radiated Energy)

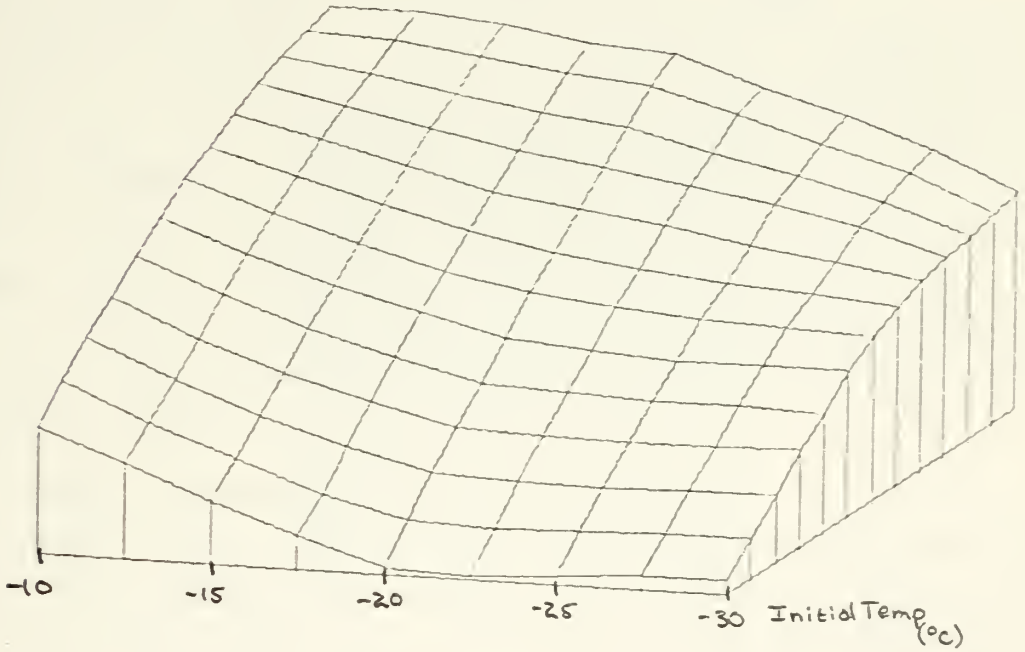

Figure 40
Density versus Radiation Parameters
(Principal Axis is Initial Temperature)

D. DYNAMIC RANGE MEASUREMENTS

The waveguide experiments were conducted to determine the dynamic range of the film, to be characterized as the product σ of contrast (ΔD) and change in energy (ΔE). These experiments were hampered by a factor not previously noted: thermal noise, that is, unwanted images due to ambient temperature in the room. The static tests were conducted with a uniform image ($\Delta D \cong 0$) so the incremental contribution of ambient temperature was not seen. However, the waveguide experiment required simultaneous imaging of high and low energy regions. An expected variation of density occured in response thereto. Additionally, though, there was a uniform density distribution due to the uniform ambient temperatures near the experiment. The effect was minimized by using long pre-exposure times, e.g. 2 seconds blue, 1 second green and low initial temperatures, e.g. -30°. This however restricted operations to the flatter regions of the surfaces presented in Figures 33 and 35. These flatter regions have a much lower and generally uniform dynamic range as measured by $\sigma = \Delta D \Delta E$.

The phenomenon is directly analogous to that of a receiver or control system in which high sensitivity and dynamic range is accompanied by poor performance because of noise response, so that optimal performance is ultimately found to be derived from a raised a.g.c. threshold or a damped system. Figures 41 and 42 show two photographs, one taken at a high sensitivity point on the surfaces, the other taken at a low sensitivity point. The preferability of the latter is obvious.

E. FIELD MEASUREMENTS

Figure 43 shows the normalized precomputed and normalized experimental values of relative power in the field of the dipole and reflector system, as a function of the corner-to-driven-element distance for a reflection

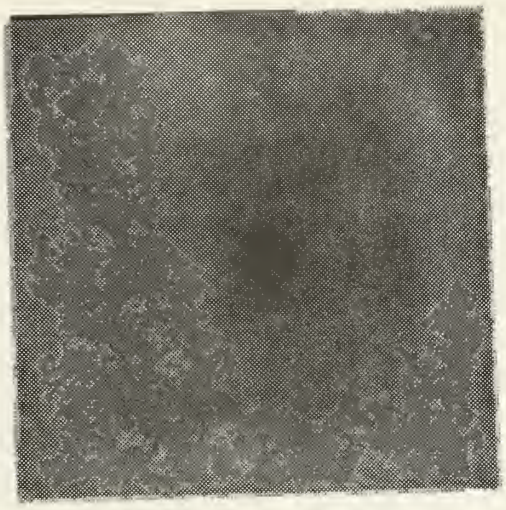

Figure 41
Blue Exposure = 4/25sec; Green Exposure = 3/100sec;
initial temp = -10°C

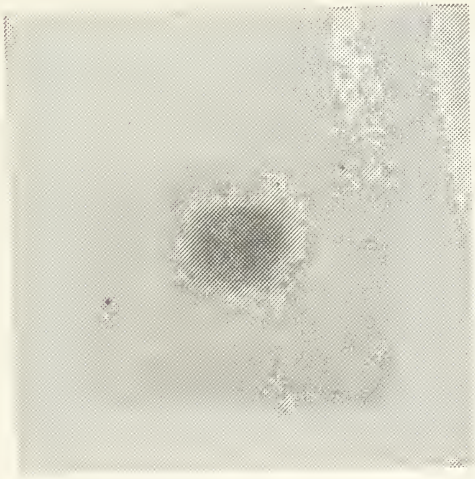

Figure 42
Blue Exposure = 6sec; Green Exposure = 2sec;
initial temp = -10°C

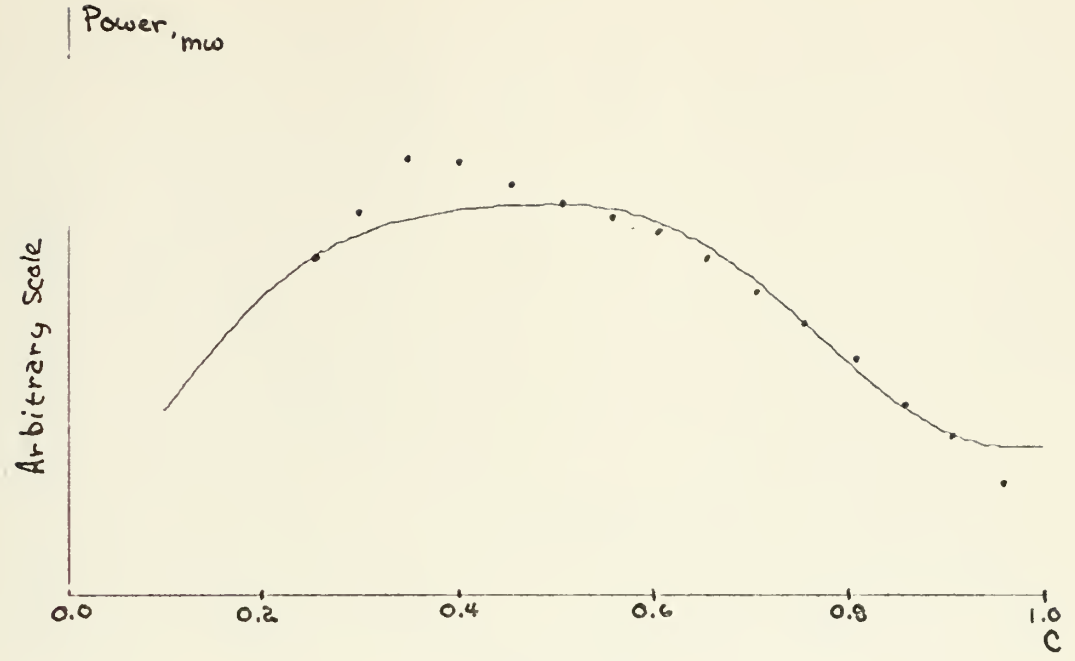

Figure 43
Field Power vs. Corner Distance $C\lambda$;
$\Gamma = -.4\angle -45^\circ$ $\lambda = 20cm$ $Y_1 = K_1\lambda = 5cm$

Figure 44
Field Power vs. Corner Distance $C\lambda$;
$\Gamma = -.9\angle -30^\circ$ $\lambda = 20cm$ $Y = K_1\lambda = 5cm$

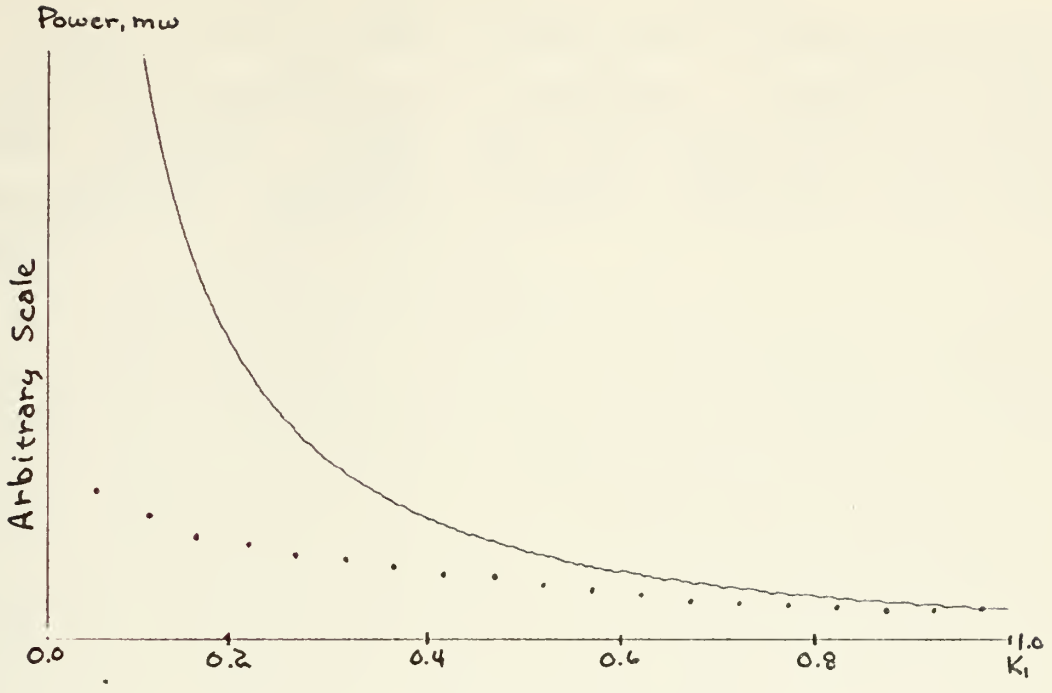

Figure 45
Field Power vs. Probe Distance K,λ;
$\tilde{\Gamma} = -.4\angle -45°$ $\lambda = 20cm$ $D = C\lambda = 10cm$

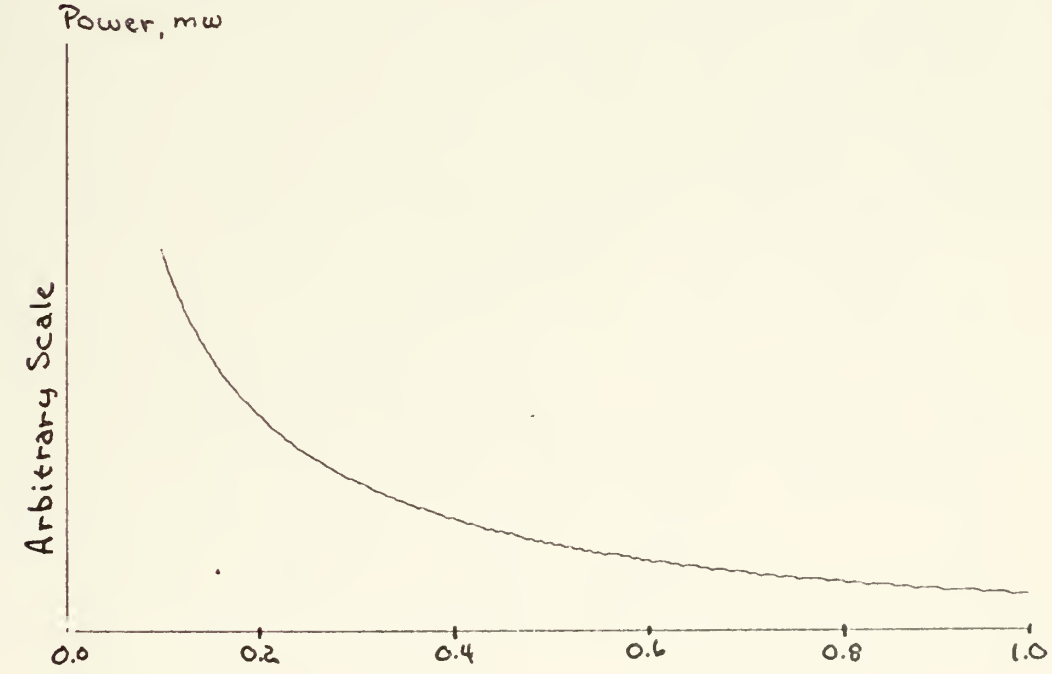

Figure 46
Field Power vs. Probe Distance K,λ;
$\tilde{\Gamma} = -.9\angle -30°$ $\lambda = 20cm$ $D = C\lambda = 10cm$

coefficient ($\tilde{\Gamma}$) equal to $-.4\angle -45^{\circ}$. Figure 44 shows the same for a reflection coefficient of $-.9\angle -30^{\circ}$.

Figure 45 and 46 show the plots for the same reflection coefficients respectively as a function of probe-to-driven element distance. These show the importance of providing good electrical connection between reflector and ground plane.

VII. EXPERIMENTAL CONCLUSIONS

A particular set of parameters was selected as being optimal. The set and the bases for its selection are presented below.

A. FILM SENSITIZING PARAMETERS

1. Light Source and Intensity

The choice of a 4800°K, 225 foot-candle source was principally an economic decision based on available devices and a consideration of the discussion in appendix A.

2. Filters

The choice of Wratten 47B (Blue) and Wratten 99 (Green) filters was based on the corresponding responses indicated in Figures 8 and 9 and on the accompanying discussion in Section IV D. These choices were considered to result in approximately equal sensitization of blue and green dyes.

3. Sensitizing Pre-exposure

Blue and Green pre-exposures of 2 and 1 second respectively were chosen on the basis of the discussion in Section VI. D to place the response in an easily controllable region of the surface of Figures 37 and 38. The shutter opening was f/5.6 with a 50mm lens focused to 60 feet. The camera was a Leicaflex.

B. FILM RADIATION PARAMETERS

1. Initial Temperature

An initial temperature of -20°C was chosen to reduce the effect of ambient temperatures while reducing the amount of time needed to be spent preparing the film. As indicated by Figure 33, this temperature is considered to have been reached after 1^m and 45^s of cooling. Figure 35 indicates that after 30^s of exposure to ambient temperatures the film would still be at less than 5°C, and after 45^s would still be at less than 10°C.

2. Radiation Frequency

A frequency of 1.5 GHz was chosen to permit the largest possible image for the desired target elements on a single film.

3. Radiation Exposure

It is concluded that ultimately the process is power limited with the facilities available to this author. At no time was there available a power density greater than approximately 300mw/cm^2. With that limitation, the only way to increase applied energy was to increase radiation time. This was counter-productive, since increased radiation time allowed increased warming, which resulted in images being fogged with responses to warmer temperatures. A choice of 45 seconds of radiation with the maximum power available of approximately 16 watts was made to optimize the process in consideration of these factors.

C. ALTERNATIVE SOLUTIONS

Within the overall aim of providing a simple and relatively inexpensive method of imaging fields, the most obvious method to improve the images beyond what was accomplished here would be to increase the available power level, which would increase the ratio of desired to undesired thermal fields in which the process operates. By thus raising the signal, the signal to noise rate is improved.

The next more obvious alternative is to reduce the noise by reducing the ambient temperature. This would require conducting the experiments in a cooled environment large enough to contain the radiation structure, or at least the scatterer and film.

VIII. FINAL RESULTS

A series of images were obtained using the parameters of Chapter VII. The target scatterers correspond to devices measured by Burton [2]. They are presented below.

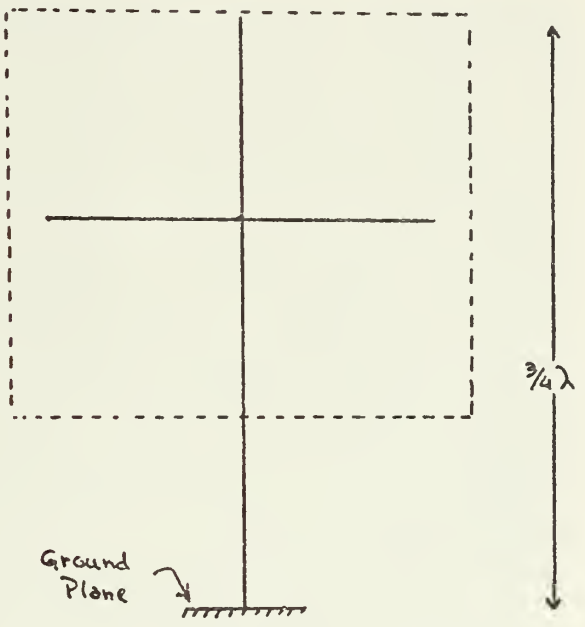

Figure 47
Region of Cross Included in DTM Images

Figure 48
DTM Image of Driven Cross

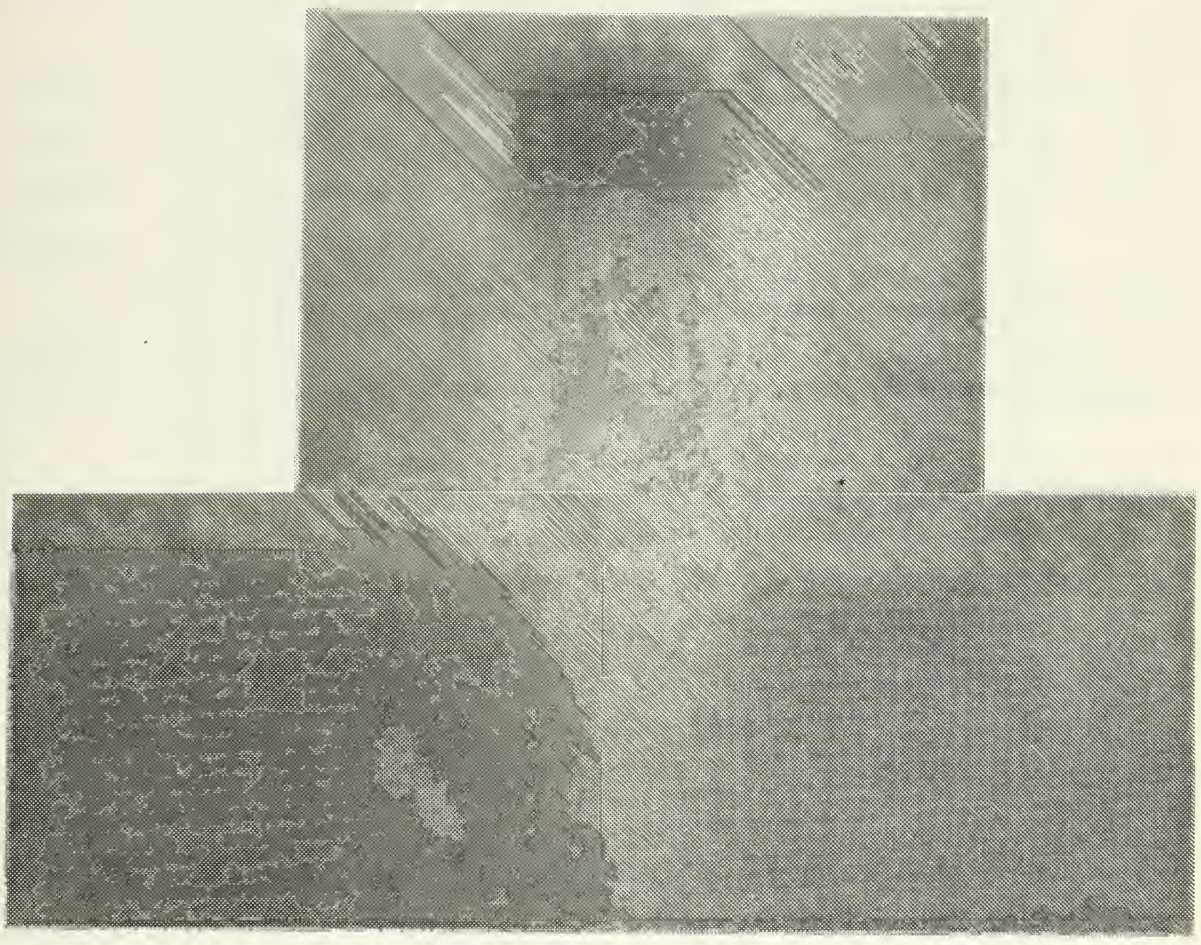

Figure 49
DTM Image of Scattering Cross Y1 = 10cm

IX. CONCLUSION

A. SUMMARY

Dye Transfer Modulation has been analyzed and parameterized. An optimum set of parameters subject to certain constraints has been identified. Results have been obtained on significant structures using those parameters.

A single major problem remains to be solved for the process to have widespread application. That problem is that of insufficient margin between power density of the applied electromagnetic field and power density of the ambient thermal field.

Two solutions have been suggested, one being to increase the available EM power density, the other being to decrease the ambient thermal field by conducting the process in a cooled enclosure.

A third alternative was determined shortly before the completion of this work. A long wavelength (2 - 5.6μm) infrared detector was obtained on a loan basis from the manufacturer.[40] The device is sensitive to temperatures in the ambient range and displays them on a television screen. An experiment was conducted by the author to determine its applicability to our purpose. A piece of ordinary carbon paper was attached to a cardboard backing with adhesive. It was then placed against a monopole scatterer which was then irradiated. The image produced on the screen was photographed. Figure 50 is the result.

The advantage lies in the fact that it expresses a change in energy as a change in hue of the image rather than simply a change in density. Since the eye is more responsive to changes in color than in density the image presents

---

[40]The device is the AGA Thermovision 470 System, manufactured by AGA Corporation, 550 County Ave., Secausus, N.J., 07904.

greater visibility. Comparison between Figure 50 and Figure 49 are invited.

Figure 50
AGA Thermovision Image of Scattering Cross

Follow up experiments were conducted with this device and are discussed in in Appendix F.

APPENDIX A

BASIC CONCEPTS RELEVANT TO FILM SENSITOMETRY

A. FILM SENSITIVITY VERSUS EXPOSURE

Direct parallels can be drawn between fundamental radiometric and photometric quantities. In sensitometry, ("the science of measurement of the sensitivity of photographic materials")[41] quantities which are of particular interest are[42]

Quantity Name	Symbol	Defining equation	Representative Units Radiometric	Photometric
Energy	Q		joule	lumen-second (lm.sec)
Energy density	ω	$\omega = \partial Q / \partial v$	joule/m^3	lm.sec/m^3
Energy Flux	Φ	$\Phi = \partial Q / \partial t$	watt	lm.
Irradiance (illumi-nance)	E	$E = \partial \Phi / \partial A$	watt/m^2	lm/m^2=lux(lx) =foot-candles
Intensity	I	$I = \partial \Phi / \partial w$ w=solid angle	watt/ste-radian (W/str)	candela (cd) =lm/steradian
Radiance (Lumi-nance)	L	$L = \partial I / \partial w$	watt per (str$\cdot m^2$)	cd/m^2

The distinction between the two measuring concepts is simply the preposition of the appropriate adjective; e.g. radiant energy in radiometry, luminous energy in photometry. This method of distinction is evidenced in the quantities E and L above. The candela was defined[43] by the 9th General Conference on Weight and Measures, in 1948, as 1/60 the luminance of a black body radiator[44] heated to the temperature of solidification of platinum. A lumen is the

---

[41] Engel, p.21.

[42] "Section 2 - Radiometry and Photometry" SPSE Handbook of Photographic Science and Engineering, 1973, pp. 146-148.

[43] Engel, p. 178.

[44] The subject of Densitometry is discussed at length in "Section 15, Densitometry," J. Paul Weiss, editor, SPSE Handbook of Photographic Science and Engineering, Wiley, 1973, p. 829, ff.

time rate of energy radiation (radiation power output present) in one steradian from a source with an intensity of one candela. Illuminance (or, illumination) is commonly measured in foot-candles in the English speaking world, which is defined as one lumen/ft^2.[45] Illuminance varies as the square of the distance from the source to the film.[46] One more quantity is the quantity exposure (H). Exposure is defined as[47] an energy density:

$$H = E\,t$$

where E is defined above and t is time. Exposure is conventionally given in units of ergs per square centimeter. In practice it is referred to as a combination of lens setting and exposure time in fractions of a second, e.g. "f/8 at 1/30." Lens settings are measured in "f-stops" where the f-stop number is defined as the ratio of focal length of the lens to the diameter of the entrance pupil.[48] F-stops are conventionally 1.4, 2.8, 4, 5.6, 8, 11, 16, 22 with one half stop in between. While most cameras are provided with "click stops" which provide specific stop settings some lenses may be varied continuously. One conventional f-stop decrease in lens opening represents an approximate doubling of illumination, hence of exposure. Precisely, the comparison is between the squares of the f/number:[49]

$$I_2 = \left[\frac{f/\#(1)}{f/\#(2)}\right]^2 \cdot I_1$$

For example:

$$f/16 \text{ to } f/11 \text{ yields } I_2 = I_1\left[\frac{16}{11}\right]^2 = 2.12\,I_1$$

Over a short range of f-stops the increase of an additional f-stop may be compensated for by cutting the exposure time in half providing a constant exposure (H). However, if a large change in either parameter is made it

---

[45] Engel, p. 178-179.

[46] Ibid. p. 79.

[47] SPSE Handbook..., p. 767.

[48] Ibid. p. 195.

[49] Engel, p. 96.

cannot be so simply compensated by changing the other parameter by a reciprocal amount. The reason for this failure of reciprocity lies in the reaction of the emulsion to very large or very short durations of illumination, with different explanations for each case. In either case the phenomenon is referred to as the Reciprocity Law Failure.[50]

Film sensitivities are conventionally provided as a plot of experimental data:

The particular emulsion type is subjected to different amounts of exposure (H) and developed under standard conditions. The density (D) of the developed negative is the logarithm of the opacity (O) where the opacity is the ratio of incident intensity to transmitted intensity:

$$O = \frac{I \text{ incident}}{I \text{ transmitted}}, \quad D = \log_{10}(O)$$

In practice, Density can be quantified by visual comparison of a projected negative image to a card standard which has been printed with different tones of grey corresponding to different densities.[51]

A plot of density versus log H is then the conventional method of documenting the sensitivity of a film to different intensities. Figure 51 gives a characteristic "Density versus log H curve" (H and D curve), showing the standard features. Various classification methods have chosen one or more of the features of the D-log H curve as a criteria for specifing some index to the film's sensitivity. In this country the most common is the "ASA" rating which has been established by the American National Standards Institute (ANSI) and generally is given by

$$\text{ASA Speed} = \frac{K}{H_m}$$

K is a constant and H_m is a particular value of H which cor-

---

[50] Ibid., pp. 97-98.

[51] The subject of Densitometry is discussed at length in "Section 15, Densitometry," J. Paul Weiss, editor, SPSE Handbook of Photographic Science and Engineering, Wiley, 1973, p. 829, ff.

relates to desired results for different emulsion types. The H and D curve for a representative color reversal film is given in Figure 52. For this emulsion type,

$$H_m = \sqrt{H_l H_s}$$

and

$$\text{ASA Speed} = \frac{8}{H_m}$$

rounded to the nearest $\sqrt[3]{2}$ step.[52]

B. FILM SENSITIVITY VERSUS COLOR OF LIGHT

A different parameter of film sensitivity is the frequency response of the film emulsion. Color sensitometry provides curves of spectral density versus wavelength for the individual layers of the film, or alternatively, an impressive array of different methods of quanitizing the response of a particular film.[53] Of particular interest is the concept of color balance. As a rule, one desires a film to reproduce the color of an object as it was seen. But for reflecting objects the color seen depends on the color of the illuminating source. Therefore, films are constructed to provide a "natural" response to objects illuminated by source of a particular color temperature. Natural response is considered to exist when neutrals are reproduced as nearly neutral.[54] The color temperature of the source is the temperature at which a black body radiator would emit a spectrum of radiation similar to the source in question.[55] If a film is exposed to light from a source of a color temperature other than that for which the film has been designed colors will not be rendered natural in the resulting image. Thus the familar yellow tinge to photograghs taken under tungsten lighting with "Daylight"

---

[52] SPSE Handbook..., pp. 810 - 816.

[53] Ibid., p. 448 - 469.

[54] Ibid., p. 469.

[55] Eastman Kodak Company, Kodak Publication No. U-72, Kodak IRTRAN Infrared Optical Materials, 1971, p. 5.

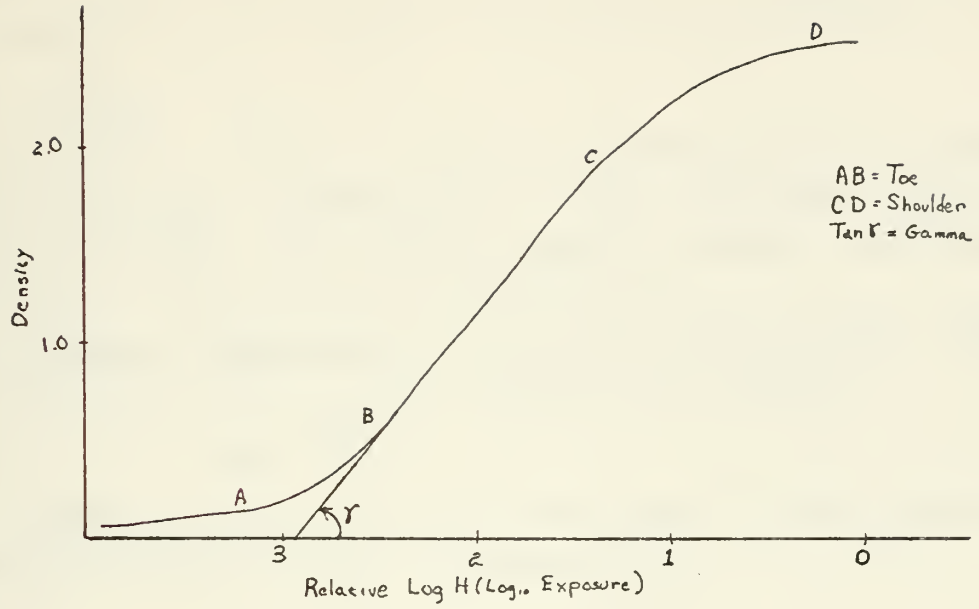

Figure 51
Typical H and D Curve

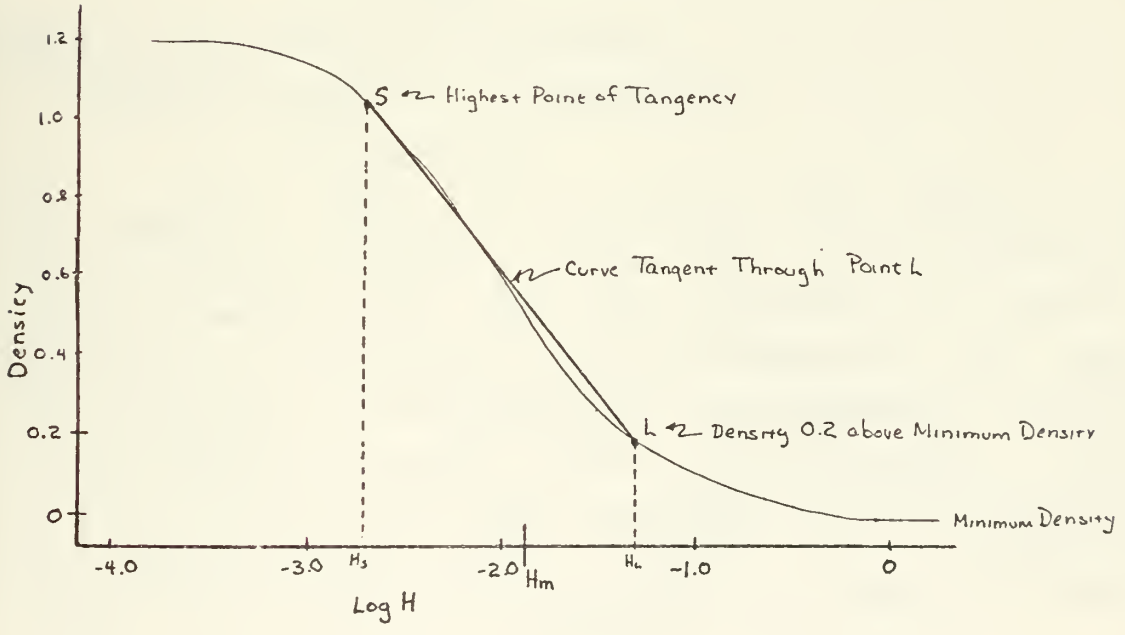

Figure 52
ASA Speed Parameters

film. This imbalance can be corrected through the use of filters whose spectral transmittance is such that the spectral intensities of light transmitted through the filter corresponds to the spectral sensitivity of the film in use.

C. FILTERS

Several classes of optical filters exist of which the class absorption filters are of interest here. Using the quantity flux (Φ) defined above various qualities of absorption filters can be considered:[56]

Spectral Reflectance ρ_λ is the ratio of flux reflected by a material (Φ_r) to flux incident on it (Φ_i):

$$\rho_\lambda = \Phi_r / \Phi_i$$

Spectral Absorption α_λ is the ratio of flux absorbed by the material (Φ_a) to the incident flux:

$$\alpha_\lambda = \Phi_a / \Phi_i$$

Spectral Transmittance τ_λ is the ratio of flux transmitted through the object (Φ_t) to the incident flux:

$$\tau_\lambda = \Phi_t / \Phi_i$$

τ_λ max is the maximum transmittance.

Spectral density D_λ is defined as

$$D_\lambda = \log_{10} \frac{1}{\tau_\lambda}$$

The spectral density of two or more filters used simultaneously is equal to the sum of the individual spectral densities.[57] The term "Spectral..." implies a dependence of the quantity on the wavelength of the energy being considered. The bandwidth or half-width $\Delta\lambda_{1/2}$ is defined as the wavelength interval between the wavelengths at which τ_λ falls to $\frac{1}{2}\tau_\lambda$ max and mean wavelength λ_m is the wavelength about which the pass band is centered. Of the absorption filters, two types are of interest, the band-pass filters and the colcr conversion filters.

---

[56] SPSE Handbook..., p. 259.

[57] Ibid., p. 302-303.

1. Band-pass filters

The more common band-pass filters are constructed of a gelatin film or colored glass. Those produced by the Eastman Kodak Company are classified by a number series, the "Wratten" numbers. These filters permit transmission of a band of wavelengths, and may be tabulated[58] by mean wavelength λ_m. The Wratten numbers increase approximately with increasing λ_m. Figure 9 above shows representative half-widths for selected filters. An important aspect of a particular filter is its peak transmittance (τ_λ max). Different filtering materials have different spectral transmittances at different frequencies. Thus one obtains a transmittance curve for a given filter similar to Figure 53. The differences in peak transmittance among the various filters gives rise to the requirement that different times be used to obtain equal negative density (D) when using filters with different peak transmittances. For example,[59] a Wratten 18A filter has a τ_λ max of 0.62 while a

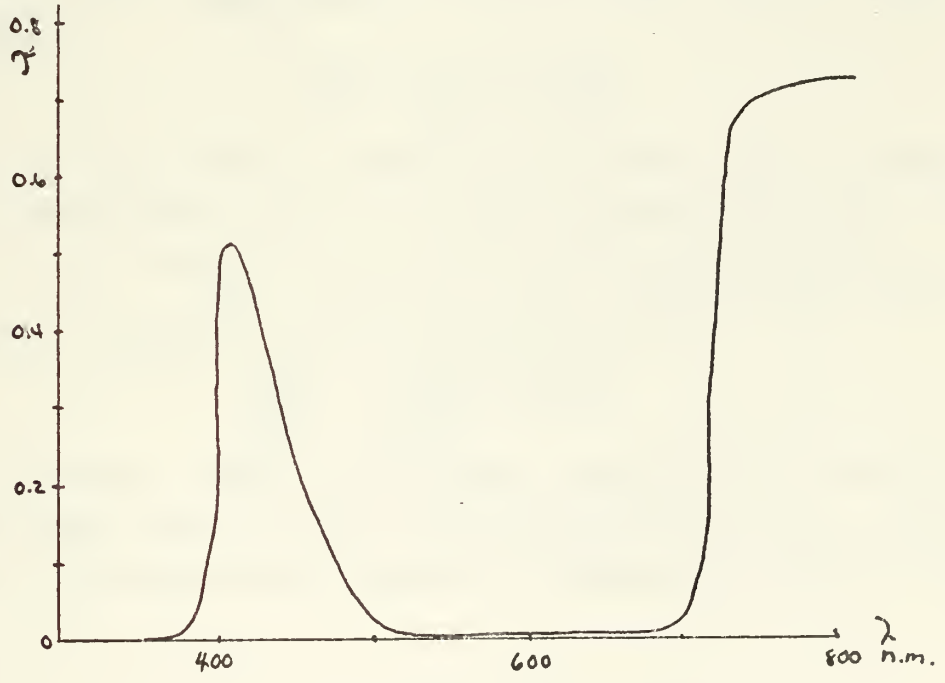

Figure 53
Transmittance of a Wratten 47 Filter

---

[58] Ibid., p. 308-309.

[59] Ibid.

Wratten 99 filter has a τ_λ max of 0.20 (approximately). Then to obtain an equal exposure at their respective should require an exposure time three times as long with the Wratten 99 filter as with the Wratten 18A. The approximate values of τ_λ max for Wratten 47B and 61 filters are respectively, .50 and .40 indicating exposure times of 1.25 longer for the green (Wratten 61) filter.

2. Color Conversion Filters

The need for matching color balances between film and source to render "natural" colors in the image is satisfied through use of color conversion filters, which adjust intensities of incoming light to provide a wavelength intensity distribution which matches the sensitivity distribution of the film in such a way as to cause the source-film system to have an overall sensitivity similar to that of the eye.[60] There exists a series of filters designed to provide this spectral shift. Each of the series is rated by its mired shift value. This value (MSV) is given by[61]

$$MSV = \frac{10^6}{T_2} - \frac{10^6}{T_1}$$

where T_1 is the color temperature of the source and T_2 is color temperature of the light transmitted by the filter (MIRED is an acronym for million-reciprocal-degrees). For example, if a film which has been balanced for 5600°K is used with a 4800°K source a mired shift of

$$\frac{10^6}{5600} - \frac{10^6}{4800} = -29.76$$

is indicated. This corresponds roughly to a Wratten 82B filter, whose Mired Shift Value is given as -32.[62] Thus an increase in temperature requires a decrease in Mired Value.

---

[60] Engel, p. 44.

[61] SPSE Handbook..., p. 312-317.

[62] Ibid., p. 315.

POLAROID CORPORATION
CAMBRIDGE, MASSACHUSETTS 02139

Thank you for calling us on the Polaroid Technical Assistance telephone line.

Enclosed is the literature we discussed. I trust that you will find it informative. If you have any questions in this area, or if you would like help with any other Polaroid industrial product, film or application, please call us again on our "Hot Line."

We appreciate your interest in Polaroid photographic products.

Sincerely,

In response to your questions regarding the slope and resolution of Polacolor film, I am pleased to pass on the following information:

Slope (of the neutral column measured between .3 and .7 densities using #92, 93 and 94 Wratten Status A Filters)

Red - 1.32 ± .15

Green - 1.40 ± .15

Blue - 1.24 ± .15

Resolution (contact print) - 13 line pairs/mm

I hope that this data along with the spectral sensitivity information given to you over the phone will prove helpful in your work.

The attached H&D curve is representative of the Type 108 Polacolor film as measured by the Polaroid system. The initial step on the horizontal exposure axis has an exposure of two meter candle seconds from a xenon strobe light source filtered to represent average outdoor daylight. The exposure scale is in density units (logarithmic scale) so the exposure at 1.0 density would be 0.2 m.c.s. The vertical scale is the sample density as measured on a reflection densitometer.

The spectral sensitivity data attached is from a study done in our laboratories several years ago, using a non-equal energy spectrophotometer on separate film samples for each wavelength measurement. The data is plotted as a function of wavelength against the log of the number of incident photons per square centimeter to reach a 1.0 density on the positive. Although we do not have an estimate of the error involved in this technique, the data is a reasonable representation. Subsequent to this study, a modification of the negative has been introduced into the product to reduce the green sensitivity in the UV and blue region of the spectrum.

Both pieces of attached data are from single film lots representative of the Type 108 Polacolor product. As such, they should not be misconstrued as an average result nor as a product specification.

Log (Number of Photons/sq cm to Reach 1.0 Read Out
Green Read Out
Blue Read Out
Green Read Out
Red Read Out
Wavelength in
Sensitivity

APPENDIX C
COMPUTER PROGRAM

A. DISCUSSION

Program PWRCK computes the values of power versus corner to monopole ($C\lambda$) and monopole to probe (K,λ) distances as described in section V. C. 2. The data thus computed is displayed as either a two- or three- dimensional plot. The type of plot generated depends on the parameters IC and IK. If either of these is set equal to the integer 1, a 2-D plot shall be generated. Otherwise a 3-D plot is generated.

Since the purpose is to provide flexibility in computation there is necessarily a finite complexity to the program. This primarily comprises determining the various parameters of interest and inserting them in the program. Insertion, rather than reading, of the values has been selected for two reasons. First, computer time is reduced, and second, once set, the majority of the parameters are not likely to be changed.

Only one other user interaction is required besides setting parameter values. That is the task (unavoidable in FORTRAN) of explicitly defining the size of the arrays. Three sets of arrays must be DIMENSIONed. The first deals with the power computations. The second deals with plot scaling for three dimensional plots. The third set affects the output routines but is fixed and does not require user interaction. Procedures are described below.

B. PARAMETERS TO BE PROVIDED

The following values are required for all types of output:

CAPH = CAP H = Monopole length H in centimeters

CLMDA = Lambda = Radiation frequency's wavelength (λ) in centimeters

IC = number of data points computed for each P versus C curve

IK = number of data points computed for each P versus K curve

L2 = number of integration steps per datum point

RC = magnitude (always positive) of the complex reflection coefficient Γ.

ARC = phase angle of in degrees

Y1 = initial monopole to probe distance $K_1\lambda$ in centimeters

YMAX = largest value of K,λ in centimeters by which data is to be computed

DY = Interval in K,λ in centimeters by which data points are to be separated

EZO = an arbitrary scale value

D = Initial corner to monopole distance $C\lambda$ in centimeters

DMAX = largest value of $C\lambda$ in centimeters for which data is to be computed

DD = Interval in $C\lambda$ in centimeters by which data points are to be separated

Z = Probe length ($S\lambda$) in centimeters

DZ = Integration interval in Z with which Simpson's rule integration is performed

TTL = a 96 character alpha-numeric title to be read in on two successive cards, with 48 characters (blanks included) per card

C. DETERMINATION OF PARAMETERS

1. Defined parameters

Certain parameters are defined in metric units

CAPH
CLMDA
RC
ARC
Y1
EZO
D
YMAX
DMAX
Z

Note that YMAX and DMAX are not explicitly required by the program.

2. Derived Parameters

In all of the derivations the issue is to determine the interval between computations in each dimension (DY, DD, DZ) which gives the smoothest results. The computer must

also be told the number of such steps (IK, IC, L2) which are being taken. There is no way to avoid mental gymnastics in deriving these values since one must be determined on the basis of the other in an iterative manner. It is considered that this is most efficiently done off-line, as described with the below formulas. It is worthwhile to note that there is always one more in the number of data points than in the number of intervals in a range, since one must account for the very first (zero-interval) computation. On these bases the following formulas generate the required derived parameters.

$$IC = \frac{DMAX - 1}{DD} + 1 \qquad DD = \frac{DMAX - DD}{IC - 1}$$

$$IK = \frac{YMAX - Y1}{DY} + 1 \qquad DY = \frac{DMAX - DD}{IK - 1}$$

$$L2 = \frac{Z}{DZ} + 1 \qquad DZ = \frac{Z}{L2 - 1}$$

D. SAMPLE PROBLEMS

The three sample problems demonstrate the use of the program.

1. Two Dimensional Plot (Power vs Y_1 for fixed D)

Consider a problem in which a two dimensional plot is desired of Power versus Y_1 for a fixed value of Cλ with a given reflection coefficient -.4$\angle$-45°. Refer to Figures 17 and 18 as desired. A wavelength of 20cm (corresponding to a frequency of 1.5 GHz) is selected with a fixed Corner-to- Monopole distance of 5cm, probe length of 2cm and monopole length (λ/4) of 5cm. Initial value of Y_1 is 2cm and data is desired out to one wavelength away from the monopole.

a. Defined parameters from this problem statement are

```
CAPH = 5.0
CLMDA = 20.
RC = 0.4
ARC = 135.
Y1 = 2.
EZO = 30.
D = 5.
YMAX = 20.
DMAX = 5.
```

$$Z = 2.$$

b. Derived Parameters

Only a single curve is desired, and there is a single value of D, thus IC = 1. In order to get a smooth plot it is likely that an interval of about 20 points per inch should give a smooth curve. But to allow easy graduation of the axes one ought to have some metric relationship between intervals and the range YMAX - Y. Since in this case YMAX - Y is 18cm., a choice of 90 intervals is suggested, giving

$$\frac{90}{DY} = YMAX - Y \text{ so that } IK = 91$$

Similarly, a choice of approximately 100 integration steps results in L2 = 101. From these we obtain

IC = 1
IK = 91
L2 = 101
DD = 1.0
DY = 0.2
DZ = 0.02

With these parameters inserted and the title cards (TTL) appended in the conventional manner as data cards, the listing on page 105 results in the 5" x 3" plot of Figure 54.

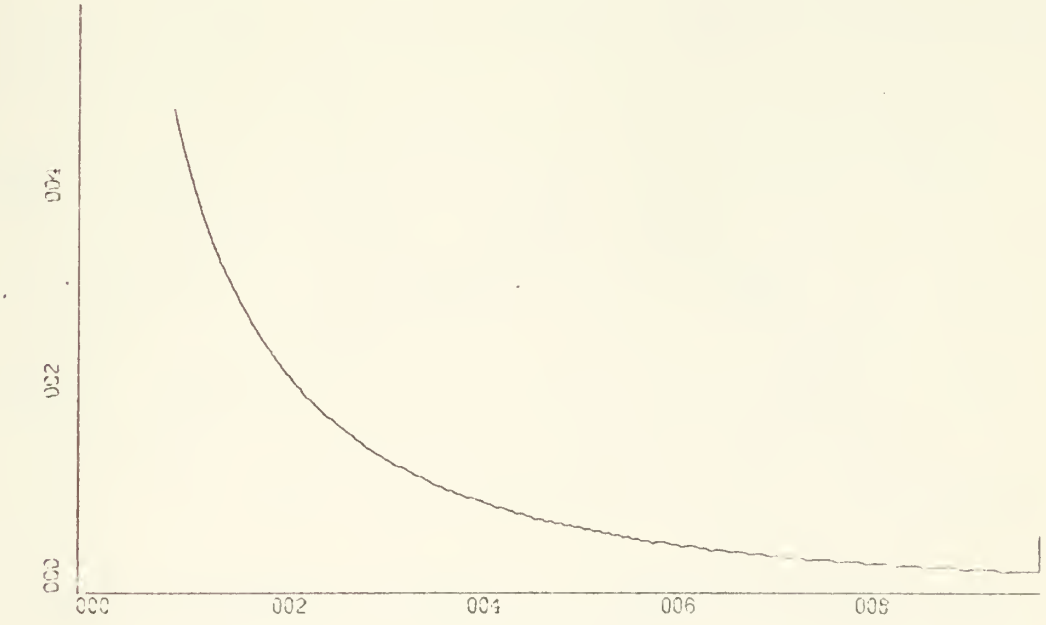

Figure 54

2. Two Dimensional Plot (Power versus D for fixed Y)

a. Defined Parameters

In this case, using the same scenario as (1) above, but plotting versus the other parameter requires only the change in Y1 and D. For example if a fixed probe distance Y1 of 18cm were selected and the initial corner distance D were selected to be 2cm, the two cards changed would be

```
Y1 = 18.0
D = 2.0
```

b. Derived parameters

Since the intervals involved have not changed, that is, probelength is the same, and the data line is still 18cm. The computations are conceptually identical with the first problem. Axes have changed, so the intervals and counters change

```
IC = 91
IK = 2
L2 = 101
DD = 0.2
DY = 1.0
DZ = 0.2
```

The resulting plot is shown in Figure 55.

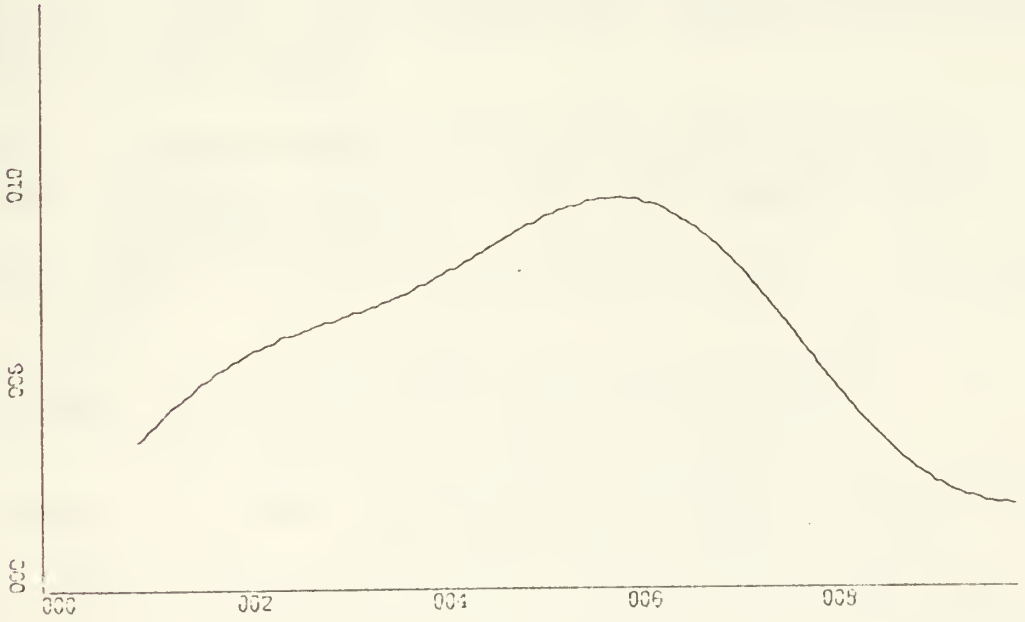

Figure 55

3. Three Dimensional Plot (Power versus Y, and D)

a. Combining the reasoning of the first two problems one might choose

```
Y1 = 2.0
D = 2.0
```

b. Derived Parameters

Now, unfortunately the number of computations has been squared unless some adjustment is made. The three dimensional plot is desireable primarily as an aid to visualization rather than for scientific accountability, so it is reasoned that a less precise plot is acceptable. Here two intervals per centimeter of data range is considered adequate. Similarly, the number of integration steps are reduced, so that

```
IC = 37
IK = 37
L2 = 51
DD = 0.5
DY = 0.5
DZ = 0.04
```

c. For the three dimensional plot, some additional user interaction is required by the plotting subroutine. These are described in detail in the Technical Memorandum for PLD3D1 available from the Computer Center Consultant Staff. This program has reduced the parameters thereof tc three items.

NKXY - a "magic number" which is determined by PLT3D1

ALPHA - rotation angle of the 3-D surface about a horizontal axis

BETA - rotation angle of the surface about a vertical axis

These three values are to be read in when provided in the abcve order in an (I10, 2F10.3) Fortran FORMAT.

(1) Initially NKXY is set to -1 and entered in column 9. ALPHA and BETA must be set to their desired value. The program provides two output plots, so two data cards must be provided. It is suggested that the angles be selected initially to be 15° and 15° respectively for ALPHA,

15° and 75° respectively for BETA. Accordingly the data cards should appear as

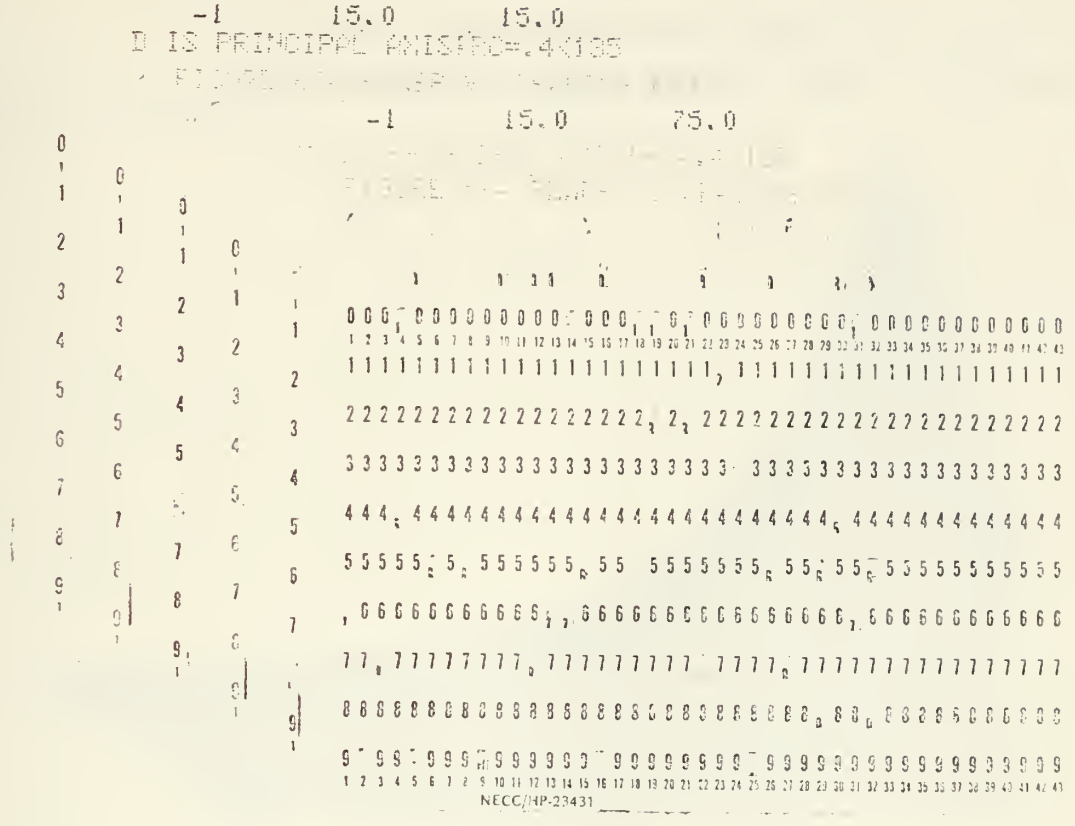

(2) When run, the program will define the required value of NKXY as follows

```
 ALPHA= 15.0      BETA= 15.0

 PLT3D1 WILL PRODUCE AN ISOMETRIC PROJECTION OF THE
 INPUT SURFACE

 THE VALUE OF NKXY FOR THIS PLOT SHOULD BE     0

 SUBROUTINE PLT3D1 HAS PLOTTED A GRAPH TITLED:

 ***POWER VS CORNER TO MONOPOLE DISTANCE (C) AND     ****
 ***MONOPOLE TO PROBE DISTANCE (K)-(IN WAVELENGTHS) ****
 ALPHA= 15.0      BETA= 75.0

 PLT3D1 WILL PRODUCE AN ISOMETRIC PROJECTION OF THE
 INPUT SURFACE.

 THE VALUE OF NKXY FOR THIS PLOT SHOULD BE     0

 SUBROUTINE PLT3D1 HAS PLOTTED A GRAPH TITLED:

 ***POWER VS CORNER TO MONOPOLE DISTANCE (C) AND     ****
 ***MONOPOLE TO PROBE DISTANCE (K)-(IN WAVELENGTHS) ****
```

At this point the user must set NKXY to the proper values, and check the DIMENSION statement in the program to insure that the arrays KX and KY are at least as large as NKXY.

When these adjustments are made the program is re-run, the resulting output plots shall result as shown in Figures 56 and 57.

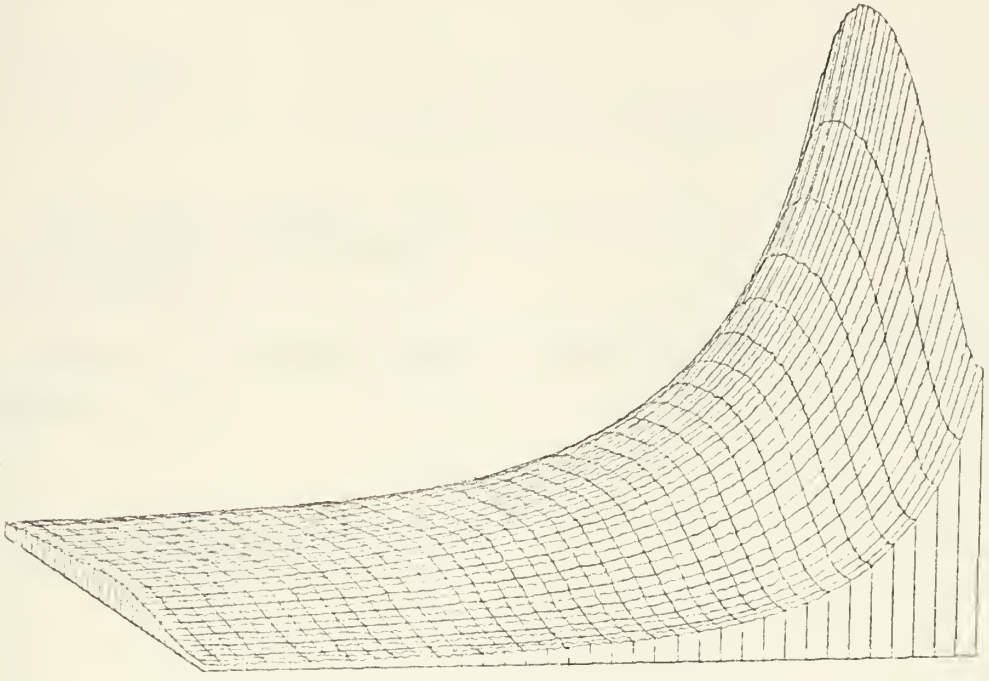

Figure 56

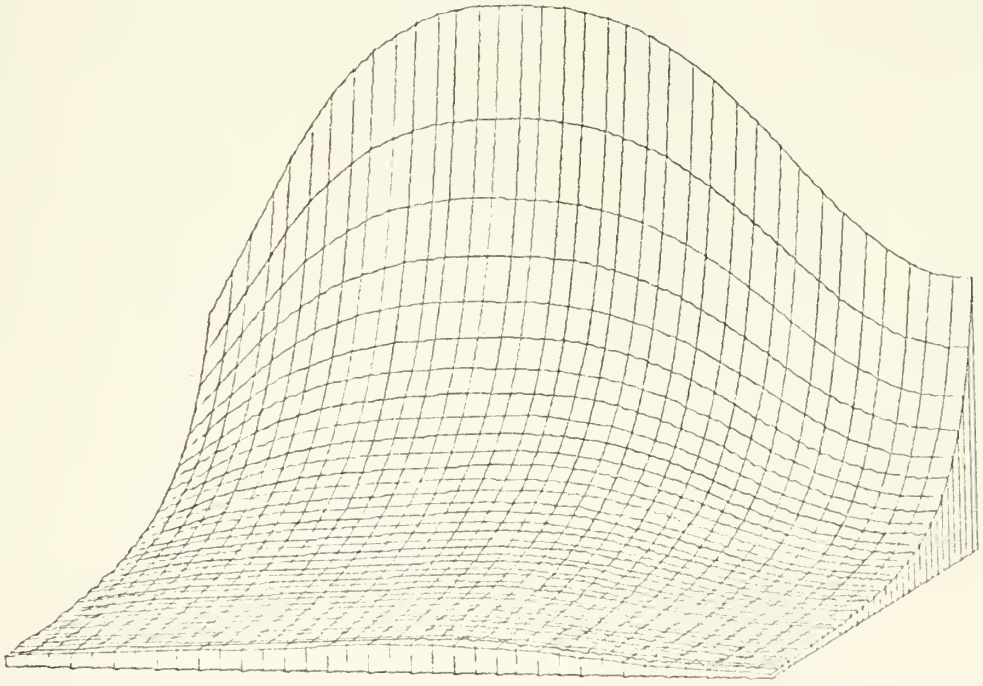

Figure 57

d. Scaling

The program is set up to provide a real valued output in mw for an input current Im of Im = EZO. It may be desired to normalize the plots to a fixed value to allow comparison of curve shapes. This is accomplished by the block of source cards from statements 2000 through 2100 as follows:

```
 2000 CONTINUE
C-------------------------------------------------------C
C                                                       C
C                                                       C
C                                                       C
C-------------------------------------------------------C
      DO 2100, I=1,IC
      P(N,I) = P(N,I)/PRMX
 2100 CONTINUE
```

Other scaling techniques may be substituted for this set of statements.

```
      DIMENSION X(91),KK(91),Y(01),CC(01),P(91,01)
      DIMENSION KX(99),KY(99)
      DIMENSION WK(37,37,3),IDN(37,37),F(2),SIZE(2)
      DIMENSION EZ(6),THTEZ(6),VALK(6)
      EQUIVALENCE (X(1),KK(1)),(Y(1),CC(1))
      REAL*8 TTL (12)
      REAL*4 KK
      LOGICAL*1 IDN
      REAL*4 LAB1 (1)/'    '/
      DATA XCMAX/1.0/,TWOPI/6.2831852/
      DATA SEZMR,SEZMJ,SHRX,SHJX/4*0.0/
C-----------------------------------------------------------------------C
C                                                                       C
C     CAPH=CAP H (MONOPOLE HEIGHT);CLMDA=WAVELENGTH(LAMBDA),ETA=FREESPACE
C     IMPEDANCE                                                         C
C                                                                       C
C-----------------------------------------------------------------------C
      CAPH=5.
      CLMDA=20.
      ETA=377.0
C-----------------------------------------------------------------------C
C                                                                       C
C     INITIALIZE INCREMENT COUNTERS ON CINC(IC), DY(IK) AND DS(L2)      C
C                                                                       C
C-----------------------------------------------------------------------C
      IC=1
      IK=91
      L2=101
C-----------------------------------------------------------------------C
      NROW=IK
      NCOL=IC
      PRMN=1.E 70
      PRMX=0.0
C-----------------------------------------------------------------------C
C                                                                       C
C     INITIALIZE REFLECTION COEFFICIENT (RC) AND ANGLE (ARC)            C
C                                                                       C
C-----------------------------------------------------------------------C
      RC=0.4
```

```
      ARC=135.
C-----------------------------------------------------------------------C
C                                                                       C
C     INITIALIZE MONOPOLE TO PROBE DISTANCE (Y1) AND INCREMENT (DY)     C
C                                                                       C
C-----------------------------------------------------------------------C
      Y1=2.
      DY=0.2
C-----------------------------------------------------------------------C
C                                                                       C
C     SELECT INTEGRATION INCREMENT(DZ)                                  C
C                                                                       C
C-----------------------------------------------------------------------C
      DZ=.02
C-----------------------------------------------------------------------C
C                                                                       C
C     SELECT AN ARBITRARY SCALE VALUE(EZO)                              C
C                                                                       C
C-----------------------------------------------------------------------C
      EZO=30.
C-----------------------------------------------------------------------C
      EZO=EZO/CLMDA
      H=CAPH/CLMDA
      DS=DZ/CLMDA
      ARC=(ARC/360.)*TWOPI
      EZ(1)=EZO
      EZ(2)=EZO*RC
      EZ(3)=EZO*(RC)**2
      EZ(4)=EZ(2)
      EZ(5)=EZ(3)
      EZ(6)=EZ(2)
      THTEZ(1)=0.
      THTEZ(2)=ARC
      THTEZ(3)=2.*ARC
      THTEZ(4)=ARC
      THTEZ(5)=2.*ARC
      THTEZ(6)=ARC
      DO 3000 N=1,IK
      VALK1=Y1/CLMDA
      KK(N)=VALK1
      VALK(1)=VALK1
C-----------------------------------------------------------------------C
C                                                                       C
C     INITIALIZE CORNER TO MONOPOLE DISTANCE (D) AND INCREMENT (DD)     C
C                                                                       C
C-----------------------------------------------------------------------C
      D=5.
      DD=1.
```

```
C-----------------------------------------------------------------------C
C                                                                       C
C     CORNER TO DRIVEN ELEMENT DISTANCE (C) IS COMPUTED                 C
C                                                                       C
C-----------------------------------------------------------------------C
      DO 2000 I=1,IC
      C=D/CLMDA
      CC(I)=C
C-----------------------------------------------------------------------C
C                                                                       C
C     COMPUTE K(M)                                                      C
C                                                                       C
C-----------------------------------------------------------------------C
      WORK=C**2+(C*VALK1)+VALK1**2
      VALK(2)=SQRT(WORK)
      WORK=(3.*C**2)+(3.*C*VALK1)+VALK1**2
      VALK(3)=SQRT(WORK)
      VALK(4)=2.*C+VALK1
      VALK(5)=VALK(3)
      VALK(6)=VALK(2)
      WALFA=(VALK1**2+(2.0*VALK1*C))/(2.0*(VALK1+C))
C-----------------------------------------------------------------------C
C                                                                       C
C     S = HEIGHT ABOVE PLANE, INCREMENTED BY H FROM 0 TO 1/CLMDA        C
C                                                                       C
C-----------------------------------------------------------------------C
      S=0.0
      DO 1900 L=1,L2
C-----------------------------------------------------------------------C
C                                                                       C
C     COMPUTE R1M, R2M, PR, SUM OF PR                                   C
C                                                                       C
C-----------------------------------------------------------------------C
      DO 1000 M=1,6
      WKKM=VALK(M)
      ALFA=ARCOS((WALFA/WKKM)+(WKKM/(2.0*(VALK1+C))))
      WORK1=WKKM**2+S**2+H**2
      WORK2=WORK1-(2.0*H*S)
      VALR1=SQRT(WORK2)
      WORK2=WORK1+(2.0*H*S)
      VALR2=SQRT(WORK2)
      RHO=SQRT(S**2+WKKM**2)
      PHI1M=TWOPI*VALR1
      PHI2M=TWOPI*VALR2
      PHI3M=TWOPI*H
      PHI4M=TWOPI*RHO
      SP1M=SIN(PHI1M)
      SP2M=SIN(PHI2M)
```

```
      SP4M=SIN(PHI4M)
      CP1M=COS(PHI1M)
      CP2M=COS(PHI2M)
      CP3M=COS(PHI3M)
      CP4M=COS(PHI4M)
      CALFA=COS(ALFA)
      EZMRE=1.00000*((SP1M/VALR1)+(SP2M/VALR2)-((2.0*CP3M*SP4M)/RHO))
      EZMJ=1.000*((CP1M/VALR1)+(CP2M/VALR2)-((2.0*CP3M*CP4M)/RHO))
      EZM=(SQRT(EZMRE**2+EZMJ**2))*EZ(M)
      THTZM=ATAN2(EZMJ,EZMRE)+THTEZ(M)
      EZMRE=EZM*COS(THTZM)
      EZMJ=EZM*SIN(THTZM)
      HREAL=(1.000/(WKKM*ETA))*(SP1M+SP2M-(2.0*CP3M*CP4M))
      HJ=(1.000/(WKKM*ETA))*(CP1M+CP2M-(2.0*CP3M*CP4M))
      HM=(SQRT(HREAL**2+HJ**2))*EZ(M)*CALFA
      THTHM=ATAN2(HJ,HREAL)+THTEZ(M)
      HRX=HM*COS(THTHM)
      HJX=HM*SIN(THTHM)
      SEZMR=SEZMR-EZMRE
      SEZMJ=SEZMJ-EZMJ
      SHRX=SHRX+HRX
      SHJX=SHJX+HJX
 1000 CONTINUE
C-----------------------------------------------------------------------C
C                                                                       C
C     INDIVIDUAL FIELD CONTRIBUTIONS ARE NOW COMBINED. FIND RESULTANT POWER
C     MAGNITUDE (PYTM), ANGLE (PYTA) AND REAL PART (SUMPR).             C
C                                                                       C
C-----------------------------------------------------------------------C
      EZT=SQRT((SEZMR**2)+(SEZMJ**2))
      THTZT=ATAN2(SEZMJ,SEZMR)
      HTX=SQRT(SHRX**2+SHJX**2)
      THTHX=ATAN2(SHJX,SHRX)
      PYTM=(-EZT)*HTX
      PYTA=THTZT-THTHX
      SUMPR=(PYTM*COS(PYTA))/2.
C-----------------------------------------------------------------------C
C                                                                       C
C     INITIALIZE FOR NEXT DS CONTRIBUTION. INTEGRATE CURRENT CONTRIBUTION
C     USING SIMPSON'S RULE.                                             C
C                                                                       C
C-----------------------------------------------------------------------C
      SEZMR=0.0
      SEZMJ=0.0
      SHRX=0.0
      SHJX=0.0
      S=S+DS
      IF (L.NE.1) GO TO 1500
```

```
      P(N,I)=SUMPR
      L1=1
      GO TO 1900
 1500 IF (L.EQ.L2) GO TO 1800
      IF (L1.EQ.2) GO TO 1600
      P(N,I)=P(N,I)+(4.*SUMPR)
      L1=L1+1
      GO TO 1900
 1600 P(N,I)=P(N,I)+(2.*SUMPR)
      L1=1
      GO TO 1900
 1800 P(N,I)=((P(N,I)+SUMPR)*DS)/3.
1900  CONTINUE
C-------------------------------------------------------------------------------C
C                                                                               C
C     POINT VALUE IS NOW DETERMINED.  MODIFY FOR SCALING AND INCREMENT D.       C
C                                                                               C
C-------------------------------------------------------------------------------C
      PNI=P(N,I)
      IF (PRMN.GT.PNI) PRMN=PNI
      IF(PRMX.LT.PNI) PRMX=PNI
      D=D+DD
 2000 CONTINUE
C-------------------------------------------------------------------------------C
C                                                                               C
C     C-LINE IS NOW COMPLETE. MODIFY FOR SCALING PURPOSES.                      C
C                                                                               C
C-------------------------------------------------------------------------------C
      DO 2100 I=1,IC
      P(N,I)=P(N,I)/PRMX
2100  CONTINUE
      PRMN=1.E 70
      PRMX=0.
C-------------------------------------------------------------------------------C
C                                                                               C
C     INCREMENT Y1 FOR NEW C-LINE.                                              C
C                                                                               C
C-------------------------------------------------------------------------------C
      Y1=Y1+DY
3000  CONTINUE


C-------------------------------------------------------------------------------C
C                                                                               C
C     NORMALIZE ALL VALUES TO LARGEST VALUE                                     C
C                                                                               C
C-------------------------------------------------------------------------------C
```

```
      DO 3050 I=1,IC
      DO 3045 N=1,IK
      P(N,I)=P(N,I)/PRMX
3045  CONTINUE
3050  CONTINUE
C-----------------------------------------------------------------------C
C                                                                       C
C     ALL POINTS ARE COMPUTED NOW AND STORED IN ARRAY P(N,I).  SELECT PLOT
C     MODE AND GENERATE OUTPUT.
C     YSCL=UNITS PER INCH FOR SUBROUTINE DRAW
C                                                                       C
C-----------------------------------------------------------------------C
      YSCL=PRMX/3.
C-----------------------------------------------------------------------C
C                                                                       C
C     READ 96-CHARACTER TITLE ON TWO CARDS (48 CHARACTERS EACH) INTO ARRAY TTL
C                                                                       C
C-----------------------------------------------------------------------C
      IF ((IC.NE.1).AND.(IK.NE.1)) GO TO 3125
      READ (5,3100) TTL
 3100 FORMAT(6A8)
      WRITE (6,3101)
 3101 FORMAT('1')
      WRITE (6,3102) TTL
 3102 FORMAT (' ',6A8)
      IF (IC.EQ.1) GO TO 5000
      IF (IK.EQ.1) GO TO 6000
 3125 F(1)= 1.E 10
      F(2)= 1.E 10
      SIZE(1)=5.
      SIZE(2)=3.5
      LINES=0
      DO 4000 K=1,4
      READ (5,3100) TTL
      READ (5,3150) NKXY,ALPHA,BETA
3150  FORMAT (I10,2F10.3)
      WRITE (6,3500) ALPHA,BETA
3500  FORMAT (' ','ALPHA=',F5.1,5X,'BETA=',F5.1)
      CALL PLT3D1(X,NROW,Y,NCOL,P,ALPHA,BETA,F,TTL,SIZE,WK,IDN,KX,KY,
     1NKXY,LINES)
4000  CONTINUE
      GO TO 7000
C-----------------------------------------------------------------------C
C                                                                       C
C     GENERATE A PLOT OF POWER VS Y1 FOR A FIXED VALUE OF D             C
C                                                                       C
C-----------------------------------------------------------------------C
5000  CONTINUE
```

```
      CALL DRAW(91,KK,P,0,0,LAB1,TTL,0.,YSCL,0,0,0,0,5,3,0,LAST)
      WRITE (6,5250)
 5250 FORMAT('0',2(7X,'KK',9X,'P',7X))
      WRITE (6,5500) (KK(I),P(I,01),I=1,91,5)
 5500 FORMAT(' ',2(1F10.3,3X,1F10.6,3X))
      WRITE (6,5501)
 5501 FORMAT('0','END OF JOB')
      WRITE (6,5502)
 5502 FORMAT('1')
      GO TO 7000
C-----------------------------------------------------------------------C
C                                                                       C
C     GENERATE A PLOT OF POWER VS D FOR A FIXED VALUE OF Y1             C
C                                                                       C
C-----------------------------------------------------------------------C
 6000 CONTINUE
      CALL DRAW(91,CC,P,0,0,LAB1,TTL,0.,YSCL,0,0,0,0,5,3,0,LAST)
      WRITE (6,6250)
 6250 FORMAT('0',2(7X,'CC',9X,'P',7X))
      WRITE (6,5500) (CC(I),P(01,I),I=1,91,5)
      WRITE (6,5501)
      WRITE (6,5502)
 7000 STOP
      END
```

APPENDIX D
MATHEMATICAL PROCEDURES

A. STATISTICAL METHODS

Data presented from the various experiments are identified as "average values" derived from the stated number of runs on the experiments. The following algorithms were used to obtain the various statistical values referred to in the text:

1. Average Value ($\bar{x}$) of a set $\{x_1, x_2, \ldots, x_N\}$:

$$\bar{x} = \sum_{i=1}^{N} x_i$$

2. Standardard Deviation (Sx) is used to characterize the accuracy of a particular average:

$$Sx = \sqrt{\frac{\sum_{i=1}^{N} x_i^2 - N\bar{x}^2}{n - 1}}$$

3. Average Standard Deviation ($\bar{Sx}$) is used to characterize the overall accuracy of a curve, each point of which is an average value with its attendant standard deviation. It is the average of those standard deviations:

$$\bar{Sx} = \frac{1}{M} \sum_{j=1}^{M} Sx_j$$

B. CURVE FITTING

1. Temperature Curves

Temperature Curves were fitted with a French curve passing through the average data points for the given set of conditions.

2. Density Curves

Density curves in Figures 37 and 38 were adjusted within one half a standard deviation on either side of the averaged datum point. These restrained adjustments in one

dimension were necessary to obtain consistency in the other planar dimension. Figure 58 shows the technique used. Averaged data points were plotted with a line showing a width equal to one standard deviation centered on the datum point. Straight lines connecting these limits created a "channel" (the hatched region) within which adjustment was allowed. Thus figures 37 through 40 show values obtained within one half a standard deviation of the mean experimental values with quasi-linear interpolation between data points.

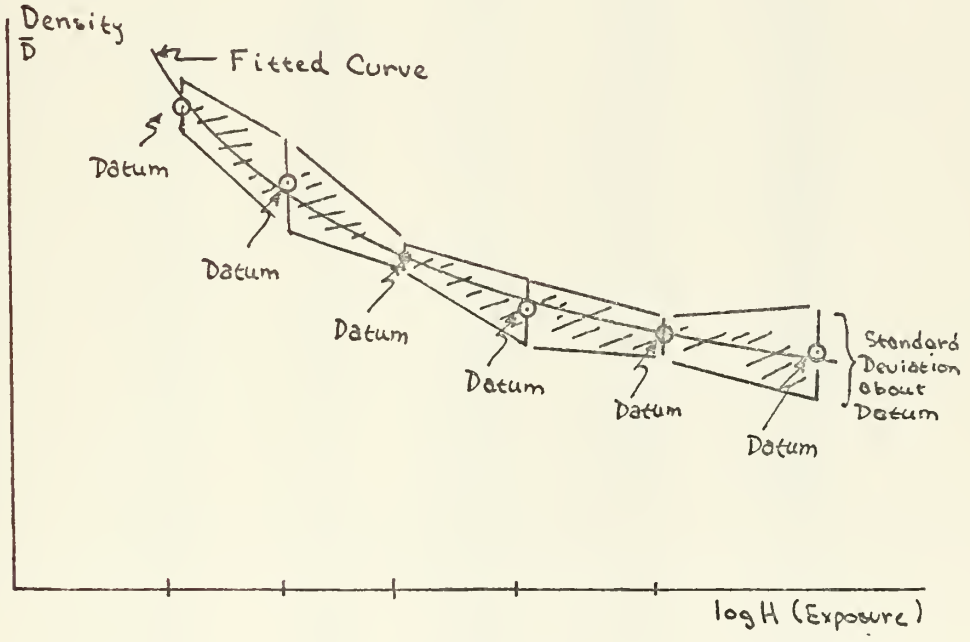

Figure 58
Region of Likely Values about a Datum Point

APPENDIX E

SMOOTH EXPERIMENTAL DATA

t sec \ Figure	26	27	30	31	32
0	22	-35	22.0	20.8	-48.8
5	20	-34	17.0	17.0	-43.3
10	15	-32	13.7	11.0	-34.0
15	10	-30	11.3	5.4	-29.6
20	6	-28	6.7	0.8	-23.3
25	3	-26	4.0	-3.6	-11.0
30	-1	-25	1.7	-8.0	-6.3
35	-4	-23	-0.3	-11.4	-2.3
40	-6	-22	-2.3	-15.0	0.5
45	-9	-22	-4.3	-18.4	2.8
50	-11	-21	-6.0	-22.0	4.5
55	-13	-21	-7.7	-25.4	6.3
1^m	-15	-21	-9.3	-28.0	7.5
5	-16	-21	-10.7	-31.0	8.5
10	-18	-21	-13.0	-33.6	9.8
15	-19	-21	-13.7	-36.0	10.8
20	-20	-21	-15.0	-38.6	11.3
25	-21	-21	-16.0	-41.0	12.3
30	-22	-21	-17.0	-43.0	12.5
35	-23	-21	-18.3	-45.0	13.5
40	-24	-21	-19.3	-46.8	13.8
45	-25	-21	-20.3	-48.6	13.8
50	-26	-21	-21.3	-50.0	14.5
55	-27	-21	-22.3	-51.6	14.8
2^m	-27	-22	-23.3	-53.2	14.8
5	-28	-22	-24.0	-54.4	15.8
10	-28	-22	-24.3	-56.2	15.8
15	-29	-22	-25.3	-57.5	15.8
20	-29	-22	-26.3	-58.8	16.0
25	-29	-23	-26.3	-59.8	16.8

t \ Figure	26	27	30	31	32
30	-30	-23	-27.3	-61.2	16.8
35	-30	-23	-28.0	-62.0	16.8
40	-30	-24	-28.3	-63.0	16.8
50	-31	-24	-29.3	-64.6	17.0
55	-31	-25	-29.7	-65.4	17.0
3^m	-32	-25	-30.3	-66.0	17.8
5	-32	-25	-30.7	-66.4	17.8
10	-32	-25	-31.3	-67.2	17.8
15	-32	-25	-31.7	-68.0	17.8
20	-32	-26	-32.3	-68.8	17.8
25	-32	-26	-32.3	-69.4	17.8
30	-32	-26	-32.7	-70.0	18.8
35	-32	-26	-33.0		18.8
40	-32	-26	-33.3		18.8
45	-33	-26	-33.7		18.8
50	-33	-27	-33.7		18.8
55	-33	-27	-34.0		18.8
4^m	-33	-27	-34.3		18.8
			Note (1)	Note (2)	Note (3)

Note (1) - Average of 3 data points
Avg.std deviation is 2°.39.

Note(2) - Average of 5 data points
Avg. std deviation is 2°.17.

Note (3) - Average of 4 data points
Avg. std deviation is 1°.4.

Figure 37

Blue	Green	D
-2.0	-1.7	.3580
-1.9	-1.7	.3575
-1.8	-1.7	.3565
-1.7	-1.7	.3555
-1.6	-1.7	.3540
-1.5	-1.7	.3530
-1.4	-1.7	.3515
-1.3	-1.7	.3500
-1.2	-1.7	.3480
-1.1	-1.7	.3460
-1.0	-1.7	.3440
-0.9	-1.7	.3405
-0.8	-1.7	.3375
-0.7	-1.7	.3335
-0.6	-1.7	.3320
-0.5	-1.7	.3300
-0.4	-1.7	.3280
-0.3	-1.7	.3265
-0.2	-1.7	.3250
-0.1	-1.7	.3230
0.0	-1.7	.3215
0.1	-1.7	.3200
0.2	-1.7	.3180
0.3	-1.7	.3165
0.4	-1.7	.3145
0.5	-1.7	.3125
0.6	-1.7	.3100
-2.0	-1.6	.3535
-1.7	-1.6	.3505
-1.4	-1.6	.3450
-1.0	-1.6	.3400

Blue	Green	$\bar{D}$
-0.7	-1.6	.3295
-0.3	-1.6	.3225
0.0	-1.6	.3155
0.3	-1.6	.3115
0.6	-1.6	.3040
-2.0	-1.5	.3500
-1.7	-1.5	.3475
-1.4	-1.5	.3400
-1.0	-1.5	.3340
-0.7	-1.5	.3255
-0.3	-1.5	.3180
0.0	-1.5	.3105
0.3	-1.5	.3070
0.6	-1.5	.2965
-2.0	-1.4	.3470
-1.9	-1.4	.3465
-1.8	-1.4	.3460
-1.7	-1.4	.3445
-1.6	-1.4	.3410
-1.5	-1.4	.3375
-1.4	-1.4	.3350
-1.3	-1.4	.3330
-1.2	-1.4	.3310
-1.1	-1.4	.3300
-1.0	-1.4	.3285
-0.9	-1.4	.3260
-0.8	-1.4	.3235
-0.7	-1.4	.3210
-0.6	-1.4	.3185
-0.5	-1.4	.3170
-0.4	-1.4	.3155
-0.3	-1.4	.3140
-0.2	-1.4	.3120
-0.1	-1.4	.3100

Blue	Green	D
0.0	-1.4	.3075
0.1	-1.4	.3060
0.2	-1.4	.3035
0.3	-1.4	.3025
0.4	-1.4	.2980
0.5	-1.4	.2940
0.6	-1.4	.2900
-2.0	-1.3	.3435
-1.7	-1.3	.3425
-1.4	-1.3	.3330
-1.0	-1.3	.3265
-0.7	-1.3	.3170
-0.3	-1.3	.3100
0.0	-1.3	.3015
0.3	-1.3	.2990
0.6	-1.3	.2850
-2.0	-1.2	.3415
-1.7	-1.2	.3405
-1.4	-1.2	.3315
-1.0	-1.2	.3225
-0.7	-1.2	.3130
-0.3	-1.2	.3050
0.0	-1.2	.2980
0.3	-1.2	.2960
0.6	-1.2	.2800
-2.0	-1.1	.3405
-1.7	-1.1	.3380
-1.4	-1.1	.3300
-1.0	-1.1	.3185
-0.7	-1.1	.3090
-0.3	-1.1	.3005
0.0	-1.1	.2940
0.3	-1.1	.2915
0.6	-1.1	.2755

Blue	Green	$\bar{D}$
-2.0	-1.0	.3395
-1.9	-1.0	.3390
-1.8	-1.0	.3370
-1.7	-1.0	.3350
-1.6	-1.0	.3330
-1.5	-1.0	.3305
-1.4	-1.0	.3280
-1.3	-1.0	.3245
-1.2	-1.0	.3205
-1.1	-1.0	.3165
-1.0	-1.0	.3130
-0.9	-1.0	.3095
-0.8	-1.0	.3070
-0.7	-1.0	.3040
-0.6	-1.0	.3020
-0.5	-1.0	.3000
-0.4	-1.0	.2980
-0.3	-1.0	.2960
-0.2	-1.0	.2945
-0.1	-1.0	.2930
0.0	-1.0	.2910
0.1	-1.0	.2890
0.2	-1.0	.2865
0.3	-1.0	.2865
0.4	-1.0	.2810
0.5	-1.0	.2770
0.6	-1.0	.2740
-2.0	-0.9	.3385
-1.7	-0.9	.3325
-1.4	-0.9	.3220
-1.0	-0.9	.3070
-0.7	-0.9	.2995
-0.3	-0.9	.2890
0.0	-0.9	.2855

Blue	Green	D
0.3	-0.9	.2800
0.6	-0.9	.2690
-2.0	-0.8	.3365
-1.7	-0.8	.3290
-1.4	-0.8	.3150
-1.0	-0.8	.3010
-0.7	-0.8	.2940
-0.3	-0.8	.2830
0.0	-0.8	.2800
0.3	-0.8	.2730
0.6	-0.8	.2665
-2.0	-0.7	.3340
-1.9	-0.7	.3310
-1.8	-0.7	.3275
-1.7	-0.7	.3235
-1.6	-0.7	.3190
-1.5	-0.7	.3140
-1.4	-0.7	.3085
-1.3	-0.7	.3035
-1.2	-0.7	.2995
-1.1	-0.7	.2960
-1.0	-0.7	.2935
-0.9	-0.7	.2915
-0.8	-0.7	.2890
-0.7	-0.7	.2875
-0.6	-0.7	.2845
-0.5	-0.7	.2825
-0.4	-0.7	.2805
-0.3	-0.7	.2785
-0.2	-0.7	.2765
-0.1	-0.7	.2745
0.0	-0.7	.2725
0.1	-0.7	.2700
0.2	-0.7	.2680

Blue	Green	$\bar{D}$
0.3	-0.7	.2660
0.4	-0.7	.2640
0.5	-0.7	.2630
0.6	-0.7	.2615
-2.0	-0.6	.3275
-1.7	-0.6	.3200
-1.4	-0.6	.2995
-1.0	-0.6	.2890
-0.7	-0.6	.2825
-0.3	-0.6	.2745
0.0	-0.6	.2690
0.3	-0.6	.2620
0.6	-0.6	.2600
-2.0	-0.5	.3195
-1.7	-0.5	.3140
-1.4	-0.5	.2925
-1.0	-0.5	.2840
-0.7	-0.5	.2785
-0.3	-0.5	.2710
0.0	-0.5	.2660
0.3	-0.5	.2590
0.6	-0.5	.2545
-2.0	-0.4	.3130
-1.7	-0.4	.3080
-1.4	-0.4	.2860
-1.0	-0.4	.2800
-0.7	-0.4	.2750
-0.3	-0.4	.2650
0.0	-0.4	.2610
0.3	-0.4	.2585
0.6	-0.4	.2495
-2.0	-0.3	.3080
-1.9	-0.3	.3060
-1.8	-0.3	.3030

Blue	Green	D
-1.7	-0.3	.3015
-1.6	-0.3	.2930
-1.5	-0.3	.2865
-1.4	-0.3	.2820
-1.3	-0.3	.2790
-1.2	-0.3	.2770
-1.1	-0.3	.2760
-1.1	-0.3	.2760
-1.0	-0.3	.2750
-0.9	-0.3	.2735
-0.8	-0.3	.2725
-0.7	-0.3	.2710
-0.6	-0.3	.2695
-0.5	-0.3	.2680
-0.4	-0.3	.2665
-0.3	-0.3	.2650
-0.2	-0.3	.2630
-0.1	-0.3	.2615
0.0	-0.3	.2595
0.1	-0.3	.2575
0.2	-0.3	.2550
0.3	-0.3	.2530
0.4	-0.3	.2505
0.5	-0.3	.2480
0.6	-0.3	.2440
-2.0	-0.2	.3045
-1.7	-0.2	.2995
-1.4	-0.2	.2790
-1.0	-0.2	.2715
-0.7	-0.2	.2685
-0.3	-0.2	.2620
0.0	-0.2	.2565
0.3	-0.2	.2510
0.6	-0.2	.2415
-2.0	-0.1	.3020

Blue	Green	D
-1.7	-0.1	.2960
-1.4	-0.1	.2755
-1.0	-0.1	.2690
-0.7	-0.1	.2655
-0.3	-0.1	.2595
0.0	-0.1	.2550
0.3	-0.1	.2485
0.6	-0.1	.2385
-2.0	0.0	.3005
-1.9	0.0	.2985
-1.8	0.0	.2955
-1.7	0.0	.2930
-1.6	0.0	.2850
-1.5	0.0	.2790
-1.4	0.0	.2750
-1.3	0.0	.2715
-1.2	0.0	.2685
-1.1	0.0	.2670
-1.0	0.0	.2660
-0.9	0.0	.2650
-0.8	0.0	.2645
-0.7	0.0	.2630
-0.6	0.0	.2615
-0.5	0.0	.2600
-0.4	0.0	.2585
-0.3	0.0	.2570
-0.2	0.0	.2550
-0.1	0.0	.2530
0.0	0.0	.2520
0.1	0.0	.2500
0.2	0.0	.2480
0.3	0.0	.2460
0.4	0.0	.2430

Blue	Green	D
0.5	0.0	.2395
0.6	0.0	.2350
-1.7	0.1	.2900
-1.4	0.1	.2715
-1.0	0.1	.2630
-0.7	0.1	.2600
-0.3	0.1	.2535
0.0	0.1	.2485
0.3	0.1	.2430
0.6	0.1	.2315
-2.0	0.2	.2960
-1.7	0.2	.2870
-1.4	0.2	.2685
-1.0	0.2	.2610
-0.7	0.2	.2570
-0.3	0.2	.2500
0.0	0.2	.2450
0.3	0.2	.2390
0.6	0.2	.2275
-2.0	0.3	.2930
-1.9	0.3	.2910
-1.8	0.3	.2880
-1.7	0.3	.2840
-1.6	0.3	.2790
-1.5	0.3	.2715
-1.4	0.3	.2660
-1.3	0.3	.2630
-1.2	0.3	.2615
-1.1	0.3	.2600
-1.0	0.3	.2590
-0.9	0.3	.2570
-0.8	0.3	.2550
-0.7	0.3	.2535
-0.6	0.3	.2520

Blue	Green	D
-0.5	0.3	.2500
-0.4	0.3	.2480
-0.3	0.3	.2460
-0.2	0.3	.2445
-0.1	0.3	.2430
0.0	0.3	.2410
0.1	0.3	.2385
0.2	0.3	.2365
0.3	0.3	.2340
0.4	0.3	.2315
0.5	0.3	.2290
0.6	0.3	.2260

Figure 39

Initial Temp	Radiation Time	Average Density
-30.0	30.0	0.1565
-30.0	32.5	0.1670
-30.0	35.0	0.1790
-30.0	37.5	0.1905
-30.0	40.0	0.2000
-30.0	42.5	0.2105
-30.0	45.0	0.2185
-30.0	47.5	0.2245
-30.0	50.0	0.2290
-30.0	52.5	0.2320
-30.0	55.0	0.2350
-30.0	57.5	0.2380
-30.0	60.0	0.2405
-27.5	30.0	0.1560
-27.5	32.5	0.1670
-27.5	35.0	0.1785
-27.5	37.5	0.1900
-27.5	40.0	0.2010
-27.5	42.5	0.2110
-27.5	45.0	0.2200
-27.5	47.5	0.2275
-27.5	50.0	0.2350
-27.5	52.5	0.2425
-27.5	55.0	0.2465
-27.5	57.5	0.2520
-27.5	60.0	0.2550
-25.0	30.0	0.1540
-25.0	32.5	0.1655
-25.0	35.0	0.1780
-25.0	37.5	0.1900
-25.0	40.0	0.2010

Initial Temp	Radiation Time	Average Density
-25.0	42.5	0.2105
-25.0	45.0	0.2220
-25.0	47.5	0.2300
-25.0	50.0	0.2390
-25.0	52.5	0.2500
-25.0	55.0	0.2550
-25.0	57.5	0.2620
-25.0	60.0	0.2670
-22.5	30.0	0.1520
-22.5	32.5	0.1650
-22.5	35.0	0.1780
-22.5	37.5	0.1900
-22.5	40.0	0.2020
-22.5	42.5	0.2130
-22.5	45.0	0.2245
-22.5	47.5	0.2335
-22.5	50.0	0.2455
-22.5	52.5	0.2550
-22.5	55.0	0.2625
-22.5	57.5	0.2720
-22.5	60.0	0.2770
-20.0	30.0	0.1535
-20.0	32.5	0.1660
-20.0	35.0	0.1800
-20.0	37.5	0.1915
-20.0	40.0	0.2035
-20.0	42.5	0.2160
-20.0	45.0	0.2283
-20.0	47.5	0.2385
-20.0	50.0	0.2500
-20.0	52.5	0.2605
-20.0	55.0	0.2710
-20.0	57.5	0.2810
-20.0	60.0	0.2885

Initial Temp	Radiation Time	Average Density
-17.5	30.0	0.1640
-17.5	32.5	0.1750
-17.5	35.0	0.1880
-17.5	37.5	0.2000
-17.5	40.0	0.2120
-17.5	42.5	0.2240
-17.5	45.0	0.2350
-17.5	47.5	0.2450
-17.5	50.0	0.2550
-17.5	52.5	0.2650
-17.5	55.0	0.2750
-17.5	57.5	0.2840
-17.5	60.0	0.2910
-15.0	30.0	0.1760
-15.0	32.5	0.1870
-15.0	35.0	0.1985
-15.0	37.5	0.2100
-15.0	40.0	0.2220
-15.0	42.5	0.2330
-15.0	45.0	0.2440
-15.0	47.5	0.2535
-15.0	50.0	0.2630
-15.0	52.5	0.2720
-15.0	55.0	0.2805
-15.0	57.5	0.2890
-15.0	60.0	0.2960
-12.5	30.0	0.1900
-12.5	32.5	0.2000
-12.5	35.0	0.2110
-12.5	37.5	0.2220
-12.5	40.0	0.2340
-12.5	42.5	0.2440
-12.5	45.0	0.2545

Initial Temp	Radiation Time	Average Density
-12.5	47.5	0.2630
-12.5	50.0	0.2720
-12.5	52.5	0.2790
-12.5	55.0	0.2865
-12.5	57.5	0.2940
-12.5	60.0	0.2990
-10.0	30.0	0.2020
-10.0	32.5	0.2150
-10.0	35.0	0.2260
-10.0	37.5	0.2365
-10.0	40.0	0.2470
-10.0	42.5	0.2570
-10.0	45.0	0.2660
-10.0	47.5	0.2730
-10.0	50.0	0.2800
-10.0	52.5	0.2860
-10.0	55.0	0.2910
-10.0	57.5	0.2950
-10.0	60.0	0.2990

$C_{\lambda,K,\lambda}$ \ Figure	43	45
6	51.45	10.387
7	66.48	9.582
8	65.86	8.739
9	63.11	8.250
10	59.44	7.438
11	57.56	6.706
12	54.95	6.116
13	51.00	5.206
14	45.55	4.693
15	41.22	4.586
16	35.82	4.380
17	28.95	3.904
18	23.00	3.643
19	15.76	3.400
20	10.72	3.323

$S\bar{x} = 1.436$

APPENDIX F
AGA THERMOVISION EXPERIMENTS

A. DISCUSSION

The author attended a general demonstration of the AGA Thermovision Device Model 750 on 22 July 1975 at NPS. The author recognized the possible application of the device to the objectives of this work, and asked the AGA representative to take part in some simple experiments that afternoon to see if the application of the device was feasible. The representative, Mr. Jack Patterson, agreed to do so. The experiment consisted simply of a Case 1A cross (described below) 10cm from the driven element irradiated with the corner reflector system with the reflector 18cm from the driven element. A Polaroid Print backing cardboard on which was attached a piece of Olde Towne carbon paper was placed next to the cross. The power density arriving at the cross was estimated to be approximately 15 mw/cm^2 and the ambient temperature was 24°C. The Thermovision was focused on the cross, resulting in the image of which Figure 53 is a conventional Polaroid photograph.

Encouraged by these results and after consultations with Professor Burton, arrangements were made for a more extensive and controlled feasibility test. Those experiments, conducted on 17 November 1975, were to determine the feasibility of using the AGA Thermovision System to detect thermal fields induced by electromagnetic fields on an assortment of structures. The form of these experiments was selected to investigate two principal elements considered likely to affect that feasibility. These elements are:

1. Conductivity

The surfaces investigated must be sufficiently conductive to allow current and charge distributions to be established. In particular, current distributions are

necessary in order to generate thermal fields which may be then sensed by the Thermovision System. However, the surfaces must not be so conductive that either (a) no significant heat is generated, or (b) any generated heat is immediately dissipated by the thermal conductivity of the material. (Thermal and electrical conductivity go virtually hand in hand in electrically conductive materials.)

2. Emissivity

The materials used must have their surfaces treated in such a manner as to assure a sufficient level of emissivity.

a. Spectral emissivity (ϵ_λ) is a measure of the difference between the spectral emittance of the object in question and that of an ideal black body:

$$\epsilon_\lambda = \frac{W_{\lambda o}}{W_{\lambda B}}$$

where $W_{\lambda o}$ is the spectral emittance of the object in question, $W_{\lambda B}$ is that of the black body.

b. The emissivity (ϵ) or total emissivity of an object is the ratio of its total emittance to that of a black body expected from the Stefan-Boltzmann formula

$$= \frac{\int_0^\infty W_{\lambda_0} d\lambda}{\sigma T^4} = \frac{W_0}{\sigma T^4}$$

where W_o is the total power density at all frequencies emitted by the object, σ is the Stefan-Boltzmann constant ($5.67 \cdot 10^{-8} \frac{\text{watt}}{m^2 \cdot \sigma K^4}$) and T is the temperature of the object in degrees Kelvin.

> "The values for ϵ obtained by using Thermovision are, in effect, the average of ϵ_λ occuring over the middle infrared wavelength interval utilized..."[63]

The emissivity of a material is highly dependent on the condition of its surface. In general,

---

[63]Thermovision Manual, Section 7, p. 7.

highly reflective surfaces are very poorly emissive, so that by increasing its absorptance, we can increase its emissivity.

B. BASIC FORM OF EXPERIMENTS

The experiments comprised three basic forms.

1. Dielectric Substrate with Carbon Paint

Various structures were made of dielectric substrate and painted with a conductive carbon paint.[64] Carbon has been seen in the first experiment to have heat generating and keeping qualities which were adequate to provide a Thermovision image. The question was whether its electrical conductivity is sufficiently high to permit induction of currents of sufficient magnitude as to match the behavior of a more perfectly conducting structure.

2. Metal Structure with and without Carbon Paint

These structures, matching those of B.1 above, were considered a likely substitute for the problem of inadequate induced currents. The question here is whether they possess enough emissivity to present an image to the Thermovision System.

3. Structures with Carbon Paper

These structures were similar to that of the earlier experiment. The principle involved is to use the carbon paper to tranduce fields in the vicinity of the structure from which charges and currents on the structure can be deduced. The phenomenon is considered to consist of currents being induced in the carbon paper. These currents are parallel to the electric lines of force (LOF) set up by the charges on the structure. As the lines of force converge on large charge concentrations, their flux density (lines per square centimeter) increases, and with it the heat generated by the ohmic resistance of the carbon paper. In high charge density regions this LOF density

---

[64]Eccocoat 256 paint, manufactured by Emerson and Cuming, Inc., Canton, Massachusettes, 02021.

and its attendant thermal energy density (joule/cm^2) is sufficient tc exceed the sensivity of the AGA detector and provide an image.

C. EXPERIMENTAL PARAMETERS

1. Types of Structures

Three basic structures were used.

a. 1.5 Wavelength (λ) Monopole over a Ground Plane

b. Aircraft Model

c. Wire crosses

2. Expected Charge and Current distributions

Various charge and current distribution are possible on the selected structures. Broadly these may be classed into various cases.[65]

---

[65]Burton, R.W., "Measured Currents and Charges on Thin Crossed Antennas in a Planewave Field", (with R.W. King) IEEE transactions on Antennas and Propagation, Vol. AP-23, No. 5, pp.657-64, September 1975.

a. Case 1A

This case uses a $^3/_4\lambda$ vertical height (h) over a ground plane, with cross arms (when present) placed $\lambda/2$ above the ground plane. These arms are each $\lambda/4$ to be compatible with the vertical member's charge and current distribution. The effect of this configuration is to place a large current maximum at the junction point, and large charge deposits at the tips of the structure.

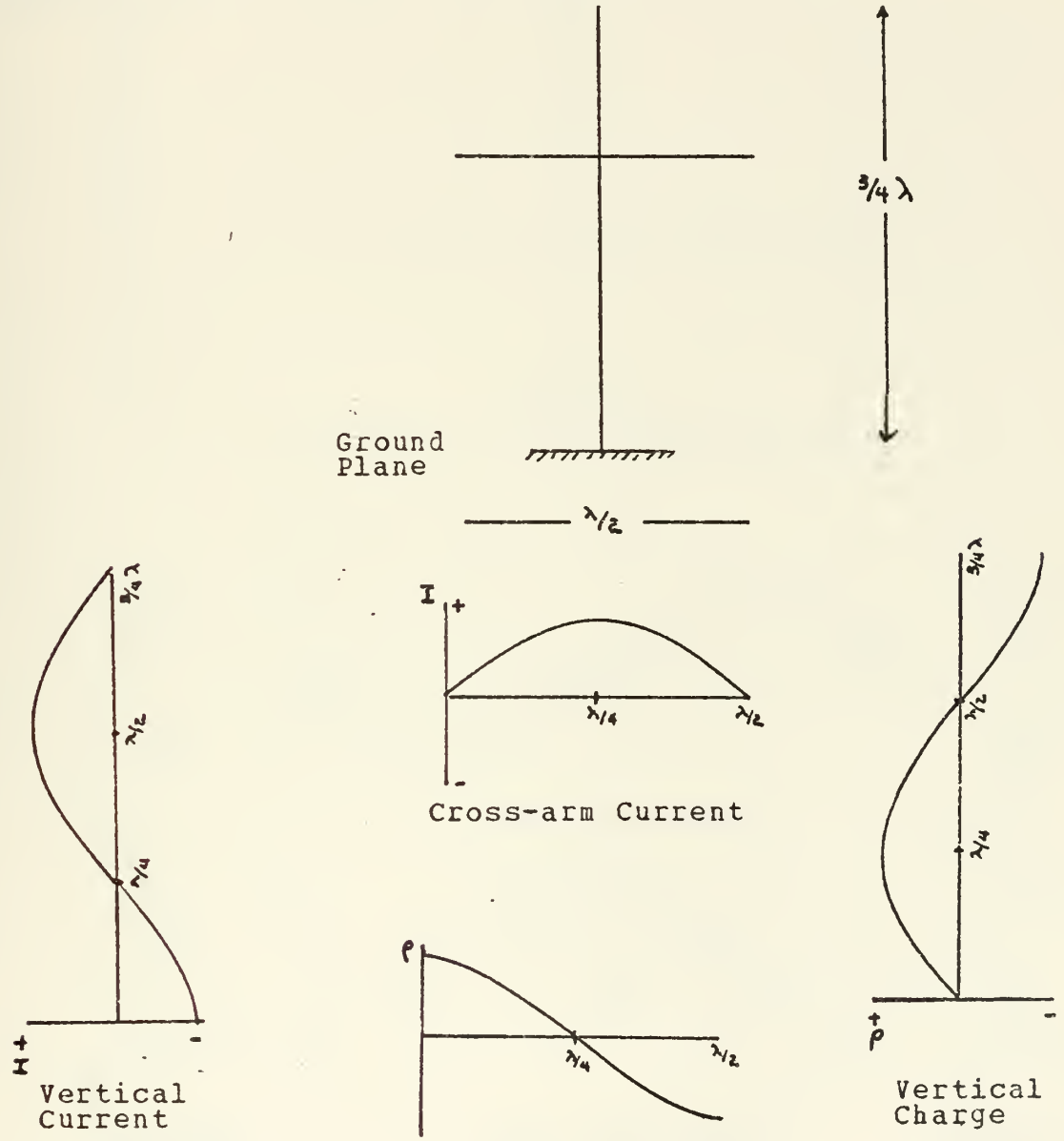

Figure 59 - Case 1A
Cross Configuration with Current and Charge Distribution

b. Case 1B

This case also uses a $\frac{3}{4}\lambda$ h but places the cross arm at a charge maximum. Now the cross arms must each be $\lambda/2$ to have their natural charge and current distributions be compatible with that of the vertical member.

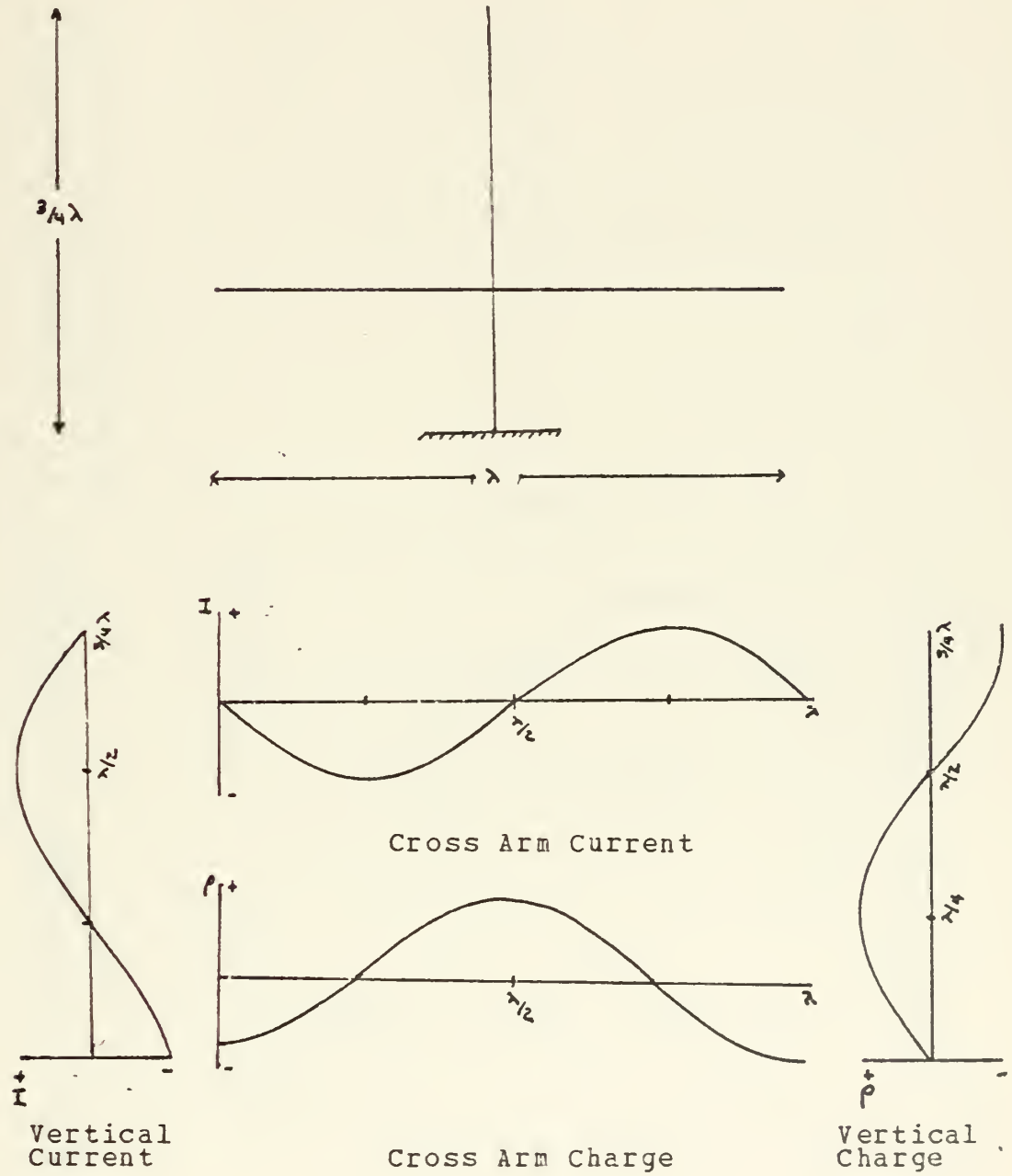

Figure 60 - Case 1B
Cross Configuration with Current and Charge Distribution

c. Case 2

This case presents a symmetric structure, with the vertical member one wavelength in length, and each arm $\lambda/2$ in length. This results in a current minimum at the junction.

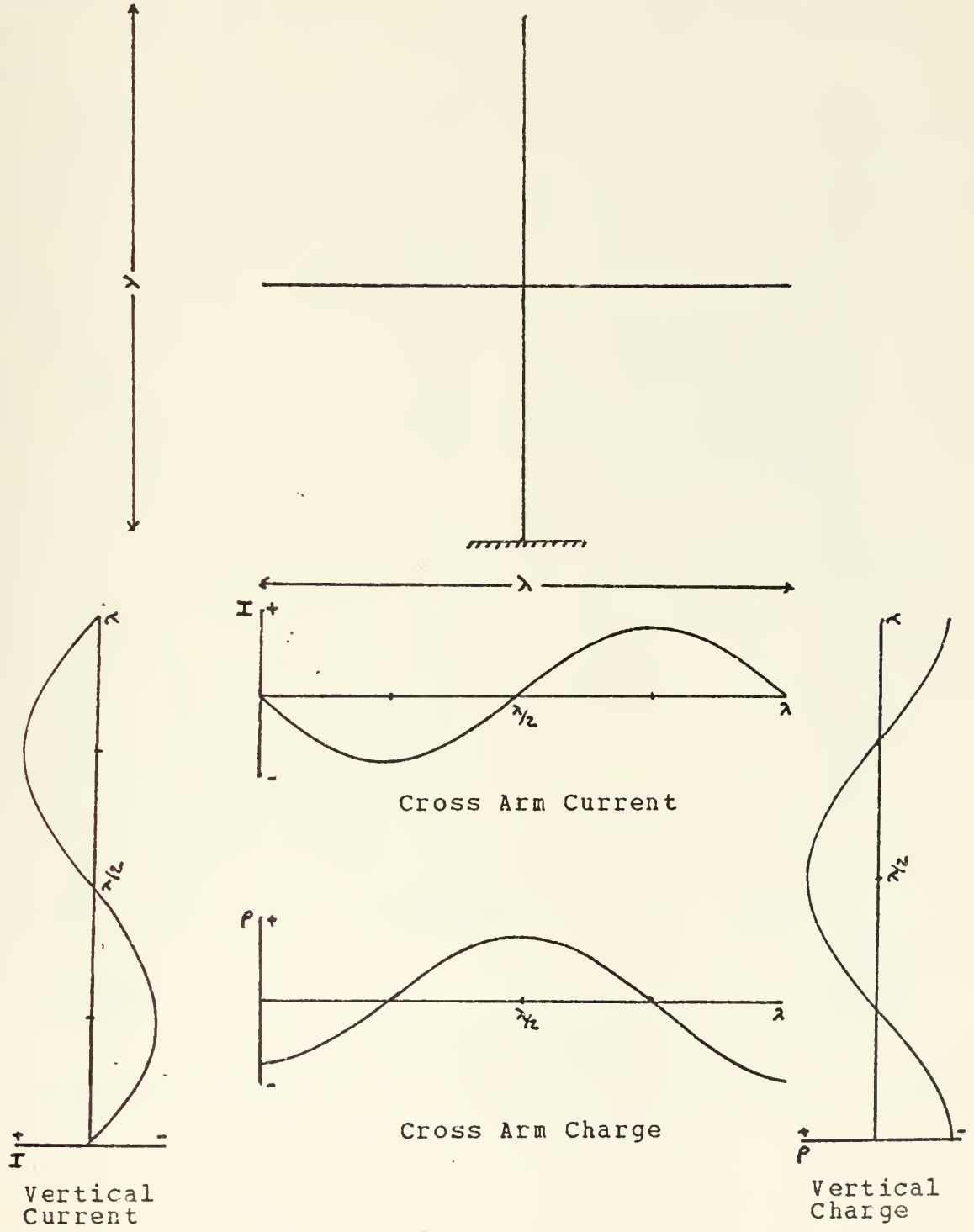

Figure 61 - Case 2
Cross Configuration with Current and Charge Distributions

d. Case 3

This case presents a 1.5λ structure without cross arms.

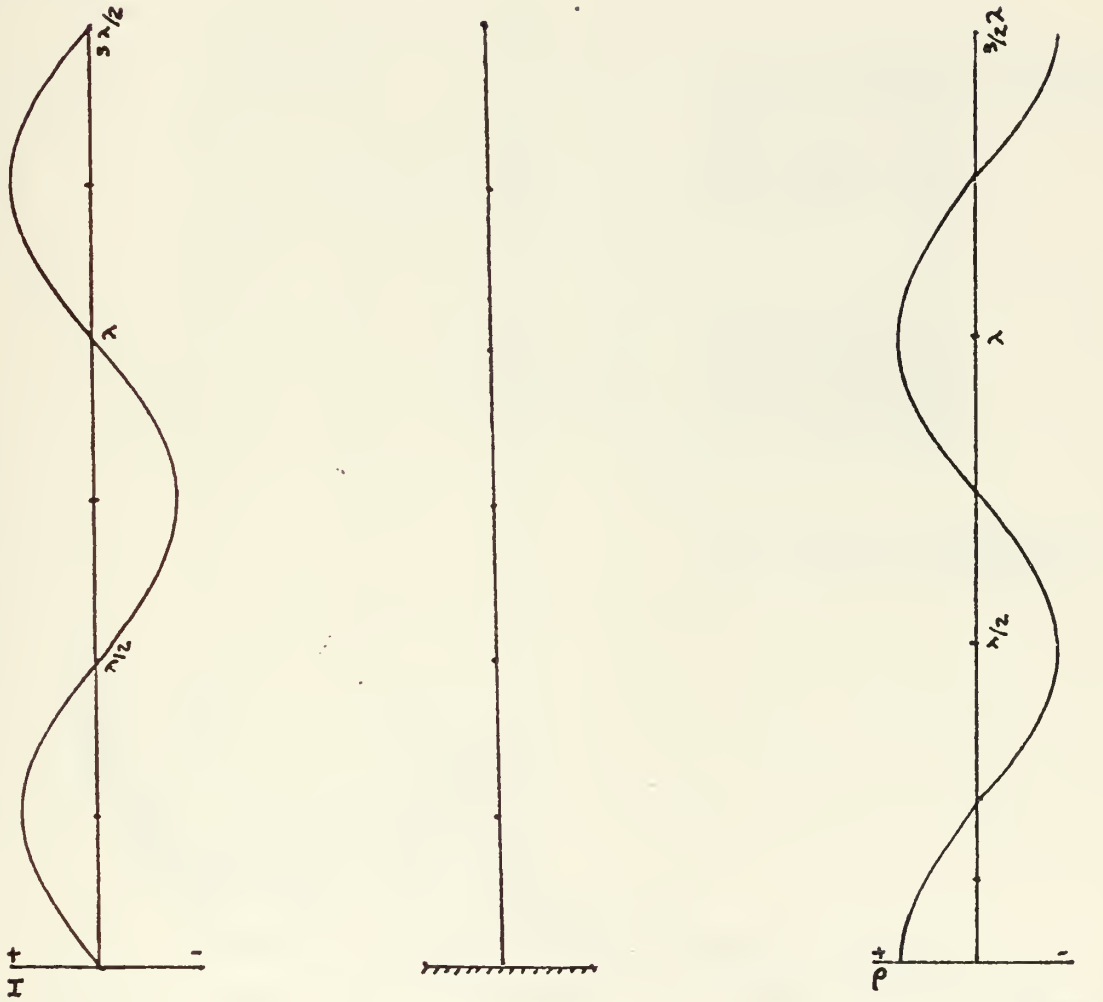

Figure 62 - Case 3
Cross Configuration with Current and Charge Distributions

3. Dimensions and Frequencies to be used

The frequencies to be used depend on the dimensions of the structures involved.

a. The available materials for construction and the considerations above of the metal monopole required a Case 3 monopole over a ground plane with dimensions as follows:

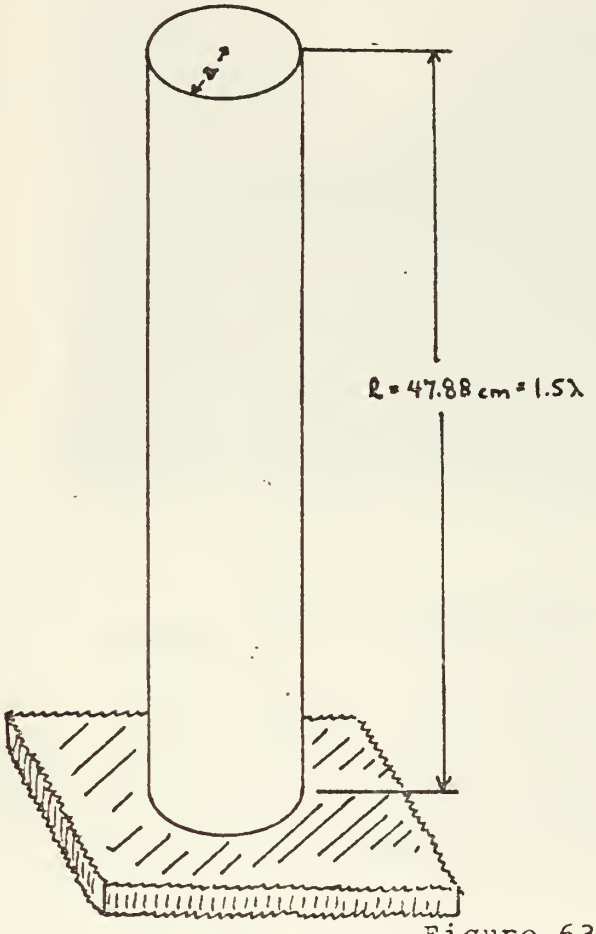

$a = 2$ inches $= 5.08$ cm

$Ka = 2a = 1.$

$\lambda = 31.92$ cm

$f = 939.39$ MHz

$l = 1.5\lambda = 47.88$ cm

Figure 63
Dimensions of the 1.5λ Wavelength Monopole

From these dimensions an operating frequency of 939.89 MHz is derived.

b. Plastic Substrate Aircraft Model

A plastic model fighter plane was selected with the dimensions shown in the figure below. From these figures the range of dimensions were obtained for

Length (L) $\qquad 26.6 \leq L \leq 27.6$ cm

Width (W) $\qquad 20.1 \leq W \leq 25.7$ cm

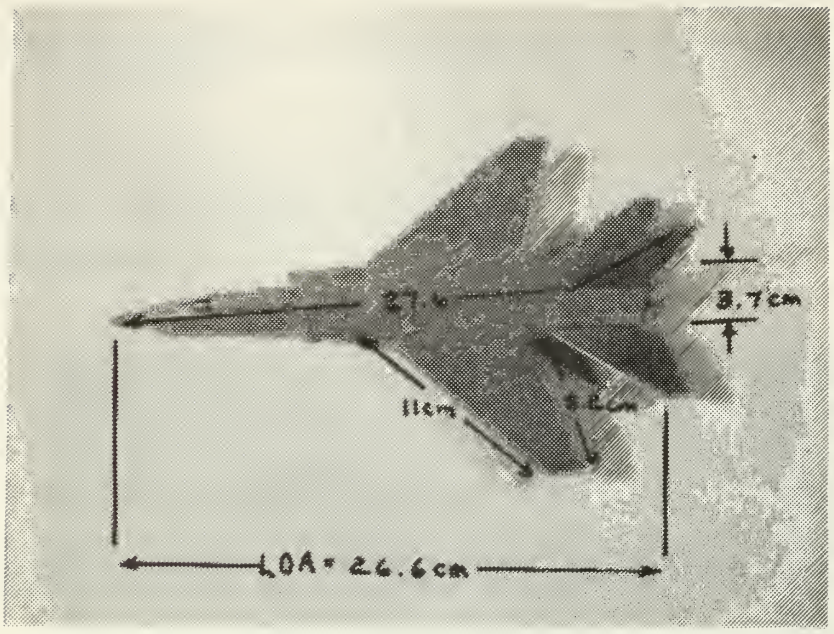

Figure 64
Dimensions of the Plastic Aircraft Model

(1) A Case 1A structure is almost achieved with a frequency selection of 815.2 MHz with the model nose down over the ground plane. In such a case L = 27.6 cm = $\frac{3}{4}\lambda$, and the arms are each .02 longer than $\lambda/4$:

$L = \frac{3}{4}\lambda = 27.6$ cm

$W = \frac{1}{2}\lambda = 18.4$ cm; $20.1 = .546\lambda$

(2) A Case 2 Configuration is obtained at 1.258 GHz with the model tail down over the ground plane. In this case the length is one wavelength but the arms are now each .02 too short:

$L = \lambda = 26.6$ cm

$W = \lambda = 26.6$ cm; $25.7 \text{ cm} = .966\lambda$

c. Metal Aircraft Model

A copper aircraft model was obtained as shown in the figure below. This structure is more symmetric than the previous one so that the only case considered favorable is a Case 2 configuration. The ranges of dimensions are

$$50 \leq L \leq 54 \text{ cm}$$
$$50 \leq W \leq 57 \text{ cm}$$

A frequency of 570 MHz provides $\lambda = 52.6$ cm, which matches these dimensions.

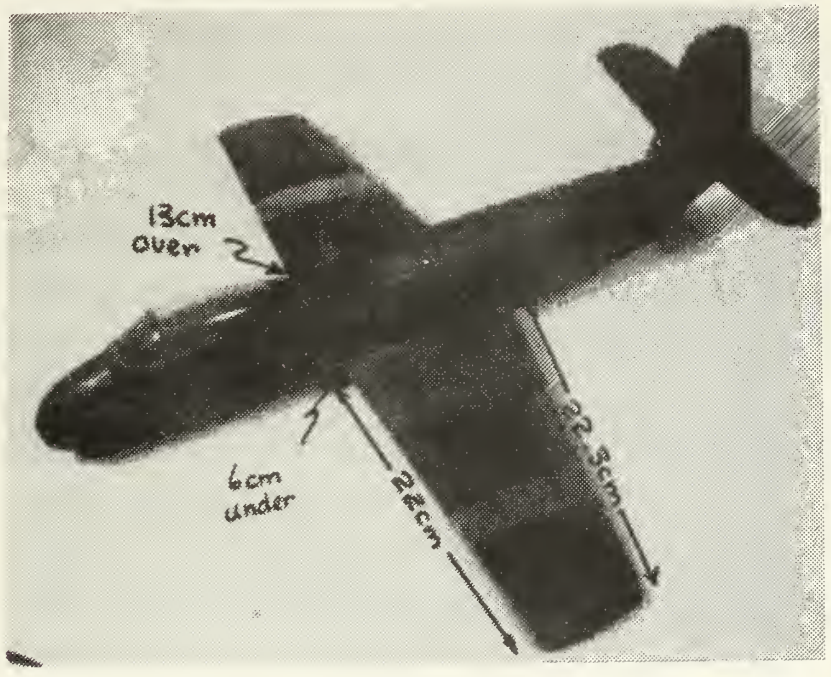

Figure 65
Dimensions of the Copper Aircraft Model

d. Wire Crosses

Wire crosses were constructed to provide Case 1A and 1B Structures. The frequency chosen on the basis of convenience is 1.5 GHz. Their dimensions are shown in the figure below:

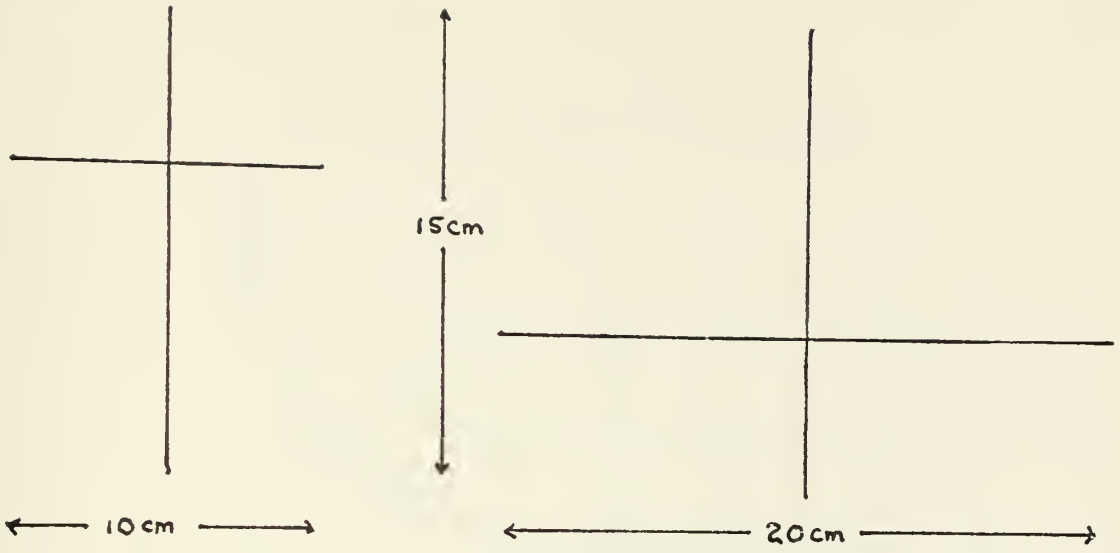

Figure 66
Dimensions of the Wire Crosses

D. EXPERIMENTAL OBJECTIVES

The experiments were to proceed through the three basic forms (dielectric, metal and wire structures) to determine

(1) Whether an image is visible

(2) What degree of difficulty exists in obtaining it.

E. EXPERIMENTAL PROCEDURES

The success or failure in determining the first objective was seen to depend principally on the amount of energy transferred to the element by the field and on its ability to reradiate that energy. The ability of the structure to accept the field energy rests principally in its resonance characteristics, and next on its ohmic conductivity. The ability of the structure to reradiate the energy then depends on its thermal conductivity and emissivity. Since ohmic and thermal conductivity essentially go hand-in-hand it is seen that there exists essentially a three dimensional matrix relationship among the parameters, as seen in Figure 67.

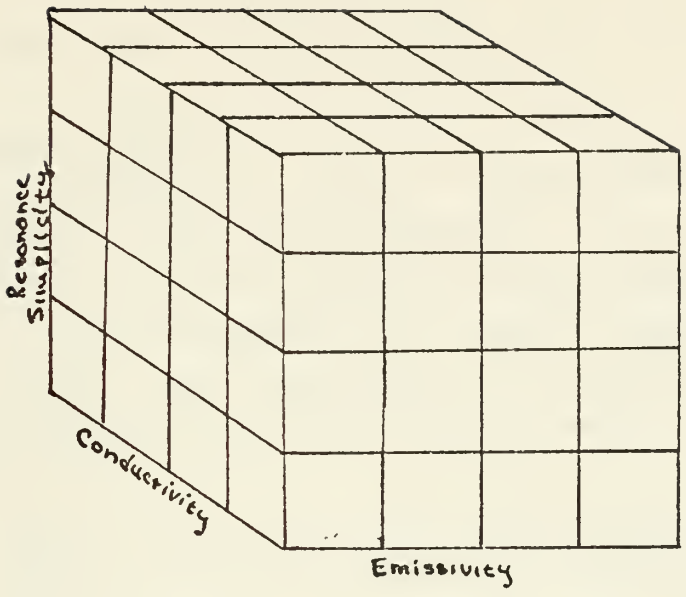

Figure 67
Matrix of the Relationship Among the Parameters

Therefore, the experiments are seen to be conducted in a matrix fashion, choosing an element with successively more complex (less simple) resonance, and for each plane level of resonance complexity investigating the response with various coordinates of conductivity and emissivity.

To implement this plan it was necessary to modify the emissivity of the metal structures. The modifications were irreversible in the short time available, so a definite procedure was followed as outlined here.

1. 1.5λ Monopoles

These provide the simplest and most predictable resonance characteristics. These were irradiated at 939.39 MHz and investigated for the surface thermal patterns in this order:

a. The dielectric base monopole.

b. The brass monopole without modification

c. The brass monopole sprayed with flat black paint on one half.

d. The brass monopole painted with carbon paint on the other half.

e. The brass monopole with large carbon paper sheet behind it.

2. Aircraft Models

These structures have significantly greater resonance complexity, but are fundamental to the research for which the use of the AGA device is being considered. The models used can be approximated by simpler structures for which there exist known measurements, notably the Case 1A and Case 2 models discussed above. These were investigated in this order:

a. Plastic Model, nose down over ground plane.

b. Plastic Model, tail down over ground plane.

c. Copper Model with oxidized surface, nose down, touching the ground plane.

d. Copper Model with oxidized surface in flight configuration at varying heights above the ground plane ($\lambda/4$, $\lambda/2$, $3/4\lambda$, and other intermediate positions).

e. Copper Model in same configurations as E. 2. b and c above but painted to obtain higher emissivity. Choice of emissive paint to be based on results of paragraph E. 1 above.

e. Painted Copper Model in configuration E. 2 b, nose down touching the ground plane, with carbon paper sheet immediately next to it.

3. Wire Crosses

These were investigated with the carbon paper in close proximity.

F. EXPERIMENTAL RESULTS

1. General

The experiment was successful in showing the ease with which the AGA device might be used to observe the fields of irregular structure. Further it showed the carbon paint and carbon paper to be effective transducer media in that it is evident that they transduce fields without

distorting them from what has been previously measured to be their correct form. It is considered important that the relative simplicity of the method be appreciated. There is no need for prechilling of the transducer medium. There is no need to get extremely close to the radiator, thereby distorting the fields or incurring the effects of nonplanar wavefronts. The experimenter is not constrained in source frequency selection since there are no size limitations. It is also evident that the power limitations cited for the DTM process are not an issue. The principal issues are how (1) to optimize the selection of a transducer medium and (2) optimize the selection of color assignment to the sensor temperature ranges discussed below. Of these two issues the latter is eminently elegible for subjective manipulation. The former may be approached on a methodical scientific basis.

2. Guide to Interpretation of Results

The photographs which accompany the following discussion are conventional Polaroid color photographs of the screen of the AGA device display monitor. The color bars across the bottoms of the photographs show the colors associated with a particular value of the temperature. The temperature range is in discrete .2° steps centered on a continuously variable temperature level. The choice of color for a particular temperature range was based simply on what combination of colors gave a percieved clarity of image. This assignment can be varied arbitarily. What is significant is that the device sensed the temperature distribution which occurred and presented it in a manner which then could be manipulated for improved human perception.

3. Experimental Parameters

The experiments used the 60° corner reflector structure as the illuminating source. It was fed with various power sources with a range of power levels from 5 to 80 watts. The corner reflector was consistently placed at

.4λ from the driven element. The target elements were generally a distance of approximately 2λ from the driven element. An additional parameter, view angle (α), emerged as one of certain interest. It is defined by Figure 68 as the angle between the direction of arrival of the illuminating wavefront and the direction along which the target element is observed.

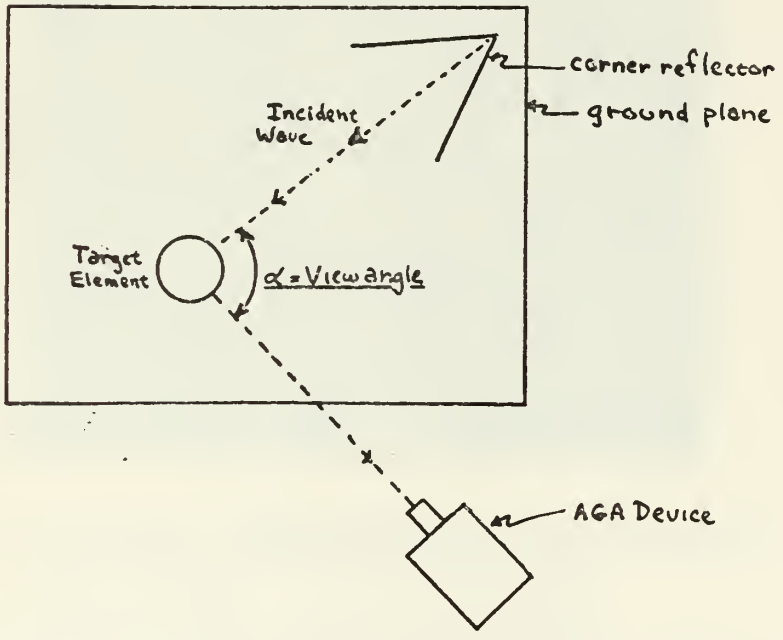

Figure 68
Top View of Experimental Setup (Not to Scale)

4. 1.5λ Monopoles

a. Dielectric base monopole

Figure 69 shows the image obtained of the dielectric base, relatively fat, 1.5λ monopole. The view angle for this image is approximately 45°. It shows the current distribution of Figure 62. Additionally it shows

the spillcver which occurs at the top of the monopole when the current, no longer able to continue longitudinally along the vertical axis becomes transverse and flows around the side of the monopole away form the incident wavefront. This phenomenon matches that measured by Burton and King for this same identical case.

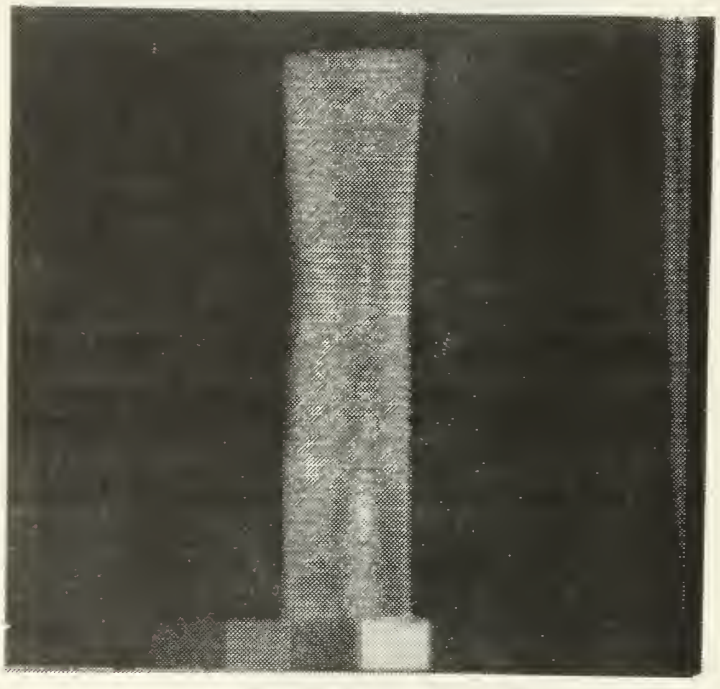

Figure 69
AGA Thermovision Image of a 1.5λ Fat Monopole

b. Brass Monopole

No image was obtained of the currents on the brass monopole. This lack of success is not considered conclusive however. Resolvable difficulties discussed below were incurred with the carbon paint coating and with obtaining a carbon paper medium large enough for the device. The time constraints did not allow these issues to be immediately resolved in this case.

5. Aircraft Models

a. Plastic Aircraft Model

Figures 70 and 71 show the image obtained of the plastic aircraft model. Figure 70 shows a view angle of 90°. The stronger currents apparent on the port wing

indicates its closer proximity to the illuminator. The overall pattern, with an apparent current maximum at the Case 1A junction, located in line with the trailing edge of the wings, is consistent with the expectations of C. 3. b. (1) above. A Case 2 image was not attempted due to time constraints.

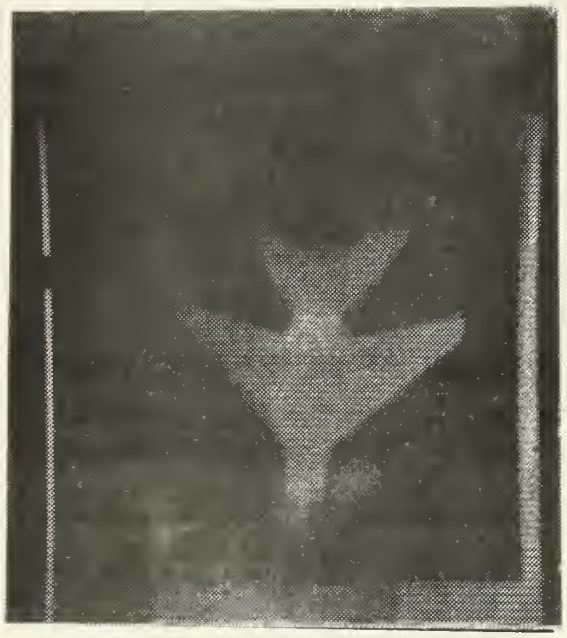

Figure 70
Plastic Aircraft Model, Case 1A View Angle = 90°

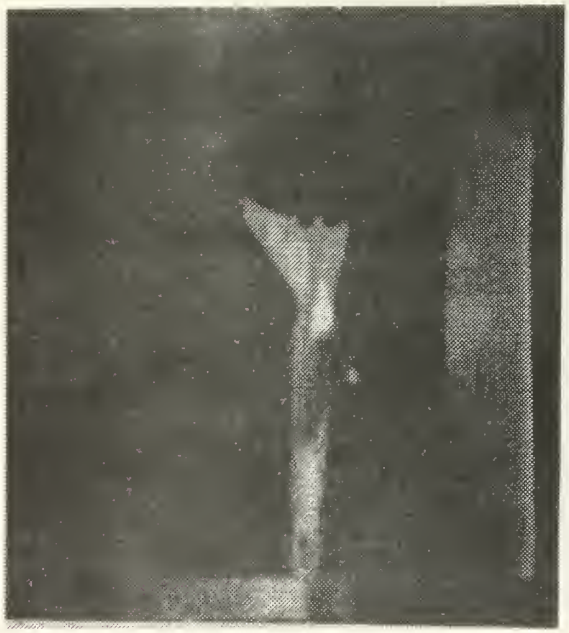

Figure 71
Plastic Aircraft Model, Case 1B View Angle = 90°

Figure 71 shows the aircraft illuminated from its underside. The hot spot on the fuselage next to the cockpit indicates the lowest current maximum of the Case 1A configuration. Additionally the junction current maximum is visible at the trailing edge of the wings. Of possible additional interest are the patterns on the vertical stabilizer indicating current distributions thereon.

b. Copper Aircraft Model

Figure 72 and 73 show the images obtained of the copper aircraft model. The highly oxidized surface of the model apparently provided the high emissivity observed, while the thinner metal thickness inhibited flow-away of the thermal fields. These results were particularly encouraging since the power levels needed were much lower than those required for the plastic model.

Of particular interest are the patterns observed on the wing surfaces where currents are not constrained by narrow structures. Apparent hot spots appear near the trailing edge of the port wing as seen in Figure 72.

Figure 72

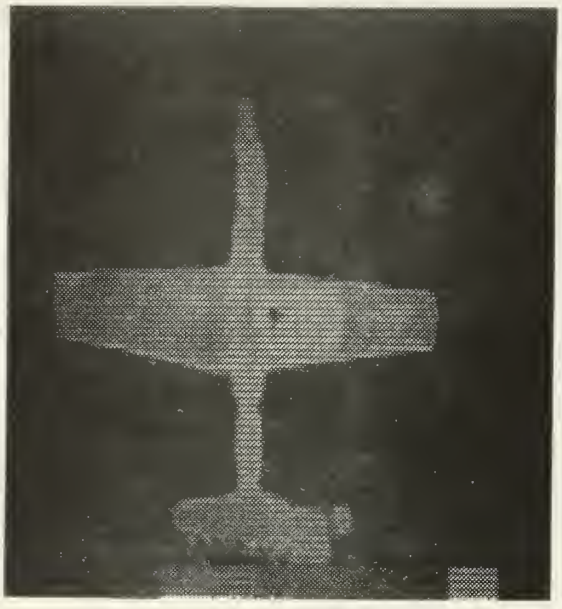

Figure 73

6. Wire crosses

Figures 74 and 75 show the Case 1A and 1B wire crosses. In all previous images the currents on the structure were being observed by their being transduced into a thermal field on the structure. Here the currents are in a piece of carbon paper placed next to the cross. The currents are apparently induced parallel to the lines of force (LOF) of the electric field so that the image obtained represents the charges on the structure. Figure 74 is completely consistent with Figure 59 and [2]. Figure 75 is completely consistent with Figure 60 and [2]. It is significant to note the diminished magnitude of the charge at the top of the Case 1A cross, caused by the sharing of charge with the cross arm tips. This phenomenon is cited in [2]. It is interesting to note the shift of charge away from the junction seen in Figure 75. This too is consistent with the measurements of [2].

Figure 74
Case 1A Wire Cross with Carbon Paper View Angle = 0°

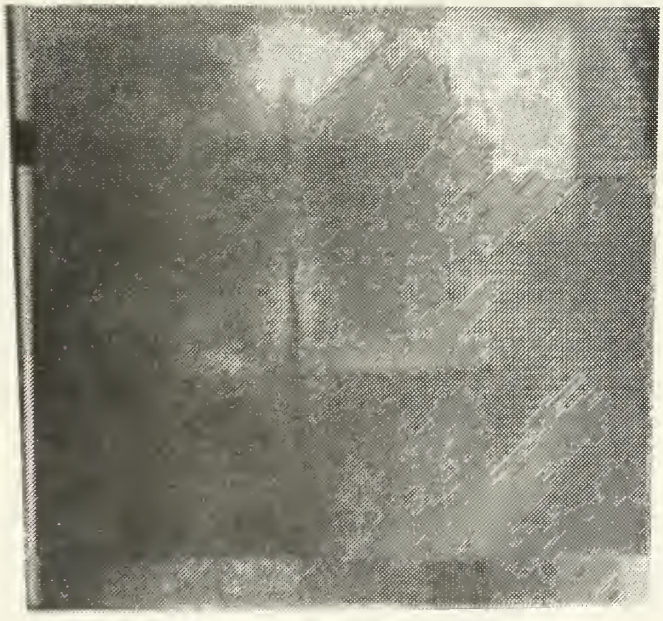

Figure 75
Case 1B Wire Cross with Carbon Paper View Angle = 0°

8. Technological Complications

Two items presented relatively minor problems.

a. Emissivity Conductive Coating

Yet to be resolved is the problem of an optimum coating for either dielectric or metal base objects. The material used contained acetone as a base, which eroded the polystyrene of the aircraft model. When placed on glass or metal this paint cracked while drying. One possible solution, that used on the dielectric base monopole, is to first coat the object with a standard lacquer[66] allowing it to dry before being painted with Eccocoat. Aquadag was also suggested, but not tried, as an alternative.

b. Large carbon paper

When using carbon paper to sense the fields in the vicinity of the structure one must allow indirection of currents in the paper along the lines of force of the electric field. To avoid distortion of such currents the carbon paper must be large enough to provide a complete circuit for the currents involved. The sheets used with the Case 1A cross were approximately twice as large as the accompanying structure. The sheet used with the Case 1B was only slightly larger than the cross, while that used with the brass monopole was approximately the same size. It appears that there is a correlation between relative size and success in imaging. It is suggested that that success is related to the freedom with which currents can be induced in the carbon paper.

G. CONCLUSION

The experiments described here clearly demonstrate the feasibility and simplicity of using the AGA Thermovision device for imaging electromagnetic fields. Its advantages over DTM are:

---

[66]The laquer used here was Tuf-On 747-S Moisture and Fungus Resistant Varnish manufactured by Brooklyn Paint and Varnish Co., Inc., 50 Jay Street, Brooklyn, N. Y.

1. Clarity of image

Because the colors may be manipulated at will, the image may be subjectively manipulated to obtain optimal perceived clarity.

2. Ease of calibration

Images may be easily measured to obtain values of field intensity. The accuracy of these measurements is limited by step size of the temperature increment and the calibration of the device, but is identifiable.

3. Ability to measure charges or current on the structure

The methods described here permit observation of current on the structure directly or of charges by inference from the near electric field observed by the currents it induces in the carbon paper. DTM is limited to observing the charges on the structure.

4. Ease of observation

Once the issues of F.1 above are resolved, the investigator simply observes the pattern. There is no need for painstaking presensitization or cooling. Since there are no frequency limitations, he can select the frequency most desirable for his objective. Since there is an apparently lower power threshold he can operate at safer power levels and at distances from the illuminator which minimize interactions with the source.

In conclusion, the use of the AGA Thermovision device in the manner described here shows significant potential as a means of observing the charges and currents on structures and the resulting electromagnetic fields.

BIBLIOGRAPHY

Beiser, Arthur, Perspectives of Modern Physics, p. 56, McGraw-Hill, 1969.

Burton, R. W., "The Crossed-Dipole Structure of Aircraft in an Electromagnetic Pulse Environment", Proceedings of the International Conference on Electromagnetic Noise, Interference and Compatibility, Advisory Group for Aerospace Research and Development (AGARD/NATO), pp. 30-1 thru 30-15, Paris, France, October 1974.

Burton, R. W., "Measured Currents and Charges on Thin Crossed Antennas in a Planewavw Field", (with R. W. King) IEEE Transactions on Antennas and Propagation Vol. AP-23, No. 5, pp. 657-64, September 1975.

Division of Engineering and Applied Physics, Harvard University, Cambridge, Massachusetts, Technical Report No. 558, A Method for Photographing Microwave with a Polaroid Film, by Keigo Iizuka, p. 3, March 1968.

Dodd, James L., A Direct Method of Visualizing the Surface Distribution on Antennas at Microwave Frequencies With Application to Cross-Wire Structures, Masters Thesis, Naval Postgraduate School, Monterey, 1974.

Eastman Kodak Company, Kodak Infrared Films, No. N - 17, p. 2, Kodak Publications, 1972.

Eastman Kodak Company, KODAK Plates and Films for Scientific Photography, P - 315, p. 3, Kodak Publications, 1973.

Eastman Kodak Company, Kodak IRTRAN Infrared Optical Materials, U - 72, p. 5, Kodak Publications, 1971.

Encyclopaedia Britannica, v. 7, p. 424, Encyclopaedia Britannica Inc., 1968.

Engel, Charles E., Photography for the Scientist, p. 2 ff., 21, 44, 45 ff., 79, 96 - 98, 178 - 179, Academic Press, 1968.

Jordan, E. C. and Balmain, K. G., Electromagnetic Waves and Radiating Systems, 2nd ed., p. 171, 250, 336, 470 - 471, Prentice-Hall, 1968.

Kraus, John D., Antennas, p. 330, McGraw-Hill, 1953.

Masterton, W. L. and Slowinski, E. J., Chemical Principles, p. 255, 380 - 382, W. B. Saunders Co. 1973.

Polaroid Corporation, Publication PX 850, p. 1, December 1972.

Polaroid Corporation Letter, Subject: Slope and Resolution of Polacolor Film; Request for report on, March 1974.

SPSE Handbook of Photographic Science and Engineering p. 195, 259, 146 - 148, 302 - 303, 308 - 309, 312 - 317, 448 - 469, 767, 810 - 816, Wiley 1973.

Thirtle, John R., "Chemistry of Color Process," SPSE Handbook of Photographic Science and Engineering, p. 567 - 568, Wiley, 1973.

Weiss, J. Paul, "Section 15 - Densitometry," SPSE Handbook of Photographic Science and Engineering, p. 829, Wiley, 1973.

INITIAL DISTRIBUTION LIST

		NO. COPIES
1.	Defense Documentation Center Cameron Station Alexandria, Virginia 22314	2
2.	Library, Code 0212 Naval Postgraduate School Monterey, CA 93940	2
3.	Department Chairman, Code 52 Department of Electrical Engineering Naval Postgraduate School Monterey, CA 93940	1
4.	Professor R. W. Burton, Code 52Zn Department of Electrical Engineering Naval Postgraduate School Monterey, CA 93940	15
5.	LCDR Claude La Varre, USN 1460 Manor Place Monterey, CA 93940	1
6.	Capt. Michael Harrison, USAF AFWL/ELP Kirtland Air Force Base, NM 87117	2
7.	Dr. A. C. Schell AFCRL/Microwave Laboratory L G Hanscom Fld Bedford, MA 01730	1
8.	LCOL A. Cupka, USAF AFWL/EL Kirtland AFB, NM 87117	2
9.	Assistant Professor Richard W. Adler, Code 52Ab Department of Electrical Engineering Naval Postgraduate School Monterey, CA 93940	2

DUDLEY KNOX LIBRARY
NAVAL POSTGRADUATE SCHOOL
MONTEREY, CALIFORNIA 93940

thesL317
Thermographic imaging of electromagnetic
3 2768 002 12295 4
DUDLEY KNOX LIBRARY